

Marquette University

e-Publications@Marquette

Dissertations (1934 -)

Dissertations, Theses, and Professional
Projects

Mechanisms of ATP-Dependent Substrate Reduction in the Nitrogenase-Like DPOR Complex

Elliot Irwin Corless
Marquette University

Follow this and additional works at: https://epublications.marquette.edu/dissertations_mu



Part of the [Biology Commons](#)

Recommended Citation

Corless, Elliot Irwin, "Mechanisms of ATP-Dependent Substrate Reduction in the Nitrogenase-Like DPOR Complex" (2020). *Dissertations (1934 -)*. 986.

https://epublications.marquette.edu/dissertations_mu/986

MECHANISMS OF ATP-DEPENDENT SUBSTRATE REDUCTION IN THE
NITROGENASE-LIKE DPOR COMPLEX

By

Elliot Irwin Corless

A dissertation submitted to the Faculty of the Graduate School,
Marquette University, in partial fulfillment of the requirements for the degree of Doctor of
Philosophy

Milwaukee, Wisconsin

August 2020

ABSTRACT

MECHANISMS OF ATP-DEPENDENT SUBSTRATE REDUCTION IN THE NITROGENASE-LIKE DPOR COMPLEX

Elliot Irwin Corless

Marquette University, 2020

Iron-Sulfur ([Fe-S]) clusters are the most common transient electron carriers in cells and are necessary for basic metabolism of all life. Bacterial systems use two operons (*isc* and *suf*) for the biogenesis and delivery of [Fe-S] clusters to various proteins. Once delivered, they serve as transient electron carriers necessary for both heterotrophic and autotrophic metabolism and reduction/oxidation chemistry. This work utilizes the hetero-octameric Dark operative Protochlorophyllide Oxido-Reductase (DPOR) complex as a platform to investigate [Fe-S] cluster biogenesis and the concerted action of its multiple [Fe-S] clusters and protein subunits.

DPOR catalyzes the penultimate step in bacterial chlorophyll synthesis and accounts for more than half of the chlorophyll produced on earth. DPOR stereo-specifically reduces the C17-C18 double bond of protochlorophyllide (Pchl_{id}) to yield chlorophyllide (Chl_{id}). This reduction requires 2 cycles of electron transfer and the hydrolysis of 4 ATP molecules. The DPOR complex is composed of two separable components. BchL exists as a stable α_2 homodimer, and BchNB exists as a stable $\alpha_2\beta_2$ heterotetramer, containing two [4Fe-4S] clusters that accept electrons from BchL and are terminally donated to one of two Pchl_{id} molecules bound to BchNB. The overall complex is arranged as two identical catalytic halves. In the presence of ATP, BchNB forms a transient complex with BchL and electron transfer to Pchl_{id} is coupled to ATP hydrolysis.

The architecture of DPOR is evolutionarily conserved, with the most notable examples being the next protein in the chlorophyll synthesis pathway Chlorophyllide Oxidoreductase (COR), and nitrogenase which share the same stoichiometry of subunits. The quaternary structure of DPOR has two pseudo C₂ axes of symmetry, one bisecting the BchL dimer, and one bisecting the BchNB tetramer. This complexity makes study of these enzymes complex but the degree of homology and conservation in these life critical enzymes begs the questions why does DPOR function in such a complicated manner? Is this complexity even necessary, and how is information communicated across the long distances between subunits of DPOR? The specific role of individual events from binding of substrate (whether ATP or Pchl_{id}), electron transfer events, and identical halves of BchL or BchNB function remains unresolved for DPOR.

This document details a classical biochemical approach that reveals mechanistic principles underlying the structural and functional complexity of DPOR. The main findings of this work are 1) proof of the non-redundancy of the *isc* and *suf* operons in the heterologous expression of proteins, 2) novel findings on the role of ATP in the BchL homodimer unique to DPOR, and 3) the sequential electron transfer in the BchNB heterotetramer. Overall it indicates that identical halves of DPOR components accomplish complex long-range allosteric communication between symmetrical structures that requires two functional identical halves for overall activity, that key features of DPOR are evolutionarily maintained because they regulate key steps that must work in harmony to accomplish the symphony of steps that allow DPOR and related enzymes to function.

ACKNOWLEDGEMENTS

To,

My mentor and advisor Edwin Antony, I would not have pursued a PHD if you didn't see what ever potential you saw in me. I can't thank you enough for believing in me and guiding me through my PHD career. Your trust and confidence in me to tackle DPOR and establish anaerobic work in our lab, and the autonomy to pursue the avenues we used has allowed me to gain the independence and confidence that are now core to my personality. I've always felt slightly in trouble since you started being my mentor, like I wasn't ever doing quite enough, but I know that it's because you wouldn't sign off on me missing my potential. Thank you for seeing the scientist inside a sarcastic, smart-assed, punk.

My mom, you always thought I was going to be the golden child that became a pediatric brain surgeon. I didn't go in that exact direction, but I hope that I've still made you proud. Thank you for supporting me even when you didn't approve of my lifestyles, for believing that I could do whatever I set my mind to.

My late grandfather, my father figure, my slave driver. Thank you for being an ornery old bastard, for drilling hard work into my soul and teaching me how to do all the things I can do with my hands. Thank you for inspiring the passions I hold dear to this day, for teaching me the gratification that comes from doing a job yourself.

My lab partner Nilisha, war makes brothers of us all, and there were times where it did feel like we were in the trenches together. More than that, I can't believe I found a kindred soul in a tiny girl from Nepal. I'm honored to call you a friend, count you as family, and to be trusted enough to give you away. I couldn't have asked for a better lab partner; I'll always be your "boyee".

Jessica, I'm so glad we became friends, even if I wasn't the greatest one when we first met. I know how close you keep your friends, and I can't express how grateful I am to count you my best friend. We've seen so much together, and you really made a new place and experience feel like home when I needed that more than anything. I don't think I would have made it through without you.

Devan, my only close male friend, thank you for being there during some of my darker moments, for making sure that we always had an event on the horizon to look forward to, and sharing your mind with me during all our totally sober talks.

Franki, you're one of the kindest people I've ever met, and you always built me up whenever we spent time together. I can't thank you enough for your friendship.

Rachelle, thank your trusting and confiding in me. Our friendship usually involved you rolling your eyes at something I said, but you always laughed afterwards, and I always knew I could count on you for anything.

My committee members. Adam, thank you for taking on the task of serving on my committee, despite not being in the same department. You could have easily passed on serving, but you went out of your way for an unknown graduate student and I thank you. Martin, the sheer amount of work you put in on my behalf is staggering. Thank you so much for taking charge on

everything and for taking me on despite all the other responsibilities you have. Thank you for your candor when we spoke one on one, and for being a genuinely good resource. Sofia, oh man, could we argue. I know you begrudgingly care about me though. Thank you for serving even though you may have preferred not to. Thank you for making me laugh and laughing at all my awesome jokes. Brain, your expertise made a lot of my dissertation possible. Thank you for sharing that expertise and for all the hard work and thought you put into my project. I counted you as a steady and calming influence on me, and I appreciate all you have done for me.

Contents

ACKNOWLEDGEMENTS.....	i
CHAPTER 1. INTRODUCTION.....	1
1.1 [Fe-S] Cluster biogenesis and function.....	1
Fig. 1.1 Cysteine desulfurase and [Fe-S] cluster biogenesis.....	3
1.2 The penultimate steps of bacteriochlorophyll synthesis.....	4
Fig. 1.2 Structure of chlorophyll synthesis intermediates.....	6
1.2.1 Electron Donor Component.....	6
1.2.2 Electron Acceptor Component.....	9
1.3 Research Directions.....	10
CHAPTER 2. DEVELOPMENT AND CHARACTERIZATION OF A NEW CELL LINE FOR INCREASED EXPRESSION OF [FE-S] CLUSTER-CONTAINING ENZYMES.....	14
2.1 INTRODUCTION.....	14
Fig. 2.1 Diagram representation of <i>isc</i> and <i>suf</i> operons.....	15
2.2 MATERIALS AND METHODS.....	16
2.2.1 Reagents and Buffers.....	16
2.2.2 Strain construction.....	17
2.2.3 Western blot analysis.....	18
2.2.4 Generation of protein synthesis plasmids.....	18
2.2.5 Generation of Pchl _{id}	19
2.2.6 Protein synthesis and purification.....	20
2.2.7 Comparison of protein induction and purification using SDS-PAGE analysis.....	21
2.2.8 Assay for substrate reduction by DPOR.....	21
2.2.9 Protein and Iron-content determination.....	22
2.2.10 Growth curve generation.....	22
2.3 RESULTS.....	23
2.3.1 Confirming the inframe partial deletion of <i>sufA</i> and <i>sufB</i> in <i>E. coli</i> BL21(DE3) and in commercial derivatives.....	23
Fig. 2.2 An inframe deletion between <i>sufA</i> and <i>sufB</i> renders the <i>suf</i> operon inactive in <i>E. coli</i> BL21(DE3).....	24
2.3.3 Designing a functional Suf-containing strain for [Fe-S] protein overexpression.....	25
2.3.4 Protein yields and [Fe-S] cluster occupancy of BchL-overproducing cultures are improved with a restored and upregulated Suf pathway.....	26

Fig. 2.3 Removing transcriptional repression of the <i>suf</i> operon results in enhanced production of the [4Fe-4S] cluster carrying BchL protein in <i>E. coli</i> BL21(DE3) cell lines. .	27
Fig. 2.4 <i>E. coli</i> BL21(DE3) Suf ⁺⁺ cells increase yield, [Fe-S] cluster formation/load ratio and maintain enzyme activity.	30
2.4 DISCUSSION.	32
CHAPTER 3. PROBING THE FUNCTIONAL ROLE OF ATP IN BChL.....	34
3.1 INTRODUCTION.	34
Fig. 3.1 Structure and substrate reduction mechanism of DPOR.	35
3.2 MATERIALS AND METHODS.....	37
3.2.1 Reagents and Buffers.	37
3.2.2 Generation of protein overexpression constructs.....	38
3.2.3 Protein purification.	38
3.2.4 Generation of Pchlide.	39
3.2.5 Pchlide Reduction Assays.....	39
3.2.6 BchL crystallization.	40
3.2.7 BchL data collection, processing and refinement.	40
3.2.8 ATP binding assay.	41
3.2.9 EPR Spectroscopy.....	42
3.2.10 Samples for EPR Spectroscopy.....	42
3.3 RESULTS.	43
3.3.1 Crystal structure of nucleotide-free BchL suggests regulation through a redox switch and a flexible N-terminal region.....	43
Table. 3.1 Crystallographic data processing and refinement statistics.	45
Fig. 3.2 Crystal structure of nucleotide-free BchL.	46
Fig. 3.3 Crystal structure of nucleotide-free BchL reveals a flexible N-terminal region capping the [4Fe-4S] cluster.	47
Fig. 3.4 Conservation of N- and C-terminal regulatory elements BchL and homologs.....	48
3.3.2 Amino acid substitutions in the flexible N-terminal region of BchL increases the rate of substrate reduction.	48
Fig. 3.5 The flexible N-terminal region is auto-inhibitory to BchL function.	50
3.3.3 ATP-binding causes changes in the local environment of the BchL [4Fe-4S] cluster affecting their EPR spectral line-shape and intensities.....	50
Fig. 3.6 EPR characteristics of BchL, BchNB and BchL tail mutant constructs under various nucleotide conditions.	52
3.3.4 A DFD amino-acid patch promotes inter-subunit cross-stabilization upon ATP binding.....	53

Fig. 3.7 Interactions between ATP and a DFD patch promotes inter-subunit cross stabilization and conformational changes in BchL.	54
Fig. 3.8 EPR characteristics of BchL, and BchL DFD mutants.....	56
3.3.5 Binding of ATP to both subunits in the BchL dimer are required to generate a concerted motion to promote inter-subunit cross stabilization and drive substrate reduction.....	57
Fig. 3.9 Crystal structures of substrate-bound BchL and the Fe-protein from Nitrogenase. .	57
Fig. 3.10 Both ATP binding sites are required for DPOR activity.	59
Fig. 3.11 Linked BchL dimer construction.	60
3.4 DISCUSSION.....	61
Fig. 3.12 Model for ATP-binding induced release of auto-inhibition by the flexible N-terminus of BchL.	64
Fig. 3.13 Perturbations in the Switch-II region change the local environment around the [4Fe-4S] cluster.....	66
CHAPTER 4. ESTABLISHMENT OF SEQUENTIAL ELECTRON TRANSFER IN BchNB.	67
4.1 INTRODUCTION.	67
Fig. 4.1 DPOR components, reaction stoichiometry, and electron transfer pathways.....	68
4.2 MATERIALS AND METHODS.....	70
4.2.1 Generation of protein expression constructs.	70
4.2.2 Generation of Pchlide.	70
4.2.3 Protein synthesis and purification.....	70
4.2.4 Western blotting.....	71
4.2.6 Assay for substrate reduction by DPOR.	72
4.2.7 EPR Spectroscopy.....	72
4.2.8 Steady State Pchlide Binding Fluorescence titrations.....	73
4.3 RESULTS.	74
4.3.1 A half-reactive DPOR complex is defective for substrate reduction.	74
Fig. 4.2 Asymmetric BchNB mutants are incapable of complete Pchlide reduction.	75
4.3.2 The [Fe-S] cluster of BchNB matches a simulated $s=7/2$ spin state which can be pre-reduced, and re-primed for sequential reactions – a ‘deficit spending’ model.	77
Fig. 4.3 The [4Fe-4S] Cluster of BchNB	78
Fig. 4.4 Electrons are re-loaded onto BchNB after catalysis	80
4.3.3 Asp274 to Ala substitution reveals unresolved electron transfer intermediates in BchNB and a sequential substrate reduction mechanism within the two halves.	81
Fig. 4.5 BchNB ^{D274A} is synthesized with electrons pre-loaded, reveals stalled intermediate.	81
Fig. 4.6 Comparison of BchNB and Pchlide-bound BchNB crystal structures	83

4.3.4 Direct measurements of Pchl _{ide} binding to BchNB reveals cooperative substrate binding and a substrate sensing mechanism that establishes functional asymmetry.....	85
Fig. 4.7 Excitation/emission spectra of Pchl _{ide}	85
Fig. 4.8 Pchl _{ide} fluorescence as a measure of Pchl _{ide} binding	87
4.4 DISCUSSION	89
CHAPTER 5: CONCLUSIONS	93
5.1 In most (or all) modern commercially available <i>E. coli</i> BL21(DE3) <i>E. coli</i> expression cell lines, one of two [Fe-S] cluster genesis operons is inoperative.	96
5.2 SufFeScent cells increase BchL Yield, and [Fe-S] cluster occupancy, while BchNB was not affected.	98
5.3 BchL utilizes a novel “cap” structure to modulate its activity.....	99
5.4 BchL has a distinct patch of amino acids necessary for stabilizing the transition state.....	100
5.5 Both molecules of ATP are required for BchL activity.....	101
5.6 BchNB requires both catalytic sites to accomplish full reduction.	102
5.7 BchNB donates electrons one at a time.	103
5.8 Stepwise electron donation in BchNB may be established by cooperative Pchl _{ide} binding.	105
5.9 Overarching themes and contributions.	107
REFERENCES CITED.....	109
APPENDIX.....	117
Appendix 1 DPOR growth protocol	117
Appendix 2 DPOR lysis and preparation protocol.....	118
Appendix 3 Bradford Assay.....	122

LIST OF FIGURES

Fig. 1.1 Cysteine desulfurase and [Fe-S] cluster biogenesis.....	3
Fig. 1.2 Structure of chlorophyll synthesis intermediates.....	6
Fig. 2.1 Diagram representation of <i>isc</i> and <i>suf</i> operons.....	15
Fig. 2.2 An inframe deletion between <i>sufA</i> and <i>sufB</i> renders the <i>suf</i> operon inactive in <i>E. coli</i> BL21(DE3).	24
Fig. 2.3 Removing transcriptional repression of the <i>suf</i> operon results in enhanced production of the [4Fe-4S] cluster carrying BchL protein in <i>E. coli</i> BL21(DE3) cell lines.	27
Fig. 2.4 <i>E. coli</i> BL21(DE3) Suf ⁺⁺ cells increase yield, [Fe-S] cluster formation/load ratio and maintain enzyme activity.	30
Fig. 3.1 Structure and substrate reduction mechanism of DPOR.	35
Table. 3.1 Crystallographic data processing and refinement statistics.	45
Fig. 3.2 Crystal structure of nucleotide-free BchL.	46
Fig. 3.3 Crystal structure of nucleotide-free BchL reveals a flexible N-terminal region capping the [4Fe-4S] cluster.....	47
Fig. 3.4 Conservation of N- and C-terminal regulatory elements BchL and homologs.	48
Fig. 3.5 The flexible N-terminal region is auto-inhibitory to BchL function.	50
Fig. 3.6 EPR characteristics of BchL, BchNB and BchL tail mutant constructs under various nucleotide conditions.	52
Fig. 3.7 Interactions between ATP and a DFD patch promotes inter-subunit cross stabilization and conformational changes in BchL.....	54
Fig. 3.8 EPR characteristics of BchL, and BchL DFD mutants.....	56
Fig. 3.9 Crystal structures of substrate-bound BchL and the Fe-protein from Nitrogenase.	57
Fig. 3.10 Both ATP binding sites are required for DPOR activity.	59
Fig. 3.11 Linked BchL dimer construction.	60
Fig. 3.12 Model for ATP-binding induced release of auto-inhibition by the flexible N-terminus of BchL.....	64

Fig. 3.13 Perturbations in the Switch-II region change the local environment around the [4Fe-4S] cluster.....	66
Fig. 4.1 DPOR components, reaction stoichiometry, and electron transfer pathways.....	68
Fig. 4.2 Asymmetric BchNB mutants are incapable of complete Pchl _{ide} reduction.....	75
Fig. 4.3 The [4Fe-4S] Cluster of BchNB.....	78
Fig. 4.4 Electrons are re-loaded onto BchNB after catalysis.....	80
Fig. 4.5 BchNB ^{D274A} is synthesized with electrons pre-loaded, reveals stalled intermediate.....	81
Fig. 4.6 Comparison of BchNB and Pchl _{ide} -bound BchNB crystal structures.....	83
Fig. 4.7 Excitation/emission spectra of Pchl _{ide}	85
Fig. 4.8 Pchl _{ide} fluorescence as a measure of Pchl _{ide} binding.....	87

LIST OF ABBREVIATIONS

[Fe-S] Iron-sulfur cluster

DNA – DeoxyriboNucleic Acid

EPR – Electron Paramagnetic Resonance

PLP – Pyrodoxal phosphate

ATP – Adenosine TriPhosphate

NADPH - Nicotinamide Adenine Dinucleotide Phosphate

Pchl_{id} – Protochlorophyllide

Chl_{id} – Chlorophyllide

DPOR – Dark-operative Protochlorophyllide Oxido-Reductase

LPOR – Light-operative Protochlorophyllide Oxido-Reductase

POR - Protochlorophyllide Oxido-Reductase

COR – Chlorophyllide Oxido-Reductase

ET – Electron Transfer

TEV - Tobacco Etch Virus

ROS - Reactive Oxygen Species

NTA – Nitriloacetic Acid

BSA – Bovine Serum Albumin

HRP – Horse-Radish Peroxidase

CHAPTER 1. INTRODUCTION.

1.1 [Fe-S] Cluster biogenesis and function.

Iron-sulfur [Fe-S] clusters are believed to be among the first prosthetic groups in the earliest of biological chemistries on earth. They are capable of controlled electron transfer, (Helmut Beinert, Holm, & Münck, 1997) a process integral to multiple cellular/biological processes including DNA metabolism, nitrogen fixation, respiration, and gene regulation. (H. Beinert, 2000; Fontecave, 2006; Kiley & Beinert, 2003) [Fe-S] cluster-containing proteins and enzymes are critical to all known forms of life, notably in auto- and heterotrophic basic metabolic processes such as respiration and photosynthesis. All [Fe-S] clusters must be assembled and matured in cells in tightly controlled pathways, because the constituent components (reactive sulfur (S^{2-}) species and Fe^{III}) are poisonous to cells. Bacteria use multiple operons to generate various [Fe-S] clusters. The first, the *nif* operon was first characterized in the 1980s. (Jacobson et al., 1989) This operon is responsible for generation of the FeMoco factor of nitrogenase, and has no redundant operon. The *isc* and *suf* operons are semi-redundant bacterial operons responsible for generation and delivery of [2Fe-2S], [4Fe-3S], [3Fe-4S], and [4Fe-4S] clusters. (Lill, Broderick, & Dean, 2015)

The simplest, lowest order iron-sulfur cluster is [2Fe-2S]. It can carry an overall charge of +2 or +1. Its oxidized state bears two Fe^{III} atoms, and its reduced state harbors an extra delocalized electron, (Fe^{III}, Fe^{II}) which is shared between the two iron ions in the cluster. Sulfurs in these complexes exist as S^{2-} , with cysteines often acting as the remaining ligands necessary for each iron to have a tetradentate coordination. This produces an overall tetrahedral orientation of the cluster, which can be further modified or combined with additional clusters through reductive coupling to form [3Fe-4S], [4Fe-4S], and higher order clusters. While cysteine is the most

common ligand in protein molecules, [Fe-S] clusters can adopt a variety of differing ligands including histidine (Reiske clusters), aspartic acid, arginine, serine, carbon monoxide, CN^- , H_2O etc. The particular [Fe-S] cluster order and ligand(s) adopted by a protein determine the role of the cluster by modulating its reduction potential, the propensity to transfer electrons. All orders of clusters can have a range of reduction potentials, from ~ 300 to $\sim -600\text{mV}$, but lower ordered clusters typically lie in the less negative end of the range, while higher order clusters run the spectrum. (Stephens, Jollie, & Warshel, 1996) The specific redox potential of a given cluster is dictated by its order, its ligands, electrostatic contributions of nearby amino acids, and exposure to solvent(s). (Stephens et al., 1996) A variety of [Fe-S] clusters are necessary for all forms of life and must be generated and regulated in all cells.

Bacterial [Fe-S] clusters are generated by the proteins encoded by the semi-redundant *isc* and *suf* operons. (Blanc, Gerez, & Ollagnier de Choudens, 2015). (Py & Barras, 2010) The *suf* operon is upregulated during stress, while the *isc* operon is constitutively expressed and is responsible for the bulk of bacterial [Fe-S] cluster biogenesis. The core enzyme of the *isc* operon is IscS, a homodimer containing one pyridoxal phosphate (PLP) cofactor per monomer. (Fig. 1.1a.) IscS abstracts sulfur from free L-cysteine, forming L-alanine as a product. This sulfur is covalently attached to a conserved cysteine on a flexible loop that does not appear in crystal structures. This creates a highly reactive persulfide with multiple potential electronic states (Fig. 1.1b). The terminal persulfide sulfur is donated to an IscU protein on each end of the IscS dimer, forming an overall hetero-tetrameric complex (Fig. 1.1a,d). IscU acts as a scaffold for the maturing [Fe-S] cluster, forming mature [2Fe-2S] clusters while bound to IscS, requiring two rounds of sulfur donation via a cysteine-sulfur intermediate (Fig. 1.1b,d) in the presence of Fe^{II} . [2Fe-2S] bound IscU can then self-dimerize once dissociated from IscS and perform reductive coupling to produce mature [4Fe-4S] clusters. (Fig. 1.1d) (Chandramouli et al., 2007) [2Fe-

2S]/[4Fe-4S] clusters are then donated directly to target proteins, are delivered via the chaperones IscU or IscA (Fig. 1.1d).

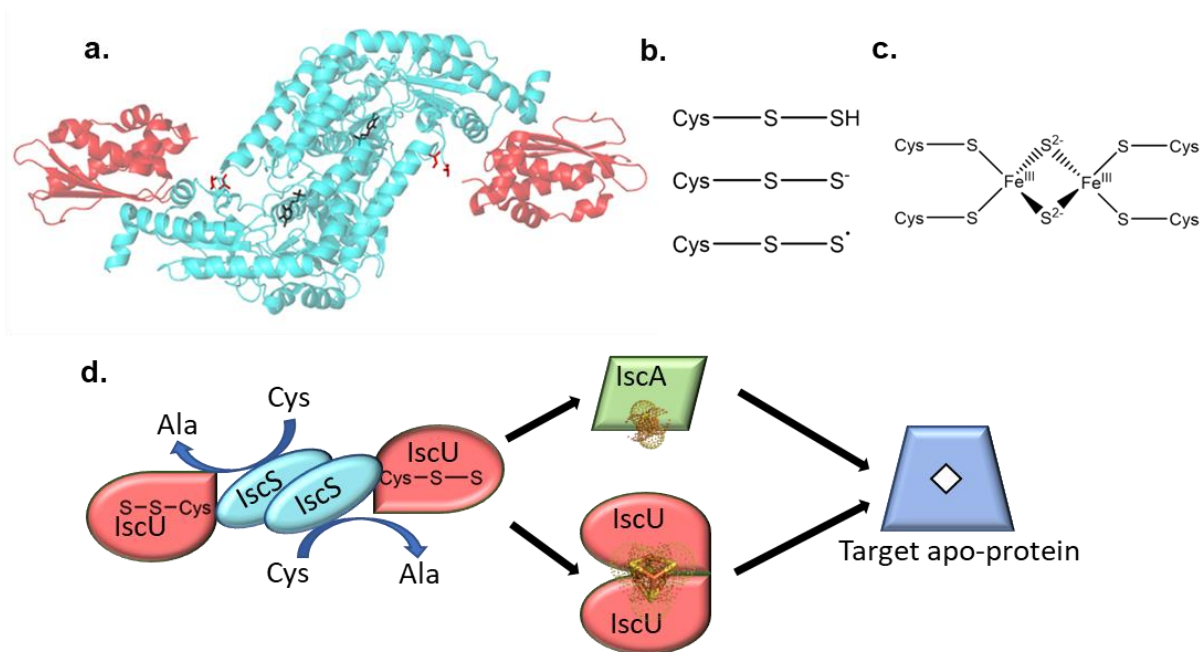


Fig. 1.1 Cysteine desulfurase and [Fe-S] cluster biogenesis.

a. IscU/IscS crystal structure. IscS dimer (Blue), and IscU (Red), PLP cofactor (Black sticks) and anchors of catalytic cysteine containing loop (Red sticks). **b.** Reactive persulfide species. **c.** Schematic of typical [2Fe-2S] cluster. **d.** Simple schematic for *isc* operon [Fe-S] cluster biogenesis. IscS shown as blue semi-circle, IscU as red teardrop(s), IscA as green parallelogram, target apo-protein as blue trapezoid, [2Fe-2S] and [4Fe-4S] clusters shown as sticks and dots.

The *suf* operon contains cognate enzymes for sulfur abstraction and donation to scaffold clusters during synthesis. This operon is upregulated during low-iron stress and oxidative stress conditions. (Ayala-Castro, Saini, & Outten, 2008; Takahashi & Tokumoto, 2002) Bacteria which are deficient in *isc* or *suf* operon are viable, demonstrating their redundant functions. However, bacteria deficient in both pathways are unsurprisingly not viable. (Tokumoto, Kitamura,

Fukuyama, & Takahashi, 2004) Additionally, the individual components of the two operons are not interchangeable. This differing functionality presents the possibility of target apoproteins proteins having a preference or even necessity for clusters generated from Isc or Suf machinery, or that chaperones/cochaperones are unable to accept or interact with scaffold proteins from one pathway.

The biochemical characterization of enzymes from any organism can be made more efficient via overexpression in commercial *E. coli* competent strains (e.g. *E. coli* BL21(DE3) and derivatives). Interestingly, all commercially available strains harbor an inframe deletion of *sufA* and *sufB*, rendering the *suf* operon inactive. (Daegelen, Studier, Lenski, Cure, & Kim, 2009; Jeong et al., 2009; Studier, Daegelen, Lenski, Maslov, & Kim, 2009) This presents an opportunity to demonstrate that native (or increased) expression of the *suf* operon may produce changes in yields or [Fe-S] cluster occupancy of heterologously expressed proteins containing [Fe-S] clusters.

1.2 The penultimate steps of bacteriochlorophyll synthesis.

The molecular basis of life on earth relies on the transfer of electrons from one substrate to another, the donor being oxidized, and recipient being reduced. The earliest formation of biomolecules on earth took advantage of the reducing power of the chemical makeup of the atmosphere at the time (H_2 , NH_3 , CH_4 , H_2S , and CO_2 .) This source of electrons was combined with light energy from the sun (photochemistry) to create some of the first lower entropy biomolecules that would eventually become amino acids, nucleic acids, lipids, and porphyrin rings. After the rise of cells, Eubacteria began using modified porphyrin rings to capture sunlight energy which allowed them to reduce the abundant CO_2 to sugars and create a proton-motive force for production of Adenosine Triphosphate (ATP). Later, cyanobacteria would acquire the

oxygen evolving complex, allowing them to use water as an electron donor for carbon dioxide reduction in lieu of the reducing gases in the early atmosphere. (Olson & Blankenship, 2004) These organisms produced the first oxygen on planet earth, and one such extant cyanobacteria *Prochlorococcus marinus* (and close relatives) produce much of the oxygen in the atmosphere today. (Munn, 2011)

All heterotrophs including humans rely on the energy capture from the environment that autotrophs produce. The most prevalent method for autotrophy revolves around the light-energy harvesting molecule chlorophyll. Chlorophyll allows autotrophs to convert the energy from photon capture to chemical potential energy, which is ultimately stored in high energy molecules of ATP and NAD(P)H. These high energy molecules are used to drive the anabolic reactions necessary to generate the complex molecules that form the basic structures of cells (DNA, proteins, lipids, sugars, etc), and are key energy storage molecules in basic hetero- and autotrophic metabolism (respiration, photosynthesis, chemosynthesis, etc). Before bacteriochlorophyll can be used to capture light for energy, it must be synthesized in the cell.

One key intermediate in the bacteriochlorophyll synthesis pathway is protochlorophyllide (Pchl_{id}e), which is converted to chlorophyllide (Chl_{id}e) through the stereospecific reduction of the C17-C18 carbon-carbon double bond of Pchl_{id}e by the enzyme Dark-operative Protochlorophyllide Oxido-Reductase (DPOR) in eubacteria and gymnosperms, or by a light dependent enzyme (LPOR) in “higher” plants. The C7-C8 carbon-carbon double bond of chlorophyllide is later reduced by Chlorophyllide Oxido-Reductase (COR), ultimately forming bacteriochlorophyllide (Bchl_{id}e) (Fig. 1.2). These reductions to the tetrapyrrole ring of maturing bacteriochlorophyll fine tune the absorbance spectra producing additional maxima, and affect the chemical properties to better perform their light harvesting role. (Nascimento, Zou, & Cheng, 2016) All carbon-carbon double bond reductions require the input of 2 electrons and 2 protons to be fully reduced. DPOR bears no homology with LPOR, a monomeric protein that uses a totally

different chemistry for the same reaction, but does bear structural and sequence homology with COR, as well as nitrogenase, which is responsible for the reduction of atmospheric nitrogen to ammonia. DPOR, COR, and nitrogenase adopt an overall octameric architecture, separable into a homodimeric electron donor component and a heterotetrameric electron acceptor component. These three enzymes have received the most attention in recent years, but several other enzymes adopt the same architecture and perform similar chemistries. This work focuses on DPOR, but its inception was reliant on work performed on Nitrogenase and COR.

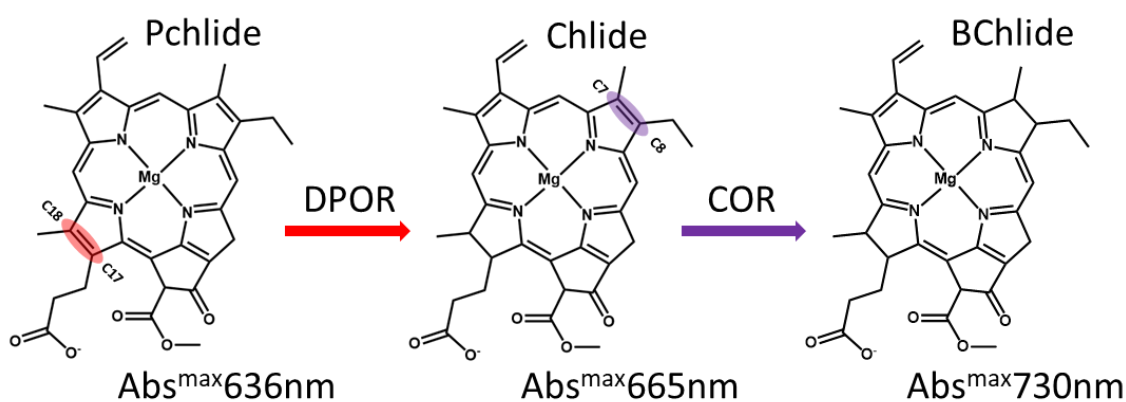


Fig. 1.2 Structure of chlorophyll synthesis intermediates.

The sequential operation of DPOR and COR in the conversion of Pchl a₀ to MV-Bchl a₀. DPOR reduces the C17-C18 double bond (red) of Pchl a₀ to produce Chl a₀, and then COR reduces the C7-C8 double bond (purple) of Chl a₀ to produce MV-Bchl a₀.

1.2.1 Electron Donor Component.

The electron donor component of this architecture (BchL, BchX, and NifH or “Fe-protein” for DPOR, COR and nitrogenase respectively) is comprised of 2 identical subunits. Each

monomer contains motifs necessary for the binding (WalkerA) and hydrolysis (WalkerB) of ATP. (Burgess & Lowe, 1996)(Nomata, Mizoguchi, Tamiaki, & Fujita, 2006)(Nomata, Mizoguchi, et al., 2006) Each subunit of the dimer provides 2 conserved cysteine residues that ligate a [4Fe-4S] cluster that bridges the dimer. This [4Fe-4S] cluster acts as the source of electrons necessary to reduce the complexes' respective substrate(s). These electrons are likely to be ultimately derived from NADPH. The first step utilizes a NADPH dependent reductase which couples the oxidation of NADPH to the reduction of the [Fe-S] cluster of a ferredoxin. A ferredoxin then serves as the biological reductant for BchL (Nomata, Swem, Bauer, & Fujita, 2005), and likely for BchX, though not yet empirically determined. NifH incorporates a Flavodoxin for this purpose the purpose of its re-reduction. (Pence et al., 2017)(Nomata et al., 2005)

For DPOR and nitrogenase, the stoichiometry of electron transfer to ATP molecules hydrolyzed has been determine to be 1:2. (Nomata, Terauchi, & Fujita, 2016)(Watt, Bulen, Burns, & Hadfield, 1975)(MCNARY & BURRIS, 1962) COR is presumed to maintain that stoichiometry but has not yet been determined. It has been shown in nitrogenase that ATP bound NifH forms a complex with its electron acceptor (NifDK or "MoFe-protein") and dissociates after ATP hydrolysis and inorganic phosphate (Pi) release. (Burgess & Lowe, 1996) Hydrolysis of ATP was originally thought to drive electron transfer, but it has been shown that ATP hydrolysis is actually a slower process than electron transfer, with Pi release being the rate limiting step for NifH. (Yang et al., 2016)(Duval et al., 2013) This suggests that electron transfer is a process that is not coupled to the free energy release of ATP hydrolysis, and that ATP hydrolysis has a role in complex formation and dissociation and/or in the modulation of the local environment or redox potential of the cluster of NifH to be properly suited to donate its electron. (Kurnikov, Charnley, & Beratan, 2001) BchL of DPOR presumably uses a similar mechanism due to its ~35% homology but has not been explored in depth. There is no molecular-level understanding of how the ATPase activity of BchL BchX and/or NifH coordinates electron transfer in these enzymes.

Presumably there is a structure-function relationship between the conformational states of ATP-free and ATP bound/hydrolysis-transition-state/ADP-Pi-bound/ADP-bound states. However, the details of how information is transmitted from the ATP binding sites on one end (the “top”) of BchL, to the [Fe-S] cluster on the other end (the “bottom”) have not been determined. BchL, despite a strong homology to NifH, contains a conserved stretch of amino acids at its N-terminus that are unresolved in existing crystal structures, and are not found in the sequence of any NifH proteins. The two are also not interchangeable, despite performing very similar functions. Finally, It has been shown that NifH can bind to two non-identical nucleotides, and still form a complex with NifDK. (Tezcan, Kaiser, Howard, & Rees, 2015) This finding suggests that despite being a symmetrical molecule, the activity of each half of the homodimer can behave differently from the other. How asymmetrical activity arises in symmetrical proteins and whether both halves must be functional for overall reactivity remain unresolved for DPOR, and many symmetric enzymes generally.

Chapter 3 of this document describes the discovery of several unknown features of BchL. Structural evidence revealed the existence of an auto-inhibitory stretch of amino acids on the N-terminus of BchL which were previously never seen in crystal structures. The existence of the dynamic interaction of an unstructured tail appears unique to BchL (among DPOR, COR, and nitrogenase). The proposed dynamic capping and uncapping of an [Fe-S] cluster appears to be a previously undescribed phenomenon. Further structural evidence suggested the existence of another feature unique to BchL, a patch of residues (DFD) that appear to communicate information between monomers of BchL by interacting in trans with the 5-carbon sugar of the nucleotide bound to the opposing monomer. I propose that this interaction is necessary to communicate the conformational state of the protein to the [Fe-S] cluster, promoting the transfer of electrons. Finally, to determine if BchL does require both the ATP molecules it can bind, a covalently attached asymmetric dimer was generated, where only half of the dimer could bind to

ATP. This variant was unable to reduce Pchlide, suggesting that both molecules of ATP are indeed necessary for reduction. The data and interpretations represented here allow the generation of a more complete reaction mechanism for the transfer of electrons from BchL to BchNB.

1.2.2 Electron Acceptor Component.

BchNB, BchYZ, and NifKD exist as stable heterotetramers and act as the catalytic electron acceptors of DPOR, COR, and nitrogenase, respectively. All use a [Fe-S] cluster to accept electrons from their respective electron donor. BchNB and BchYZ use a [4Fe-4S] cluster to receive electrons, whereas nitrogenase uses a higher order cluster ([8Fe-7S]) called a P-cluster to receive electrons. (Burgess & Lowe, 1996)(Nomata et al., 2005)(Nomata, Mizoguchi, et al., 2006) Electrons are ultimately funneled to the substrate and coupled with proton donations to accomplish reduction. These complexes all contain two clusters to accept electrons, and two substrate binding sites.

In nitrogenase, a resting P-cluster cannot receive electrons. This inspired the idea that a resting P-cluster donates one electron to its substrate (nitrogen bound to the FeMo-cofactor) and is then re-reduced by NifH. This first donation is conformationally gated, and this phenomenon was coined “deficit spending”. (Danyal, Mayweather, Dean, Seefeldt, & Hoffman, 2010)(Seefeldt, Hoffman, & Dean, 2012). The molecular details of how docking of NifH activates the first electron transfer are unknown. A reasonable explanation involves conformational gating that is induced by docking of NifH, but the specifics of how information is relayed across the long distance from the binding interface of NifH and the FeMo-cofactor in NifKD remain unknown. It is unknown whether all enzymes with this architecture use the deficit spending mechanism. DPOR and COR use a [4Fe-4S] cluster in contrast to that of the P-cluster of nitrogenase to initially accept electrons, and do not have the FeMo-cofactor of nitrogenase. The

differences in substrate(s) and chemistries implies that DPOR and COR may have evolved a different strategy for controlled electron transfer.

Models that describe the deficit spending mechanism focus on the communication of the electron accepting cluster, and the substrate of the enzyme. (Seefeldt et al., 2018) These models consider only one half of the heterotetramer. It is possible that the two active sites of this architecture are independent, one half of the tetramer functioning without input from the other. It remains unknown if the chemistry occurring in one active site affects the other, and if so, how information is transmitted between them. Additionally, it is unknown the degree of interdependence between the two halves if it does exist. Chapter 4 of this document describes the establishment of sequential electron transfer in DPOR, proposes an electron transfer scheme similar to the deficit spending model, and describes a novel binding assay that indicates that substrate binding establishes sequential electron transfer.

1.3 Research Directions.

DPOR was chosen as a model system for the study of this architecture for several reasons. The main advantages of DPOR over nitrogenase are describe. First, unlike nitrogenase which must be expressed in its native organism, DPOR is expressible in non-native systems such as *E. coli*, facilitating more traditional expression schemes. Second, the substrate of DPOR has strong absorbance and fluorescence properties, unlike the negligible spectroscopic properties of gaseous nitrogen, making the substrate binding event impossible to observe in nitrogenase. The spectral properties of Pchlide and Chlide also allow simple spectroscopic monitoring of the reaction as it proceed. Third, the chemistry of DPOR is much simpler than that of nitrogenase, 2 electrons and 2 protons in DPOR compared to 8 electrons and protons in nitrogenase. Overall,

DPOR provides a robust model system to study phenomena in multi-subunit oxido-reductases like DPOR, COR, and nitrogenase.

The biochemical characterization of DPOR detailed in this document relied heavily on large quantities of DPOR components over expressed in *E. coli*. The activity of DPOR is completely reliant on the activity and integrity of its [Fe-S] clusters. Commercially available cell lines designed for heterologous expression of proteins all have a flaw in their genome. *E. coli* and other bacteria have two native operons (*isc* and *suf*) for the production and incorporation of [Fe-S] clusters, but *E. coli* BL21(DE3) and its many variations all have a non-functional *suf* operon due to deletion that occurred early on in the usage of this abundant cell line. Chapter 2 of this document details the generation of a derivative commercial *E. coli* BL21(DE3) *E. coli* cell line wherein the *suf* operon has been restored and/or derepressed. The effects of this restoration on the yield and integrity of heterologously expressed DPOR are detailed.

DPOR is an ancient enzyme, and the overall architecture that it adopts to accomplish bond reduction is adopted by multiple enzymes that perform similar reduction reactions. Enzymes exist to speed up reactions, and DPOR is a very slow enzyme, operating at $\sim 0.2 \cdot \text{M}^{-1} \cdot \text{s}^{-1}$. The reaction catalyzed by DPOR has a high energy demand, with a cost of two ATP per electron transferred, at the secondary expense of one molecule of NADPH (the original source of the electrons). Finally, DPOR is complex, made up of 8 subunits in the captured ADP-AlF₃ ATP hydrolysis transition state shown in the crystal structure of the full DPOR complex. (Moser et al., 2013) This structural and energetic complexity/demand are not necessary for all enzymes that reduce Pchl_a to Chl_a. The non-homologous enzyme Light-operative Protochlorophyllide Oxido-Reductase (LPOR) accomplishes the reduction utilizing a hydride transfer chemistry, at the cost of only one molecule of NADPH and sunlight. It exists as a monomer, much smaller than the quaternary complex of DPOR, and performs at greater rates in-vitro. The existence of a simpler enzyme suggests intrinsic value in the architecture and chemistry of DPOR. This work

attempts to deconvolute and illustrate the elegance in DPOR and similar enzymes despite their non-intuitive complexity.

The current unknowns about the electron donor component of DPOR (BchL) are largely similar to those of NifH described earlier. Like NifH, BchL requires ATP to function, but the specific role of ATP remains unknown. Presumably, ATP hydrolysis does not drive electron transfer, as electron transfer precedes ATP hydrolysis in nitrogenase (NifK). (Duval et al., 2013) If ATP hydrolysis is not driving electron transfer, what is its role in the electron transfer event? Does BchL even need both ATP molecules to function? If so, how is the conformational landscape of BchL across its reaction cycle communicated across the dimer, and to the reduced [4Fe-4S] cluster?

BchNB, in a thematically similar pattern binds to two substrates (2 ATP in BchL) in a structurally symmetrical way across both halves of the heterotetramer. Conformational gating exists for electron transfer between the P-cluster and FeMo-cofactor of nitrogenase, and electron transfer does show negative cooperativity in nitrogenase, (Danyal et al., 2016) but no system has attempted to tackle how information is communicated from one active site to the other in the BchNB/NifKD tetramer. It is unknown if DPOR uses a deficit spending mechanism like nitrogenase, whether electrons are donated sequentially, how electron and proton donation events are coupled, and whether substrate binding is cooperative. Chapter 4 of this document describes using the intrinsic fluorescence of the substrate Pchlide as a reporter for substrate binding. This allowed the determination of both the affinity of BchNB for PChlide, but also the cooperative nature of its binding events suggest that the sequence of electron and proton donation to Pchlide is established upon substrate binding. Using a multiple affinity tag, dual expression, and dual column purification method, an asymmetric mutant of BchNB was generated, wherein one half was unable to donate a proton from the conserved proton source (Asp 274 of BchB). Like the necessity of both halves in BchL, BchNB does indeed require both halves to function. The

transfer of electrons was monitored by Electron Paramagnetic Resonance (EPR) in both the wild-type and mutant context of BchNB. EPR spectra were used to determine the unique spin state of the cluster found in BchNB ($s=7/2$) and revealed a stalled intermediate in which only one electron had been donated to half of the tetramer. This is the first evidence to support the notion that BchNB and DPOR as a whole does not function as independent halves. Individual stepwise events are necessary for the overall reaction catalyzed by DPOR. This knowledge enables further refinement of the poorly defined reaction mechanism for DPOR and related enzymes.

CHAPTER 2. DEVELOPMENT AND CHARACTERIZATION OF A NEW CELL LINE FOR INCREASED EXPRESSION OF [FE-S] CLUSTER-CONTAINING ENZYMES.

2.1 INTRODUCTION.

Iron-sulfur [Fe-S] proteins are integral to the activity of numerous biological processes including respiration, nitrogen fixation, photosynthesis, DNA replication and repair, RNA modification, and gene regulation. (H. Beinert, 2000; Fontecave, 2006; Kiley & Beinert, 2003) In *Escherichia coli* K-12, there are two multiprotein systems, Isc and Suf, dedicated to the biosynthesis of various [Fe-S] clusters and their incorporation into 140 known [Fe-S] proteins. (Blanc et al., 2015; Boyd, Thomas, Dai, Boyd, & Outten, 2014; Pérard & Ollagnier de Choudens, 2018; Py & Barras, 2010; Wayne Outten, 2015) The Isc system is encoded by the *isc* operon, composed of the *iscRSUA-hscBA-fdx-iscX* genes (Fig. 2.1). The Suf system is encoded by its cognate *sufABCDSE (suf)* operon (Fig. 2.1). *E. coli* carrying defects in both systems are not viable due to a non-functional isoprenoid biosynthetic pathway, which relies on two [Fe-S] enzymes, (Pérard & Ollagnier de Choudens, 2018; Rocha & Dancis, 2016) highlighting the significance of these [Fe-S] cluster biogenesis systems for essential life processes. (Vinella, Brochier-Armanet, Loiseau, Talla, & Barras, 2009) However, the Isc and Suf systems display some functional redundancy, as cells lacking only one system remain viable. Nevertheless, individual enzyme components of the two systems are not interchangeable, reinforcing that the scaffolds for building [Fe-S] clusters are functionally different. (Takahashi & Tokumoto, 2002; Tanaka et al., 2016) Further, little is known about the preferences of these biogenesis pathways for client proteins. Under normal growth conditions, the Isc system is thought to play the major role in [Fe-S] cluster biogenesis, but under conditions of stress, such as oxidative stress or iron-limiting conditions, the Suf system is reported to assume a greater role. (Tokumoto et al., 2004) Interestingly, some bacteria, archaea, and plant plastids contain only the Suf machinery, serving as the sole [Fe-S] cluster biogenesis machinery. (Blanc et al., 2015; Boyd et al., 2014; Outten,

Djaman, & Storz, 2004; Py & Barras, 2010; Wayne Outten, 2015) The basic biochemical characterization of individual [Fe-S] cluster containing proteins will add to our fundamental understanding of metabolism as well as disease.

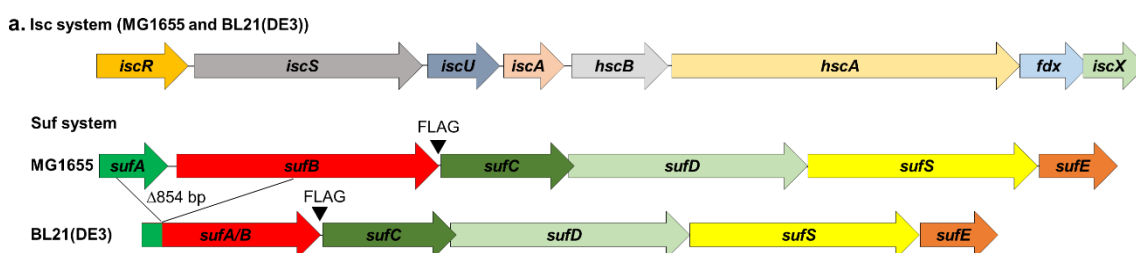


Fig. 2.1 Diagram representation of *isc* and *suf* operons.

a. Diagram of the *isc* and *suf* operons present in MG1655 and *E. coli* BL21(DE3); *E. coli* BL21(DE3) has an 854 bp deletion in the *suf* operon resulting in an inframe fusion of the *sufA* and *sufB* genes.

To accelerate biochemical studies of [Fe-S] proteins, genes encoding proteins of interest are often heterologously expressed in engineered *E. coli* strains designed for overproduction of proteins. A major challenge in the field is to obtain large enough quantities of proteins at high concentrations that are also maximally occupied with [Fe-S] clusters (Tsai & Tainer, 2018) to enable spectroscopic and structural studies. Increasing the expression of the housekeeping *isc* operon pathway imparts variable improvement in [Fe-S] cluster protein yields. (Gräwert et al., 2004; Kriek, Peters, Takahashi, & Roach, 2003; Nakamura, Saeki, & Takahashi, 1999; Tsai & Tainer, 2018) However, a similar approach has not been examined for the Suf pathway despite it being the sole pathway for [Fe-S] biogenesis in many organisms.

A commonly used strain for [Fe-S] protein overexpression is *E. coli* BL21(DE3) or one of its many derivatives. The ancestry of the parent strain for the modern day *E. coli* BL21(DE3)

can be traced back to *E. coli* B strains established by Delbrück and Luria in the 1920s. (Daegelen et al., 2009) The sequence of the *E. coli* BL21(DE3) genome, published in 2009, revealed many sequence changes compared to another *E. coli* B strain, REL606. (Daegelen et al., 2009; Jeong et al., 2009; Studier et al., 2009) Amongst these differences was an inframe deletion between *sufA* and *sufB* within the *suf* operon, encoding the Suf [Fe-S] biogenesis pathway. Here it is shown that *E. coli* BL21(DE3) is defective for Suf dependent [Fe-S] biogenesis and the deletion with sequences found in *E. coli* K12 was corrected. Commercially available *E. coli* BL21(DE3) derivatives were also tested to determine if they carry the same deletion of *sufAB*, which was suggested to arise from UV treatment early in the lineage of *E. coli* BL21. (Studier et al., 2009) By altering the promoter sequences of the corrected allele in *E. coli* BL21(DE3) a strain with increased levels of the Suf pathway was developed and tested whether it improved the yield of [Fe-S] proteins. This strain may be of general use in applications that require overproduction of [Fe-S] proteins for structural and spectroscopic studies where large quantities of protein are required.

2.2 MATERIALS AND METHODS.

2.2.1 Reagents and Buffers.

Chemicals were purchased from Sigma-Millipore Inc. (St. Louis, MO), Research Products International Inc. (Mount Prospect, IL) and Gold Biotechnology Inc. (St. Louis, MO). Oligonucleotides were purchased from Integrated DNA Technologies (Coralville, IA). Enzymes were purchased from New England Biolabs (Ipswich, MA). All reagents and buffers used for protein purification were thoroughly degassed using alternating cycles of vacuum and nitrogen pressure on a home built Schlenk line apparatus. Anaerobic conditions were maintained via

airtight syringes, excess reductant and a vinyl glove box (Coy Laboratories, MI) under an atmosphere of nitrogen (95%) and hydrogen (5%).

2.2.2 Strain construction.

A *E. coli* BL21(DE3) strain derivative (PK11465) was constructed to produce a functional *sufABCDSE* operon. This was accomplished using P1 vir transduction to move a cat-*PsufA* allele (Mettert & Kiley, 2014; Mettert, Outten, Wanta, & Kiley, 2008) from strain PK10028 to *E. coli* BL21(DE3) and selecting for growth on TYE agar plates containing 10 µg/ml chloramphenicol and 10 mM citrate. After streak purification, colony PCR and DNA sequencing were carried out to confirm the genotype. Using the same method, *E. coli* BL21(DE3) strain derivative PK11466 was constructed to produce a functional *sufABCDSE* operon, but one that also lacks transcriptional repression by Fur; the cat-*PsufA*(-26ATA-24 changed to -26TAT-24) allele, which contains a mutation within the Fur binding site, from PK10882 was moved to *E. coli* BL21(DE3) via P1 vir transduction.

Derivatives of MG1655 and *E. coli* BL21(DE3) were constructed to produce chromosomally derived, epitope-tagged variants of SufB [SufA/B in the case of *E. coli* BL21(DE3)] or SufS. First, a TAA stop codon was inserted directly after the 3XFLAG sequence on pIND4-3XFLAG(n) using Quikchange (Stratagene) to form pPK8629. Following PCR amplification of cat flanked by FLP recognition target (FRT) sites from pKD32 using primers containing BamHI and NdeI restriction sites, the PCR fragment was cloned into the same sites of pPK8629 to make pPK8630. To recombine 3XFLAG-TAA-FRT-cat-FRT directly before the native stop codons of the SufA/B fusion protein or SufS in *E. coli* BL21(DE3), this construct was PCR amplified with primers containing homology to either region of the chromosome,

electroporated into a derivative of *E. coli* BL21(DE3) that harbored pKD46, and selected for CmR (forming strains PK13232 and PK13233). Epitope-tagged variants of *sufB* and *sufS* were made in a similar manner in MG1655 (forming strains PK13230 and PK13231). All alleles were verified by DNA sequencing. Finally, P1 vir transduction was used to introduce *sufB*-3XFLAG-TAA-FRT-cat-FRT and *sufS*-3XFLAG-TAA-FRT-cat-FRT from the MG1655 derivatives PK13230 and PK13231 into *E. coli* BL21(DE3), forming strains PK13235 and PK13237, respectively.

2.2.3 Western blot analysis.

Cultures were grown aerobically to an optical density at 600 nm of 0.1 in M9 minimal medium containing 0.2% glucose, 0.2% casamino acids, 1 mM MgSO₄, 10 µg ml⁻¹ ferric ammonium citrate, 4 µg ml⁻¹ thiamine, and 0.1 mM CaCl₂. Aliquots (1 ml) of cells were pelleted and levels of SufB-FLAG, SufA/B-FLAG, or SufS-FLAG were measured by Western blot analysis as previously described (Mettert et al., 2008; Nesbit, Giel, Rose, & Kiley, 2009) except that purified anti-DYKDDDDK epitope tag antibody (Biolegend) was used.

2.2.4 Generation of protein synthesis plasmids.

Plasmids used to produce BchL, BchN, and BchB were generated from PCR amplified *Rhodobacter sphaeroides* genomic DNA. BchL and BchB open reading frames were engineered to carry an N-terminal poly-histidine (6x-His) tag and 3C protease recognition sites and were cloned into pRSF-Duet1 using BamH1/Not1 and Sac1/Sal1 restriction sites, respectively. BchN contained no modifications and was cloned into a pET-Duet1 vector using Nde1/Kpn1 restriction sites.

2.2.5 Generation of Pchl_{ide}.

Pchl_{ide} was isolated from supernatants of cultures of *Rhodobacter sphaeroides* ZY-5 strain harboring a deletion of BchL (a kind gift from Dr. Carl Bauer, Indiana University). (Yamamoto, Kato, Yamanashi, & Fujita, 2014) Ten ml of an overnight culture of ZY-5 grown with shaking (200 RPM) in RCV 2/3 medium with 50 µg/mL kanamycin, at 37°C was used to inoculate a 125 mL culture with RCV 2/3 medium containing 5 µg/mL kanamycin in a foil-wrapped 250 ml flask and grown for 24 hours at 34°C, 130 RPM. Cells were removed by centrifugation at 4,392 x g, and the green-colored supernatant was stored at 4°C. The cell pellet was then resuspended in 500 mL fresh RCV 2/3 medium with 5 µg/mL kanamycin and grown with shaking (130 RPM) for 24 hours at 34°C, in the dark and again the supernatant was separated from the cells by centrifugation. This process was repeated twice and the combined supernatant containing Pchl_{ide} was centrifuged at 4,392 x g, 4°C for 1 hour to remove any remaining cells, filtered through a white nylon 0.44 µm filter (Millipore, catalog #HNWP04700) and extracted in 500 ml aliquots with 1/3 volume di-ethyl ether in a 1L separatory funnel taking care to vent built up pressure from volatile ether after vigorous shaking. The organic phase containing the green colored Pchl_{ide} was removed, centrifuged at 4122 x g at 4°C for 5 minutes to further separate any lipid or aqueous contamination, and then decanted and evaporated to dryness under a stream of nitrogen. Water droplets formed on the inside and outside of the vessel were allowed to evaporate inside the fume hood. The resulting dark green flaky material was then resuspended in 250 µL DMSO/500 mL extract. The suspended Pchl_{ide} was aliquoted and stored in amber colored 1.5 mL conical tubes (Fisher Scientific; Catalog #05-408-134) at 4°C. Concentration of Pchl_{ide} was determined spectrophotometrically using 4 dilutions, three replicates each in 80 % acetone using the molar extinction coefficient 30,400 M⁻¹cm⁻¹.

2.2.6 Protein synthesis and purification.

Bacterial cells freshly transformed with the appropriate plasmid for recombinant protein production were used to inoculate 1 L Luria Broth medium supplemented with appropriate antibiotic (100 $\mu\text{g}/\text{mL}$ ampicillin and/or 50 $\mu\text{g}/\text{mL}$ kanamycin), 1 mM ferric citrate and 1 mM L-cysteine in 2.8 L baffled-flasks and were grown aerobically at 37°C shaking at 200 RPM. Protein synthesis was induced at a culture OD600 of 0.6 with 35 μM IPTG, and then cultures were shifted to 25°C, shaking at 150 RPM overnight. Cells were harvested after a 3-hour incubation with sodium dithionite (0.3 g/L growth) in 1 L airtight centrifuge tubes at 17°C with no shaking. All subsequent steps were performed in the glove box, or in airtight septum sealed bottles under positive nitrogen pressure unless otherwise noted. Cell pellets were resuspended in degassed STD buffer (100 mM HEPES pH 7.5, 150 mM NaCl, 1.7 mM sodium dithionite), transferred to a septa-sealed glass bottle and stored at -20 °C until lysis.

Cell lysis was performed using lysozyme (0.5 mg/ml) for 30 minutes at room temperature in septum sealed bottles. Cells were then sonicated inside a glovebox for 3 minutes on ice (Branson sonifier, 50 % duty cycle, 60 seconds on, 60 seconds off for 3 cycles). Cell lysates were clarified via centrifugation (37,157 x g, 60 minutes) and loaded onto a Nickel-nitrilotriacetic acid (Ni^{2+} -NTA) column, equilibrated with STD buffer. After washing away non-specific binding proteins with STD buffer containing 20 mM imidazole, bound proteins were eluted into a septum sealed bottle using 30 mL STD buffer containing 250 mM imidazole. For BchN-BchB, the eluted proteins were concentrated using an Amicon 15 mL 30 kDa molecular weight cut-off spin concentrator (Sigma-Millipore Inc., St. Louis, MO), by centrifugation for 8 minutes at 4122 x g at 4°C. For BchL, protein eluted from the Ni^{2+} -NTA affinity column was subsequently purified over a 10 mL Q-Sepharose column (GE Healthcare). The Q-column was first sequentially equilibrated with 150 mM HEPES pH 7.5 containing 1 M NaCl followed by 150 mM HEPES pH 7.5 (no

NaCl). BchL pooled from the affinity step was then loaded and the column was subsequently washed with STD buffer. Bound BchL was eluted using 100 mL STD buffer containing a 0.15 – 1 M NaCl gradient elution, and the fractions were collected inside the glovebox. Fractions containing BchL protein were concentrated using a spin concentrator as described above. Proteins were aliquoted into 1.2 mL cryo-tubes (Cat # 430487 Corning) and capped in the glove box. Sealed tubes were removed from the glove box, flash frozen using liquid nitrogen and stored under liquid nitrogen.

2.2.7 Comparison of protein induction and purification using SDS-PAGE analysis.

10 % SDS polyacrylamide gels were used to visualize protein samples. Uninduced and induced samples (1.0 mL and 0.5 mL, respectively) were centrifuged in a table-top centrifuge (13,222 x g, 60 sec, 4°C), and the supernatant was decanted. Sample cell pellets were resuspended in 100 µL water. Tenfold dilutions of resuspended cells were used to record the OD600 and this value was used to normalize all sample optical densities. Equivalent units of OD600 of undiluted samples were then diluted to 100µL and mixed with 100 µl of 2X SDS Laemmli sample buffer, boiled for 10 min and 10 µl were analyzed by SDS-PAGE. PageRuler Plus Prestained Ladder (Thermo Scientific) was used as a protein size ladder for reference.

2.2.8 Assay for substrate reduction by DPOR.

Reduction of Pchlide to Chlide was measured spectroscopically by mixing BchN-BchB protein (3 µM tetramer), BchL-protein (9 µM dimer), and 35 µM Pchlide, in the absence or presence of ATP (3 mM) in STD buffer + 10mM MgCl₂. Reactions (40 µl) were quenched with 160 µl of 100 % acetone (80% v/v final concentration). Precipitated proteins were removed by

centrifugation in a table-top centrifuge (13,226 x g for 4 minutes). The supernatant (160 μ l) was transferred to a cyclic olefin half-area well plate (catalog #4680 Corning) and absorbance scans from 600 nm to 725 nm were recorded on a SpectraMax i3x plate reader (Molecular Devices). Chlide appearance was quantified using its molar extinction coefficient 74,900 $M^{-1}cm^{-1}$ at 666 nm.

2.2.9 Protein and Iron-content determination.

Protein concentrations were determined using the Bradford Assay reagent (BioRad) and Bovine Serum Albumin (Gold Biotechnology Inc.) as a standard. Iron content was determined by colorimetric assay using 2,2'-dipyridyl absorbance at 520nm and $Fe(NH_4)_2(SO_4)_2$ (Fisher) as a standard after sample denaturation and iron reduction (60 minute exposure to 5% HCl and boiling, followed by exposure to excess (10%) hydroxylamine.)

2.2.10 Growth curve generation.

E. coli BL21(DE3) and *E. coli* BL21(DE3)Suf⁺⁺ cell lines were transformed with BchL plasmid and plated on LB-Agar containing 50 μ g/mL kanamycin. Six individual colonies from both cell lines were used to inoculate 5 mL cultures (LB + 50 μ g/mL kanamycin). Overnight cultures were normalized to an OD₆₀₀ of 0.01 with LB containing 50 μ g/mL kanamycin. Two μ L of OD₆₀₀ corrected starter cultures were used to inoculate 200 μ L of media in a polystyrene 96-well cell-culture plate (Cole-Palmer). Six wells containing only 200 μ L LB and 50 μ g/mL kanamycin served as a blank and negative control. Cells were grown in a SpectraMax i3x plate reader (Molecular Devices Inc.) at 37°C, shaken for 10 seconds before each read. OD₆₀₀ was measured every 2.5 minutes. Blank measurements were averaged, and individual growth curves

were corrected by subtracting averaged blank values at each time point, then averaged after correction for Fig. 2.4d. Doubling rates (“r”) were calculated from t=2 and t=4 hours using $r = (\ln[OD2/OD1]) / (t_2 - t_1)$. Doubling time was calculated using $\ln(2)/r$.

2.3 RESULTS.

2.3.1 Confirming the inframe partial deletion of *sufA* and *sufB* in *E. coli* BL21(DE3) and in commercial derivatives.

Previous sequencing of the *E. coli* BL21(DE3) genome indicated that it contains a genomic deletion encompassing portions of the *sufA* gene product, a chaperone protein which functions in delivering [Fe-S] clusters to apoproteins, and the *sufB* gene product, a protein which acts as a scaffold for building [Fe-S] clusters. (Studier et al., 2009) PCR amplification of the *suf* operon from a laboratory stock of *E. coli* BL21(DE3), using primers flanking the two genes, generated a DNA fragment that is 854 bp smaller than the size expected for intact *sufA – sufB* observed for the reference strain *E. coli* K-12 MG1655 (Fig. 2.2a), indicating the presence of the deletion. The presence of the deletion was then tested for other commercially available strain derivatives of *E. coli* BL21(DE3). PCR amplification of the *sufA – sufB* genes from 7 different commercial strains [Ni-Co21(DE3), Lemo21(DE3), C41(DE3), Rosetta2(DE3)pLysS, BLR(DE3)pLysS, *E. coli* BL21(DE3)Ai, and *E. coli* BL21(DE3)codon plus] revealed the same 854 bp deletion in the *sufA – sufB* genes as observed for the parent *E. coli* BL21(DE3) (Fig. 2.2a).

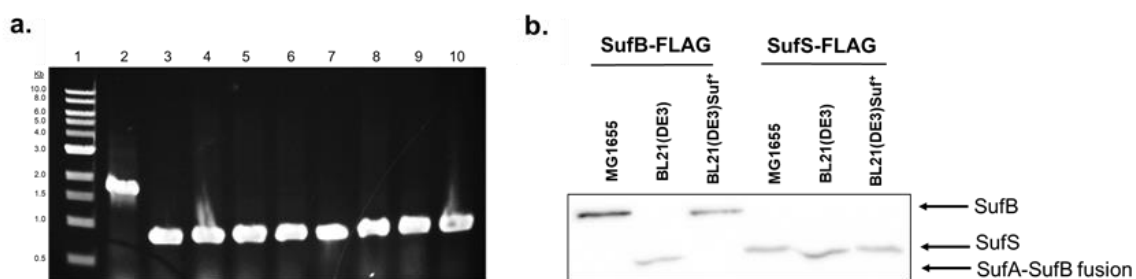


Fig. 2.2 An inframe deletion between *sufA* and *sufB* renders the *suf* operon inactive in *E. coli* BL21(DE3).

a. The presence of the 854 bp deletion was tested in commercial lineages of *E. coli* BL21(DE3) using PCR analysis. Lane 2 shows the expected 1641 bp product from MG1655. Lanes 3 through 10 show the 787 bp product predicted from the 854 bp deletion present in strains *E. coli* BL21(DE3), NiCo21(DE3), Lemo21(DE3), C41(DE3), Rosetta2(DE3)pLysS, BLR(DE3)pLysS, *E. coli* BL21(DE3)Ai, and *E. coli* BL21(DE3)codon plus. **b.** Western blot analysis using an anti-FLAG antibody reveals the production of full length c-terminally FLAG-tagged SufB protein in MG1655 and in strain *E. coli* BL21(DE3)Suf+, in which the *sufA sufB* genes are properly restored. Full length C-terminally FLAG-tagged SufS protein is present in all strains.

2.3.2 The 854 bp deletion within the *suf* operon renders the Suf pathway nonfunctional.

DNA sequencing of *sufA* and *sufB* of *E. coli* BL21(DE3) also confirmed the same nucleotide deletion boundaries within *sufA* and *sufB* as reported previously. (Studier et al., 2009) Comparison of the *sufABCDSE* operon DNA sequence from *E. coli* K12 strain MG1655 and *E. coli* B strain *E. coli* BL21(DE3) indicated that the 854bp inframe deletion within the *E. coli* BL21(DE3) *sufABCDSE* operon encompassed the last 79 codons of *sufA* and the first 202 codons of the *sufB* coding sequences, generating a predicted SufA/B fusion protein of ~37 kDa (Fig. 2.1a). A FLAG epitope was engineered at the C-terminal end of SufB to test whether this fusion protein accumulated in cells by Western blotting using an anti-FLAG antibody. In the *E. coli* BL21(DE3) strain background, a protein that was smaller than that present in the reference strain

MG1655 was detected, consistent with the size of the predicted fusion protein between SufA and SufB (Fig. 2.2b). This deletion had no effect on downstream *sufS* expression since similar levels of FLAG-tagged SufS were observed comparing MG1655 and *E. coli* BL21(DE3) (Fig. 2.2b).

Activity of this mutant fusion protein was tested using P1 vir to transduce into *E. coli* BL21(DE3) a $\Delta iscSUAhscBAfdx::kan$ allele which requires a functional Suf pathway for growth. (Mettert & Kiley, 2014) No *E. coli* BL21(DE3) derivatives were recovered, suggesting that this fusion protein, and consequently, the Suf pathway, is non-functional in this strain. To quantitatively demonstrate this, the $\Delta iscSUAhscBAfdx::kan$ allele was genetically fused to a *gusA::Tn10 (TetR)* allele and established the co-transduction linkage between these two markers upon their subsequent transduction into MG1655 and *E. coli* BL21(DE3). After initially selecting for transductants on tetracycline-containing medium and then screening ~50 of these colonies for KanR, 38% of the MG1655 transductants exhibited KanR. In contrast, none of the *E. coli* BL21(DE3) transductants were KanR, thus providing further evidence of a non-functional Suf pathway in this strain.

A derivative of *E. coli* BL21(DE3) was then constructed in which the mutant *suf* operon was replaced with an intact *suf* operon from MG1655 using P1 vir transduction. Instead of the fused protein observed in *E. coli* BL21(DE3), this genetically restored *E. coli* BL21(DE3)*Suf*⁺ strain (PK13235) generates full length SufB as confirmed by Western blot analysis (Fig. 2.2a,b).

2.3.3 Designing a functional Suf-containing strain for [Fe-S] protein overexpression.

Since many laboratories routinely utilize *E. coli* BL21(DE3) to overexpress recombinant [Fe-S] cluster-containing proteins, I tested whether restoring the Suf system would improve the yield of recombinant [Fe-S] cluster-containing proteins. Because the *suf* operon is repressed by the transcriptional regulator Fur under standard growth conditions, (Outten et al., 2004; Wayne

Outten, 2015) a variant of *E. coli* BL21(DE3)Suf⁺ was constructed that also contains a mutated (deleted) Fur binding site (designated here as Suf⁺⁺) within the *sufA* promoter region. This mutation was chosen as the Fur binding site is a transcriptional repressor that binds iron. This mutation increases *suf* expression at least 4-fold under aerobic conditions. (Mettert & Kiley, 2014) Thus, this *E. coli* BL21(DE3)Suf⁺⁺ strain (PK11466) is expected to have enhanced levels of the Suf machinery, in addition to functional SufA and SufB proteins. In contrast to *E. coli* BL21(DE3), viable colonies of *E. coli* BL21(DE3)Suf⁺ and *E. coli* BL21(DE3)Suf⁺⁺ were recovered upon deletion of the *isc* operon, indicating that the Suf pathway is indeed functional in this variant.

2.3.4 Protein yields and [Fe-S] cluster occupancy of BchL-overproducing cultures are improved with a restored and upregulated Suf pathway.

Production and yield of recombinant [Fe-S] cluster-containing proteins was assessed in *E. coli* BL21(DE3)Suf⁺ and *E. coli* BL21(DE3)Suf⁺⁺ to determine if the restoration and/or up-regulation of the *suf* operon had any beneficial effects on [Fe-S] cluster biogenesis. The Dark-operative Protochlorophyllide Oxido-Reductase (DPOR) enzyme from *Rhodobacter sphaeroides*, was chosen as a model system, as its native organism has only the Suf system for [Fe-S] biogenesis. DPOR catalyzes the ATP-dependent reduction of protochlorophyllide (Pchlide) to chlorophyllide (Chlide) in plant and photosynthetic bacterial systems under low-light or dark conditions. (Nomata, Kitashima, Inoue, & Fujita, 2006a; Nomata et al., 2005) DPOR is comprised of two components (Fig. 2.3a): an electron donor (BchL) and an electron acceptor enzyme (BchN-BchB). BchL exists as a homodimer stabilized by a bridging [4Fe-4S] cluster ligated by 2 cysteine residues from each monomer. (Bröcker et al., 2010; Muraki et al., 2010) BchN and BchB exist as an $\alpha_2\beta_2$ heterotetramer with two symmetric halves (Fig. 2.3a). Each half contains one [4Fe-4S] cluster that accepts an electron from reduced BchL and an active site for

substrate (Pchlide) binding and reduction. (Moser et al., 2013) Two rounds of electron transfer from BchL to BchN-BchB are required to reduce the C17-C18 double bond in Pchlide to form Chlide. (Nomata, Kondo, Mizoguchi, & Tamiaki, 2014) Additional details of DPOR mechanistic specifics can be found in Chapter 1 of this document.

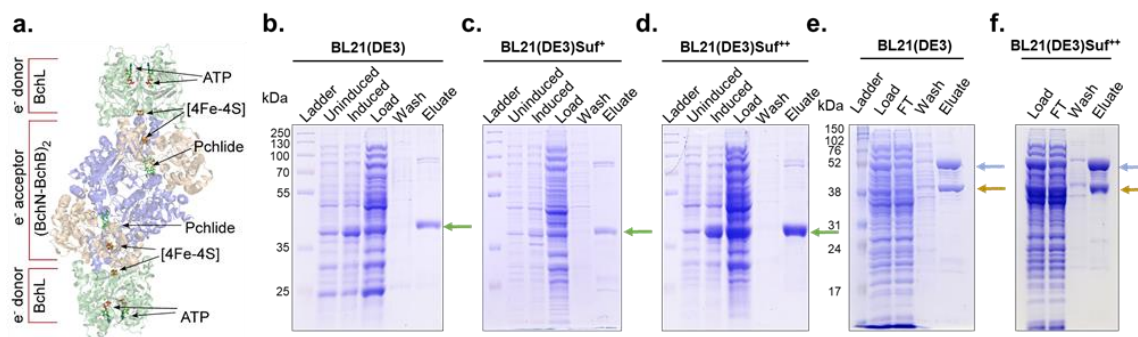


Fig. 2.3 Removing transcriptional repression of the *suf* operon results in enhanced production of the [4Fe-4S] cluster carrying BchL protein in *E. coli* BL21(DE3) cell lines.

a. Crystal structure of the DPOR complex (PDB ID:2YNM) consisting of BchL (green) and BchB(blue)-BchN(brown) proteins. Locations of [4Fe-4S] clusters and the binding sites for Pchlide and ATP are denoted. Synthesis and affinity purification of BchL from **b.** *E. coli* BL21(DE3), **c.** *E. coli* BL21(DE3)Suf⁺, and **d.** *E. coli* BL21(DE3)Suf⁺⁺ cells. Green arrow indicates the position of BchL following SDS-PAGE. Analogous purification of the BchN-BchB complex from **e.** *E. coli* BL21(DE3), **f.** and *E. coli* BL21(DE3)Suf⁺⁺ cells. Brown and green arrows indicate position of BchN and BchB respectively. Gels are representative of three independent experiments.

BchL and BchN-BchB synthesis, protein yield, iron content, and protein activity from three strains: a) *E. coli* BL21(DE3), b) *E. coli* BL21(DE3)Suf⁺, and c) *E. coli* BL21(DE3)Suf⁺⁺ were compared. Strains containing plasmids carrying open reading frames for BchL or BchN-BchB under the control of an IPTG-inducible T7 promoter were grown and used for synthesis and purification of the proteins under identical conditions. For BchL, protein accumulated to similar cellular levels after induction when comparing *E. coli* BL21(DE3) and *E. coli* BL21(DE3)Suf⁺ (Fig. 2.3b,c) but was markedly higher for *E. coli* BL21(DE3)Suf⁺⁺ (Fig. 2.3d). BchL protein was

then purified from each strain using affinity Ni²⁺-NTA chromatography. The elevated protein levels in *E. coli* BL21(DE3)Suf⁺⁺ resulted in a reproducible ~3-fold increase in the overall yield of purified BchL protein obtained from one liter of cells (3.62±0.54 mg/L) as compared to *E. coli* BL21(DE3) (1.32±0.63 mg/L) or *E. coli* BL21(DE3)Suf⁺ cells (0.81±0.23 mg/L) (Fig. 2.4a). The increased yield from *E. coli* BL21(DE3)Suf⁺⁺ may reflect increased stability of BchL if loading of the protein with [4Fe-4S] clusters protects the protein from proteolysis. If this is the case, then the levels of the Fe-S cluster biogenesis machinery but not BchL protein is limiting for formation of [4Fe-4S]-BchL in this strain background.

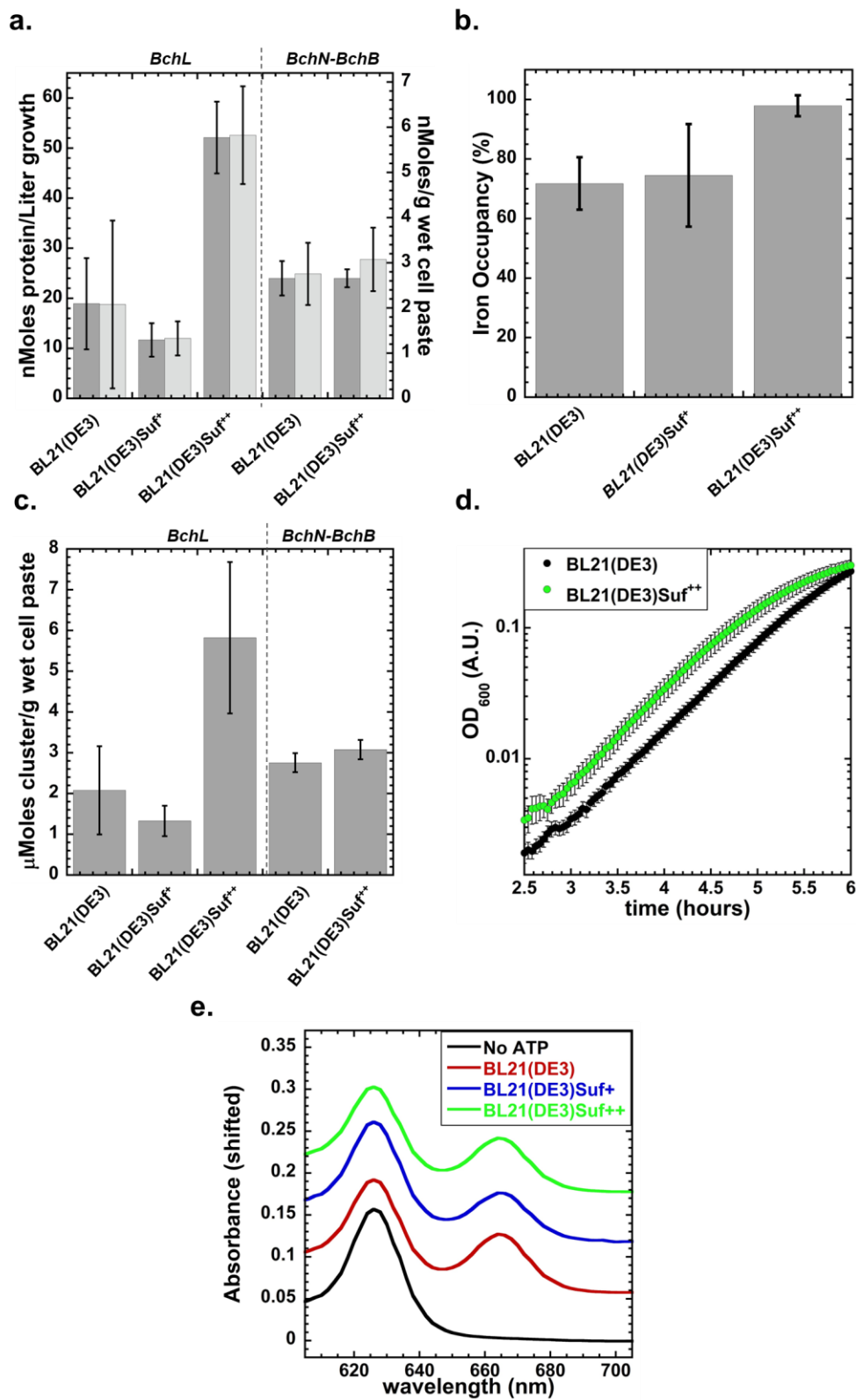


Fig. 2.4 *E. coli* BL21(DE3) Suf⁺⁺ cells increase yield, [Fe-S] cluster formation/load ratio and maintain enzyme activity.

Quantification of the final yield of BchL and BchN-BchB proteins are plotted and show enhanced yield of the BchL protein in the *E. coli* BL21(DE3)Suf⁺⁺ cells. No difference in the yield of BchN-BchB protein complex is observed. Left axis refers to dark gray bars, right axis refers to light gray bars. **b.** The total iron content in the purified BchL protein was measured and plotted as a percent of total occupancy. *E. coli* BL21(DE3) and *E. coli* BL21(DE3)Suf⁺ produced similar (2 tailed students t-test assuming unequal variance, n=3) iron content (P=0.72). however, *E. coli* BL21(DE3)Suf⁺⁺ had significantly improved iron content compared to *E. coli* BL21(DE3) or *E. coli* BL21(DE3)Suf⁺ (P= 0.0053 and 0.0226 respectively) **c.** The ratio of [4Fe-4S] cluster per gram of wet cell paste is plotted for BchL and BchNBchB. **D.** Log-phase of Growth curves of *E. coli* BL21(DE3) (black circles) and *E. coli* BL21(DE3)Suf⁺⁺ cells (green circles) that carry the BchL overexpression plasmid are plotted. Cells show similar doubling times (0.43 ± 0.10 , and 0.41 ± 0.058 hours for *E. coli* BL21(DE3) cells and *E. coli* BL21(DE3)Suf⁺⁺ cells, respectively, P= 0.61 from 2 tailed students t-test assuming unequal variance, n=9) but reach OD₆₀₀=0.2 at different times (5.91 ± 0.12 , and 5.19 ± 0.17 hrs, for *E. coli* BL21(DE3) and *E. coli* BL21(DE3)Suf⁺⁺ cells respectively, P=4.92E-08 from 2 tailed students t-test assuming unequal variance, n=9). **E.** BchL and BchN-BchB proteins purified from all three cell lines reduce Pchlde to Chlide. The lack of reduction in the absence of ATP is shown as control. The y-axis displays absorbance corresponding to the no-ATP dataset. The other three experimental traces have been numerically shifted up to better overlay the traces. Data in all panels show averaged results from three independent experiments and S.D. from n=3 (unless otherwise noted) is plotted.

I next tested whether the strain modifications influenced the production or yield of the larger BchN-BchB heterotetramer, containing two [4Fe-4S] clusters. Unlike for BchL, BchN and BchB accumulated to similar cellular levels in *E. coli* BL21(DE3) and *E. coli* BL21(DE3) Suf⁺⁺ (Fig. 2.3e,f). Consequently, I did not obtain enhanced yield of the BchN-BchB complex with *E. coli* BL21(DE3)Suf⁺⁺ (Fig. 2.3i, 4.94 ± 0.24 and 4.94 ± 0.13 mg/L BchN-BchB from *E. coli* BL21(DE3), and *E. coli* BL21(DE3)Suf⁺⁺, respectively).

I also compared the total iron occupancy within the purified BchL proteins from the three strains. Iron occupancy was determined from (Molar [Fe] assayed from isolated protein)/(theoretical Molar [Fe] assuming 4 Fe molecules per BchL dimer) $\times 100$. Approximately 70–80% iron occupancy for the BchL dimer was observed when purified from *E. coli* BL21(DE3) and *E. coli* BL21(DE3)Suf⁺, compared to 100% occupancy when isolated from *E. coli* BL21(DE3)Suf⁺⁺ (Fig. 2.4b). These data suggest that, in addition to enhancing overall protein accumulation and increasing isolated protein yields, the amount of protein carrying an intact

[4Fe-4S] cluster is also higher in the *E. coli* BL21(DE3)Suf⁺⁺ cells. In contrast, BchN-BchB showed full [4Fe-4S] cluster occupancy when purified from any of the three strains (data not shown).

To explain why a ~3-fold increase in BchL production was observed in the *E. coli* BL21(DE3)Suf⁺⁺ cells, I compared the [4Fe-4S] cluster formation/load ratio, which I define as the moles of [4Fe-4S] cluster recovered from purified enzyme per gram of wet cell mass (Fig. 2.4c). For BchL, *E. coli* BL21(DE3)Suf⁺⁺ cells generate and incorporate roughly three-fold more (5 μ moles) clusters/g of wet cell mass compared to the other strains. This ratio does not scale for the BchN-BchB protein complex, even though the levels of BchN-BchB polypeptide synthesis is lower than BchL. The structural complexity of BchN-BchB and the mechanism of [Fe-S] cluster incorporation might be limiting protein folding, possibly explaining the lack of increased yields for the BchN-BchB complex. The doubling times for the both cell lines are also similar (Fig. 2.4d), although I did consistently observe the *E. coli* BL21(DE3)Suf⁺⁺ cells exiting lag phase faster than *E. coli* BL21(DE3) cells.

To ensure that the protein complexes purified from all the strains were active, substrate reduction by their respective BchL and BchN-BchB proteins was compared in vitro. Protochlorophyllide (substrate) and Chlide (reduced product) have unique spectral characteristics that were monitored through absorbance changes. (Yuichi Fujita & Bauer, 2000) Protochlorophyllide was monitored at its characteristic absorbance peak at 625 nm and formation of Chlide was captured at its absorbance peak at 668 nm (Fig. 2.4e). In the absence of ATP no formation of Chlide was observed (black trace, Fig. 2.4c), and addition of ATP triggered formation of a Chlide peak (red trace, Fig. 2.4c). The kinetics of substrate reduction are similar between the preparations when purified protein concentrations are normalized for reactions (0.24 ± 0.02 , 0.27 ± 0.03 , and 0.24 ± 0.001 μ M min⁻¹ for proteins produced from *E. coli* BL21(DE3), *E. coli* BL21(DE3)Suf⁺, and *E. coli* BL21(DE3)Suf⁺⁺ cells, respectively).

2.4 DISCUSSION.

Restoring the Suf [Fe-S] cluster biogenesis pathway and removing its transcriptional repression leads to a marked enhancement in the production and purification of a [4Fe-4S] cluster protein. Myself and collaborators call this *E. coli* BL21(DE3)Suf⁺⁺ strain ‘SufFeScient’ for its potential application in improving production and yields of other [Fe-S] cluster-containing proteins. The SufFeScient cells can improve yields in at least the case shown here; however, its utility must be experimentally determined for given target proteins since the community does not yet have a sophisticated understanding of how subunit complexity, protein structure and local cluster environment impact biogenesis of target enzymes. For the BchL homodimer, the [4Fe-4S] cluster is exposed (Fig. 2.3a), whereas the two [4Fe-4S] clusters in the BchN-BchB complex are buried deep within the dimer interface in the context of a heterotetramer (Fig. 2.3a). Additionally, the relative efficiencies and preferences of the Isc versus Suf systems in incorporating [Fe-S] clusters into specific proteins are also not known but might account for the differences observed.

E. coli BL21(DE3) is considered a workhorse strain for recombinant protein production because of the efficient control provided by T7 RNA polymerase whose gene is integrated into the genome and the wide range of plasmid vectors containing T7 promoters used for protein synthesis or other biotechnological applications. (S. Kim et al., 2017) The in-depth analysis of its genome sequence in 2009 provided a very important history of the progenitors of this strain as well as revealing several large deletions presumed to have been caused by UV irradiation that are specific to the *E. coli* BL21 lineage [see Table 4 of (Studier et al., 2009)]. Transcriptomics and metabolic modeling have provided additional insights into differences in the metabolic and transcriptional networks of this strain compared to other *E. coli* strains. (H. Kim, Kim, & Yoon, 2018; S. Kim et al., 2017; Monk et al., 2016) Despite this wealth of knowledge, the genotype established in 2009 has not propagated to those listed by source companies and, as a

consequence, the genotype listed in publications is typically incomplete. Thus, the function of genes of interest in *E. coli* BL21(DE3) should be verified depending on experimental needs.

In fact, a previous study (Pinske, Bönn, Krüger, Lindenstrauß, & Sawers, 2011) noted the limitation of *E. coli* BL21(DE3) in producing other metal containing anaerobic respiratory enzymes. In this case, the deficiency in producing some of these enzymes could be tracked to a nonsense mutation in the gene encoding the anaerobic transcription factor FNR and consequently lead to inefficient expression of proteins required for nickel transport. In addition, poor activity of some enzymes was also caused by a large 17, 247 bp deletion that removed the high affinity molybdate transport system, compromising the ability of *E. coli* BL21(DE3) to make the molybdenum cofactor necessary for function of several anaerobic respiratory enzymes. Of note, defects in activity for formate dehydrogenases-N and H were still detected even when these other systems were restored, suggesting additional components in metalloenzyme synthesis are limiting in *E. coli* BL21(DE3). However, it seems unlikely that Suf machinery-dependent [Fe-S] cluster assembly was the step that was impaired since the Suf pathway is expressed at lower levels under anaerobic conditions. (Mettert & Kiley, 2014)

In summary, *E. coli* BL21(DE3) is a highly utilized host strain for producing [Fe-S] proteins and correction of the deletion within the *suf* operon coupled with elevating its expression should provide researchers with another option for production of [Fe-S] proteins. Finally, additional details of [Fe-S] cluster biogenesis are constantly being discovered. As these discoveries continues, there will opportunities to further refine and fine-tune competent cell lines for generation of [Fe-S] cluster proteins.

CHAPTER 3. PROBING THE FUNCTIONAL ROLE OF ATP IN BCHL

3.1 INTRODUCTION.

Photosynthetic organisms utilize chlorophyll or bacteriochlorophyll to capture light for their energy requirements. The multi-step enzymatic biosynthesis of both these compounds are similar in the cell except for the penultimate reduction of protochlorophyllide (Pchl_{id}) to produce chlorophyllide (Chl_{id}). (Y Fujita, Takagi, & Hase, 1998; Yuichi Fujita, Takagi, & Hase, 1996) Angiosperms use a light-dependent protochlorophyllide oxidoreductase to catalyze the reduction, whereas gymnosperms, cyanobacteria, algae, bryophytes and pteridophytes possess a light-independent enzyme called dark-operative protochlorophyllide oxidoreductase (DPOR; Fig. 3.1a). (Reinbothe et al., 2010) Photosynthetic bacteria that are anoxygenic, such as *Rhodobacter capsulatus*, rely exclusively on the activity of DPOR for synthesis of bacteriochlorophyll. (Reinbothe et al., 2010) DPOR catalyzes the stereospecific reduction of the C17-C18 double bond of Pchl_{id} to form Chl_{id} (Fig. 3.1b). This reduction forms the conjugated π -system in the chlorin structure of chlorophyll-a which leads to a shift in the spectral properties required for photosynthesis. (Bröcker et al., 2010; Nomata et al., 2014)

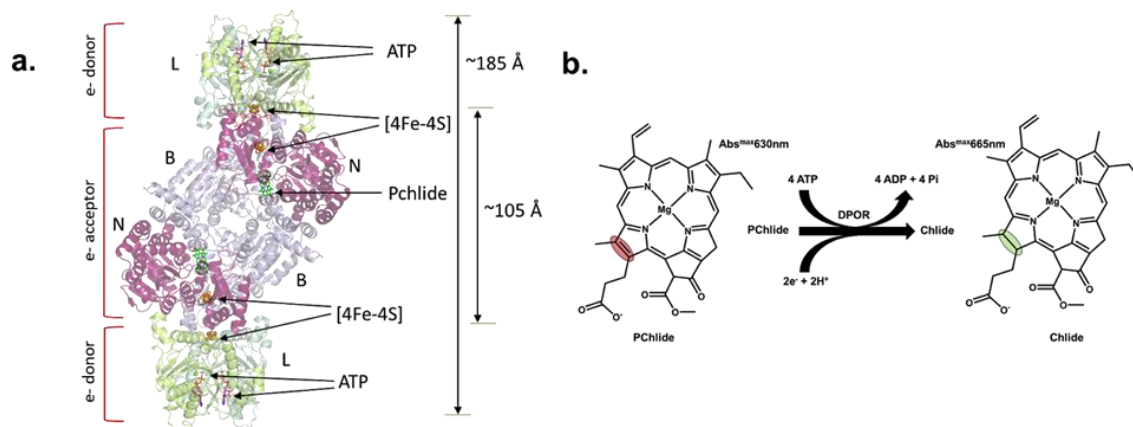
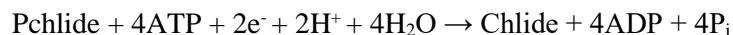


Fig. 3.1 Structure and substrate reduction mechanism of DPOR.

a. Crystal structure of the complete, ADP-AlF₃-stabilized, DPOR complex (PDB:2YNM). BchL subunits are colored green, BchN is colored purple, and BchB is violet. The four [4Fe-4S] clusters are shown as spheres, and ADP-AlF₃ and Pchlde are shown as sticks. **(b)** Schematic of Pchlde reduction to Chlide by DPOR. Two cycles of electron transfer from BchL to BchNB are required for the reduction of the C17-C18 double bond (marked by the colored ovals).

DPOR is structurally homologous to nitrogenase, with ~35% identity between matching components. Nitrogenase is responsible for reducing dinitrogen to ammonia. DPOR is composed of two components: a homodimeric L-protein (BchL), (NifH of nitrogenase) and a heterotetrameric NB-protein (BchNB), (NifKD of nitrogenase). (Bröcker et al., 2010; Muraki et al., 2010) BchL serves as the ATP-dependent electron donor, and BchNB is the electron acceptor containing the active site for Pchlde binding and reduction (Fig. 3.1a). A multi-step reaction cycle has been proposed for DPOR function with the following overall reaction stoichiometry (Fig. 3.1b): (Nomata et al., 2014)



Given the structural similarity to nitrogenase, ATP binding to BchL is thought to promote its transient association with BchNB followed by a single electron transfer (ET) to Pchlde. ATP hydrolysis drives the dissociation of the protein complex. Two such rounds of ATP-dependent ET

are necessary for Pchlide reduction, and the minimum stoichiometry of ATP/molecule of Chlide formed has been determined to be 4. (Nomata et al., 2016) However, the details of how ATP binding promotes complex formation between BchL and BchNB are poorly resolved.

High-resolution crystal structures of the BchL dimer complexed with ADP (PDB:3FWY), (Sarma et al., 2008) and stabilized in a higher-order complex with the BchNB tetramer by ADP-AlF₃ (PDB:2YNM; Fig. 3.1a) (Moser et al., 2013) provide several key molecular insights: BchL contains one [4Fe-4S] cluster ligated by 2 conserved cysteine residues from each subunit of the dimer. The subunits of BchL each have an active site for ATP, including conserved binding (Walker A) and hydrolysis (Walker B) motifs. Each half of the BchNB tetramer contains a substrate (Pchlide) binding site and one [4Fe-4S] cluster which functions as the electron acceptor from BchL (Fig. 3.1a). This cluster is ligated by 3 cysteine residues from BchN and one uncommon aspartic acid ligand from BchB. BchL sits across the top of BchNB, placing their metal clusters in relative proximity (~ 16 Å; Fig. 3.1a). (Moser et al., 2013) Thus, ATP binding is hypothesized to drive formation of the complex. ATP hydrolysis may therefore drive electron transfer. In the homologous nitrogenase system, ATP hydrolysis occurs post-ET, suggesting that hydrolysis likely drives complex dissociation post-ET. (Danyal et al., 2016; Duval et al., 2013) Given the structural similarities between DPOR and nitrogenase, I hypothesize ATP hydrolysis is also likely to promote complex dissociation in DPOR. In this chapter, I address three key questions about ATP usage by BchL: How does binding of 2 ATP molecules collectively transmit information from the ATP binding sites to the [4Fe-4S] cluster of BchL along with the interface where it complexes with BchNB? What role does ATP play in electron transfer? Are both ATP binding events necessary?

This chapter presents a crystal structure of *Rhodobacter sphaeroides* BchL in the nucleotide-free state. This structure reveals novel electron density for a flexible N-terminal region that is bound across the face of the BchL [4Fe-4S] cluster, suggesting a potential regulatory role. I

show that amino acid substitutions within this flexible N-terminal region enhance the kinetics of substrate reduction, pointing to a functionally suppressive role for this interaction. Additionally, inter-subunit contacts between BchL and bound ATP are critical for substrate reduction activity. Finally, I show that ATP binding to both subunits is required to promote conformational changes requisite for reduction of Pchlide to Chlide. I propose a model where ATP-driven cross stabilization of the homodimer promotes the release of the flexible N-terminus and drives formation of the DPOR complex towards ET and substrate reduction.

3.2 MATERIALS AND METHODS.

3.2.1 Reagents and Buffers.

Chemicals were purchased from Sigma-Millipore Inc. (St. Louis, MO), Research Products International Inc. (Mount Prospect, IL) and Gold Biotechnology Inc. (St. Louis, MO). Oligonucleotides for cloning were purchased from Integrated DNA Technologies (Coralville, IA). Enzymes for molecular biology were purchased from New England Biolabs (Ipswich, MA). All reagents and buffers were thoroughly degassed using alternating cycles of vacuum and nitrogen pressure on a home built Schlenk line apparatus. Anaerobic conditions were maintained via airtight syringes, excess reductant and a vinyl glove box (Coy Laboratories, MI) under a Nitrogen (95%) Hydrogen (5%) mix atmosphere.

3.2.2 Generation of protein overexpression constructs.

The coding regions for BchL, BchN, and BchB were PCR amplified from *Rhodobacter sphaeroides* genomic DNA and cloned into pRSF-Duet 1 or pET-Duet 1 plasmids as described. (Nomata, Kitashima, Inoue, & Fujita, 2006b) Mutations in BchL were generated using Q5 site-directed mutagenesis (New England Biolabs, Ipswich, MA). Plasmids used to express the linked-BchL-proteins carrying glycine linkers of various lengths were synthesized as codon-optimized genes (Genscript Inc., Piscataway, NJ). The longest iteration of the linked-BchL-protein was generated as described in Fig. 3.11.

3.2.3 Protein purification.

BchL and BchNB proteins were overexpressed and purified as originally described, (Nomata et al., 2005) with modifications as recently reported. (Corless, Mettert, Kiley, & Antony, 2020) The following additional steps were added to the purification of the linked-L-proteins. During cell lysis and all subsequent steps, protease inhibitors (protease inhibitor cocktail, Millipore-Sigma Inc – catalog #P2714) and 1 mM PMSF were added to all buffers. As an additional purification step, the concentrated linked-L-protein from the Q-Sepharose eluate was subsequently fractionated over a Sephadex S200 26/600 PG (GE Life Sciences) column using STD buffer (100 mM HEPES, pH 7.5, 150 mM NaCl, 10 mM MgCl₂, 1.7 mM sodium dithionite, 1 mM PMSF and protease inhibitors). Protein concentrations were determined using the Bradford assay and Bovine Serum Albumin as a standard.

3.2.4 Generation of Pchl_{id}.

Pchl_{id} was generated from a *Rhodobacter sphaeroides* ZY-5 strain harboring a deletion of the BchL gene (a kind gift from Dr. Carl Bauer, Indiana University) and purified as described. (Nomata, Kitashima, et al., 2006b)

3.2.5 Pchl_{id} Reduction Assays.

Reduction of Pchl_{id} to Chl_{id} was measured spectroscopically by mixing BchNB (5 μ M tetramer), BchL (20 μ M dimer), and 35 μ M Pchl_{id}, in the absence or presence of ATP (3 mM) in STD buffer with 10 mM MgCl₂. Substrate reduction experiments were carried out in 200 μ l reactions and quenched at the denoted timepoints with 800 μ l of 100 % acetone. The acetone/reaction mixture was spun down in a table-top centrifuge at 13,226 x g for 4 minutes. The supernatant was transferred to a cuvette and absorbance scans from 600nm to 725nm were recorded on a Cary 100 UV-Vis spectrophotometer (Agilent Technologies, Santa Clara, CA). Chl_{id} appearance was quantified using the molar extinction coefficient 74,900 M⁻¹cm⁻¹ at 666 nm. For substrate reduction experiments shown in Fig. 3.5 Chl_{id} appearance was measured in aqueous solution inside a Type 41 macro cuvette with a screw cap (Firefly Scientific, Staten Island, NY). Reactions contained BchNB (1 μ M tetramer), BchL (4 μ M dimer), 35 μ M Pchl_{id}, and ATP (3 mM) in STD buffer containing 10 mM MgCl₂. Reactions were initiated by addition of degassed ATP via a gas-tight syringe, and spectra were recorded from 400-800nm every 60s as described above. Fig. 3b shows absorbance values from difference spectra generated by subtracting timepoints from the first spectra recorded before ATP addition.

3.2.6 BchL crystallization.

BchL crystals were grown anaerobically (100% N₂ environment with <0.1 ppm O₂) inside a Unilab Pro glovebox (mBraun, Stratham, NH) at 15 °C using the vapor diffusion method. All materials and buffers were pre-treated to remove oxygen as previously described. (Lanz et al., 2012) Initial sparse matrix screens were set up anaerobically using a Mosquito Crystal robotic liquid handler (TTP Labtech, Boston, MA). 1 µL of 200 mM sodium dithionite solution was added to every well to ensure complete removal of any dissolved oxygen. For each drop, 200 nL of well solution and 200 nL of 100 µM dimeric BchL (in 100 mM HEPES pH 7.5, 150 mM NaCl, 10% (v/v) glycerol) were mixed. A crystal was observed after approximately one month with the well solution consisting of 0.6 M sodium chloride, 0.1 M MES:NaOH pH 6.5, 20% (w/v) PEG 4000. Larger volume (3-4 µL) drops of the same well solution and protein concentration in 1:1, 1:2 and 2:1 ratios of protein to well solution yielded large single crystals after ~2-3 months. Prior to freezing, the well solution was mixed in an equal volume of cryoprotectant solution with a final concentration of 9% sucrose (w/v), 2% glucose (w/v), 8% glycerol (v/v), and 8% ethylene glycol (v/v). Crystals were soaked for a few seconds in the cryoprotectant before being cryo-cooled in liquid nitrogen. A crystal from a drop set up with 2 µL well solution and 2 µL protein solution was used for in-house data collection, while different crystals that grew with 2 µL well solution and 1 µL protein solution were used for synchrotron data collection.

3.2.7 BchL data collection, processing and refinement.

An initial model was built using data collected with an in-house Rigaku MicroMax 007HF X-ray source equipped with a Pilatus 300K detector. A complete dataset at cryogenic temperature (100K) was collected to 2.92-Å resolution, which was integrated using HKL2000 and merged and scaled using SCALA in the CCP4 suite. (Winn et al., 2011) Phase determination

was initially estimated through molecular replacement (PHASER) using the *Rhodobacter sphaeroides* ADP-bound BchL structure (PDB ID: 3FWY, with all ligands re-moved) as the search model. (Sarma et al., 2008)(Adams et al., 2010) A solution was found with two dimers in the asymmetric unit. Following molecular replacement, rigid-body refinement was performed in Phenix. A starting model was built using AutoBuild and further improved with iterative rounds of model building and refinement using COOT and Phenix.

Higher resolution data were collected on a different crystal at beamline 17-ID-1 (AMX), National Synchrotron Lightsource-II, at the Brookhaven National Laboratory on a Dectris Eiger 9M detector. Two complete datasets collected at 100K were integrated, scaled and merged to 2.6-Å resolution using HKL2000. The partially refined model from home-source data was used as a molecular replacement model for solving the structure in Phenix. The resulting model was improved through iterative rounds of model building using COOT and Phenix. Data processing and refinement statistics are presented in Fig. 3.2.

3.2.8 ATP binding assay.

Nitrocellulose membranes, cut into 2×2 cm squares, were pretreated with 0.5 N NaOH for 2 min, washed extensively with H₂O, and equilibrated in binding buffer (100 mM Hepes, pH 7.5, 150 mM NaCl, and 10 mM MgCl₂). In the reactions (100 μ L), BchL (4 μ M) was incubated with 1 mM ATP + 0.3 μ Ci γ ³²P-ATP for 10 min at 25 °C, and 20 μ L aliquots of the reaction were filtered through the membrane on a single filter holder (VWR Scientific Products). The membranes were washed before and after filtration with 250 μ L of nucleotide binding buffer and air dried before overnight exposure onto a PhosphorImaging screen. 1 μ L aliquots were spotted onto a separate membrane to measure total nucleotide in the reaction. Radioactivity on the membrane was quantitated on a PhosphorImager (GE Life Sciences). Total ³²P-ATP bound was calculated using the following equation: $\frac{[\text{bound signal}]}{([\text{total signal}] \times 20)} \times [\text{ATP}]$

3.2.9 EPR Spectroscopy.

EPR spectra were obtained at 5, 10, 17.5, and 30 K on an updated Bruker EMX-AA-TDU/L spectrometer equipped with an ER4112-SHQ resonator (9.48 GHz) and an HP 5350B microwave counter for precise frequency measurement. Temperature was maintained with a ColdEdge/Bruker Stinger S5-L recirculating helium refrigerator, and an Oxford ESR900 cryostat and MercuryITC temperature controller. Spectra were recorded with either 0.3 G (3×10^{-5} T) or 1.2 G (0.12 mT) digital field resolution with equal values for the conversion time and the time constant, 1.0 mW incident microwave power, and 12 G (1.2 mT) magnetic field modulation at 100 kHz. EPR simulations were carried out using Easyspin. (Stoll & Schweiger, 2006)

3.2.10 Samples for EPR Spectroscopy.

200 μ l EPR samples contained 40 μ M BchL (or mutant), 1.7mM dithionite, and, where indicated 3mM ATP, 3mM ADP and/or 20uM BchNB. For a subset of the experiments, EPR experiments were carried out with 20 μ M BchNB, 40 μ M Pchl_a, and, where indicated, 3 mM ATP. Protein samples were prepared and transferred to the EPR tubes in the glove box and stoppered with a butyl rubber stopper. Samples were removed from the glove box and immediately flash frozen in liquid nitrogen and then analyzed by EPR.

3.3 RESULTS.

3.3.1 Crystal structure of nucleotide-free BchL suggests regulation through a redox switch and a flexible N-terminal region.

BchL was purified to >95% purity determined by SDS-PAGE and was crystallized by a collaborator, Dr. Nozomi Ando. BchL was crystallized by Ando lab members anaerobically in the absence of nucleotides, and a crystal structure was determined to a resolution of 2.6 Å (Table 3.1). The asymmetric unit contains four BchL chains: chains A and B form one BchL dimer, and chains C and D comprise the other (Fig. 3.2a,b). The overall structure of BchL is similar to previously published crystal structures (Fig. 3.3.a-c), but in this nucleotide-free state, the top face of the dimer is more open compared to ADP-bound BchL (Fig. 3.3b) and ADP-AIF₃-NB-bound BchL (Fig. 3.3c). (Moser et al., 2013) Unexpectedly, although the N-terminus is disordered and not observed in all previous BchL structures (residues 1-29 in 3FWY and residues 1-27 in 2YNM from *P. marinus*), there is clear electron density at the N-terminus of chain C in the nucleotide-free structure, which was modeled as residues 16 to 29 (Fig. 3.2b). Interestingly, the flexible N-terminal region is observed bound across the [4Fe-4S] cluster in the nucleotide-free structure (Fig. 3.3a) covering a surface that is normally used to interface with BchNB (Fig. 3.3c). In the chain C/D dimer, Asp23 of the N-terminal region interacts with Gln168, Gly16 forms an H-bond to Cys126 (an [4Fe-4S] cluster ligating residue) of the opposing chain, while Ser17 interacts with Gly161 of chain C via the backbone of G125 in chain D (Fig. 3.2c, 3.3d). Based on the structure of the ADP-AIF₃-stabilized DPOR complex (PDB: 2NYM), (Moser et al., 2013) the residues corresponding to Cys126, Gly161, and Gln168 in BchL (*R. sphaeroides* numbering) are three of the twelve residues that interact with BchNB during the formation of the active complex, as predicted by PDBePISA interface analysis (Krissinel & Henrick, 2007) (Fig. 3.3c, purple surface). Notably, the flexible N-terminal protective region (residues 1-29) is only conserved among DPOR BchL-proteins and is not observed in other homologous proteins such as NifH of

nitrogenase and the BchX protein of chlorophyllide oxidoreductase (Fig. 3.4). The position and interactions of the N-terminal residues in the nucleotide-free structure suggests a possible auto-inhibitory role by forming a barrier to docking and shielding the [4Fe-4S] cluster of BchL.

Diffraction Statistics	
Space Group	I121
Unit cell (Å)	a = 92.51 b = 100.92 c = 117.79 $\alpha = 90.00^\circ \quad \beta = 99.27^\circ \quad \gamma = 90.00^\circ$
Wavelength (Å)	1.008
Resolution Range (Å)	42.20 – 2.60 (2.69-2.60)
Total observations	303261
Unique reflections	32733 (3125)*
R_{merge}	0.193(0.908)
R_{pim}	0.057(0.413)
$\langle I/\sigma(I) \rangle$	9.2(1.5)
$CC_{1/2}$	0.990 (0.573)
Completeness (%)	99.5 (95.3)
Multiplicity	9.3 (5.1)
$R_{\text{work}}/ R_{\text{free}}$	0.231/0.277
Mean B-factor for all atoms (Å ²)	85.6
Anisotropy	0.076
Total number of atoms refined	7667
Clashscore	6
Ramachandran favored/allowed (%)	96.2/3.9
Ramachandran outliers	0
RMSD of bond lengths (Å)/angles (°)	0.002/0.393
Sidechain outliers (%)	2.4

* Values in parentheses refer to the highest resolution shell

Table. 3.1 Crystallographic data processing and refinement statistics.

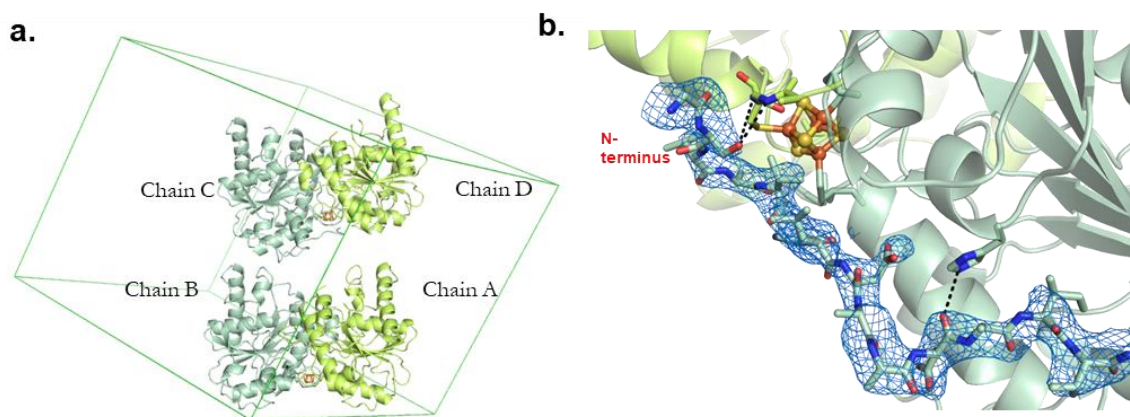


Fig. 3.2 Crystal structure of nucleotide-free BchL.

a. The asymmetric unit of the crystal structure comprises two dimers of BchL chains. The unit cell is outlined in green. **b.** Fo-Fc map of density for the previously unresolved N-terminal tail in chain C (shown as blue mesh, contoured at 1.0 σ). Clear, continuous density is visible for the backbone of the entire tail up to residue 16. Interactions of tail residue Ser17 with residues Gly125 and Cys126 on chain D as well as the hydrogen-bonding interaction between Asp26 and His169 of chain C are highlighted.

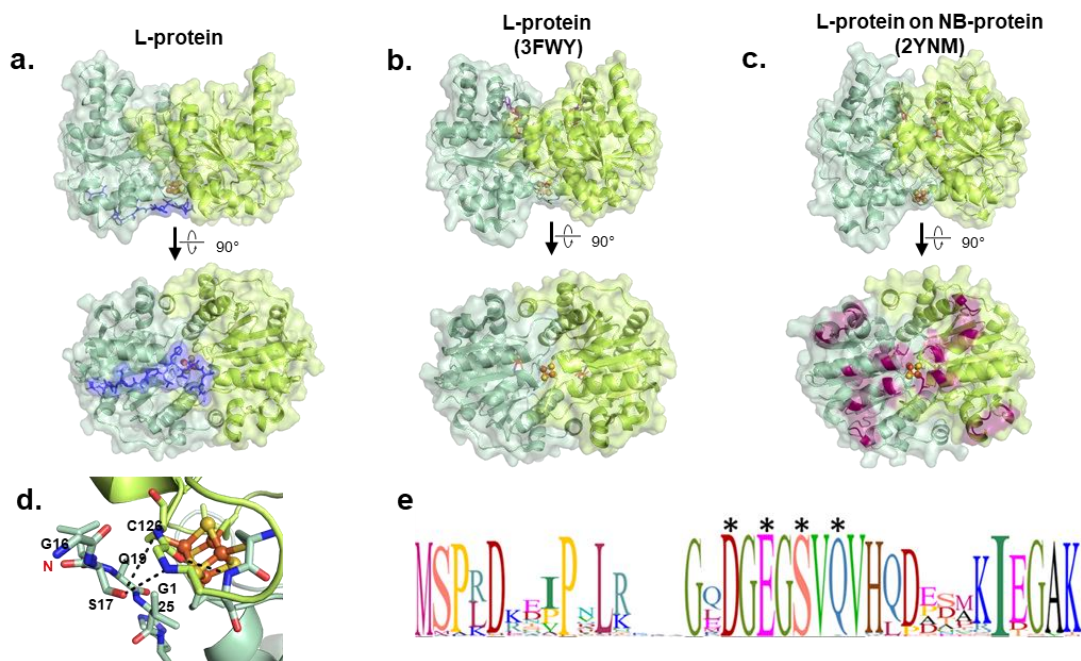


Fig. 3.3 Crystal structure of nucleotide-free BchL reveals a flexible N-terminal region capping the [4Fe-4S] cluster.

Side views (top row) and bottom views (bottom row) of the BchL structure **a.** in the absence of nucleotides, **b.** with ADP bound (PDB: 2YNM), and **c.** in complex with BchNB (PDB: 3FWY). A slight compaction upon the addition of ADP, and a further compaction when in complex with BchNB, can clearly be seen by comparing the side views. The flexible N-terminal region resolved in the nucleotide-free structure (residues 16-29, colored blue in panel **a.** clearly covers the [4Fe-4S] cluster in addition to blocking or directly interacting with several residues predicted to directly interact with BchNB (highlighted in dark purple in panel **c.**). **d.** Residues in the flexible N-terminus of chain C interact with important residues near the [4Fe-4S] cluster. The highly conserved Ser17 forms hydrogen bonds with both Cys126 and Gly125 on chain C, the former of which directly interacts with BchNB in the 2YNM structure and the latter additionally interacts with Gly161 on chain D, another predicted BchL-BchNB interface residue. **e.** Sequence logo of the N-terminus of BchL generated from alignment of $n=89$ species. Letter height corresponds to the degree of sequence conservation, and the residues mutated in this study are labeled.

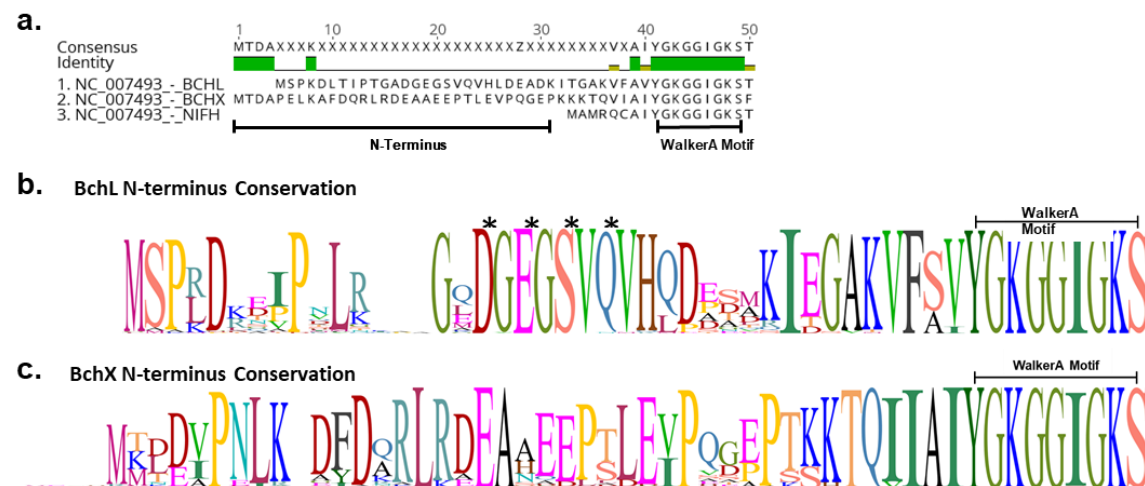


Fig. 3.4 Conservation of N- and C-terminal regulatory elements BchL and homologs.

a. Sequence alignment BchL, BchX, and NifH (the Nitrogenase Fe-protein). N-terminus length highlighted for BchL and BchX. Walker A motif sequence conservation is also labeled. **b.** Sequence logo of the N-terminus of BchL generated from alignment of $n=89$ species. Letter height represents sequence conservation. Critical amino acids for capping and generation of BchLS17A and BchL4A are labeled with asterisks. **c.** Sequence logo of the N-terminus of BchX generated from alignment of $n=89$ species. Letter height represents sequence conservation. Figure demonstrates lack of conservation in N-terminus of BchX. NifH N-terminus conservation is not shown as it lacks enough residues to potentially cap its cluster.

3.3.2 Amino acid substitutions in the flexible N-terminal region of BchL increases the rate of substrate reduction.

To test whether the flexible N-terminal region of BchL plays an auto-inhibitory role, based on the contacts observed in the crystal structure (Fig. 3.3d) and sequence alignments (Fig. 3.3e), I generated a singly mutated constructs where Asp13 (BchL^{D13A}), Glu15(BchL^{E15A}), Ser17(BchL^{S17A}), or Gln19(BchL^{W19A}) were mutated to Ala, and a quadruple mutated construct (BchL^{4A}) where Asp13, Glu15, Ser17 and Gln19 were all substituted with Ala. Though density for residues 1-15 is not seen in any BchL structure, Ser17 and Gln19 are observed in the nucleotide free structure positioned across from the [4Fe-4S] cluster (Fig. 3.2b). It should be noted that in all instances noted here that all constructs bore a N-terminal poly-histidine tag. I have tested the effect of a C-terminal affinity tag and it has no effect on activity (data not shown).

BchL^{S17A} was chosen as the first mutant to study due to its positioning on the cluster seeming to be most impactful. BchL^{S17A} was mixed with Pchlide and BchNB and found to possess reductase activity after purification (Fig. 3.5b) (Fig. 3b). However, amino acids substitutions in this N-terminal region affected protein stability: Both BchL^{S17A} and BchL^{4A} are soluble to a lesser degree compared to the wild-type protein and formed cloudy precipitates within 30 minutes of initiating reduction reactions. The decrease in stability could be due to improper interactions with BchNB, the result of unstable conformations upon binding to ATP, or just intrinsic to the mutant protein after one round of freeze-thaw. Substrate reducing activity with purified protein was assayed by mixing purified BchL, BchL^{S17A}, or BchL^{4A} (4 μ M) with BchNB (1 μ M) and Pchlide (35 μ M) and spectroscopically monitoring the reaction over time in the absence or presence of ATP (3 mM). Pchlide and Chlide have characteristic absorbance maxima at 630 nm and 680 nm, respectively, in aqueous solution. Formation of Chlide was observed as an increase in absorbance at 680 nm in the presence of ATP (Fig. 3b). Both BchL^{S17A} and BchL^{4A} are active for substrate reduction and show Chlide formation rates ~2-2.5 fold that of wild type BchL ($k_{\text{obs}} = 0.044 \pm 0.014$, 0.084 ± 0.019 , and 0.087 ± 0.016 μ M/min for BchL, BchL^{S17A} and BchL^{4A}, respectively; Fig. 3.5b.) I speculate that actual differences in activity are likely much larger as the effective concentrations of the mutant BchL proteins are likely lower than calculated during the experiment due to protein instability. I also generated a truncated version of BchL missing the first 27 amino acids (BchL^{NA27}), bearing a C-terminal poly-histidine tag. I was successfully able to overexpress BchL^{NA27}, however it was poorly soluble, and was unable to obtain sufficiently pure protein for biochemical studies. These difficulties provide additional evidence that the flexible N-terminus might play an important role in BchL function and stability.

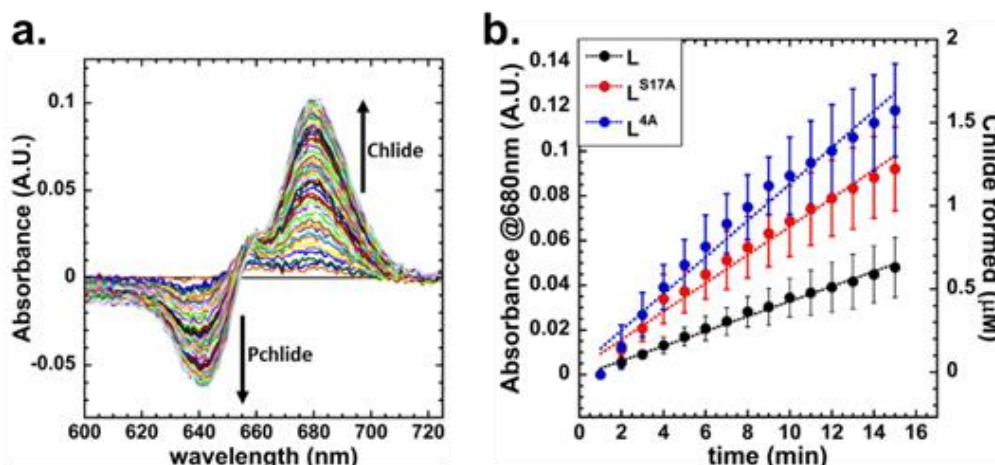


Fig. 3.5 The flexible N-terminal region is auto-inhibitory to BchL function.

a. Representative traces of wild-type reaction in aqueous solution. Arrows represent the trend in absorbance associated with substrate consumption and product formation as a function of time. **b.** Absorbance plot at 680nm (A680) of the in vitro reaction comparing reduction rates as a change in A680 (left axis) and apparent Chlide formation rates (right axis) of BchL (black circles, $k_{obs} = 0.046 \pm 0.014 \mu\text{M}\cdot\text{min}^{-1}$) BchLS17A (red circles, $k_{obs} = 0.0734 \pm 0.19 \mu\text{M}\cdot\text{min}^{-1}$), and BchL4A (blue circles, $k_{obs} = 0.100 \pm 0.016 \mu\text{M}\cdot\text{min}^{-1}$).

3.3.3 ATP-binding causes changes in the local environment of the BchL [4Fe-4S] cluster affecting their EPR spectral line-shape and intensities.

Since the flexible N-terminal region binds to the BchNB interaction interface within BchL, I hypothesized that ATP binding could promote conformational changes in BchL to relieve autoinhibition by altering the local environment of the [Fe-S] cluster. I thus recruited Dr. Brian Bennett to help me use electron paramagnetic resonance (EPR) to probe local changes in the [4Fe-4S] cluster environment, which includes the binding site for the N-terminus. Interpretation of the g-tensors of [4Fe-4S] clusters in direct structural terms is rarely possible, but EPR can nevertheless provide information about relative conformational changes around the cluster. Previous studies have described the [4Fe-4S] cluster of BchL as an axial species, while others reported a rhombic species. Here, EPR at different temperatures indicated that two distinct EPR

signals were exhibited by the [4Fe-4S] cluster (Fig. 3.6a). At 5 K, a signal termed FeS^A was observed that appears axial but was best simulated with rhombic g -values of 2.00, 1.94, and 1.85; both g_1 and g_3 are atypically low for a prototypical Cys₄-ligated [4Fe-4S] cluster, and the associated resonances exhibit large line widths (Fig. 3.6a). This signal was very fast-relaxing and was no longer detectable at 17.5 K. At this higher temperature (17.5 K), a more typical rhombic signal, FeS^B, with $g_{1,2,3} = 2.04, 1.94, \text{ and } 1.89$ was observed, and at an intermediate temperature (10 K) the observed signal was well replicated by a 40%:60% mixture of the simulations of FeS^A and FeS^B, respectively. As expected for a [4Fe-4S] cluster, the EPR signals were fast-relaxing and were not detectable at 30 K or higher temperature. BchL exhibited analogous signals to FeS^A and FeS^B when incubated with BchNB and ADP (Fig. 3.6b,c) although, notably, both ADP and BchNB served to increase the relaxation rate of the FeS^B EPR signal, suggesting a more efficient coupling of the cluster to the lattice via increased strain energy. In addition, with ADP, the proportion of the FeS^A species was diminished by a factor of two. Based on the structural data for BchL and the relaxation properties of the EPR signals, I interpret this as the FeS^A species as having a 'cap' across the cluster, formed by the flexible N-terminus, whereas the FeS^B species is uncapped; in solution, these two species are likely in dynamic equilibrium. Upon the addition of ATP, the relaxation rate of the FeS^B species was further enhanced and was undetectable at 17.5 K (Fig. 3.6c), while the FeS^A signal exhibited rapid-passage distortion at 5 K, indicating a diminution of the relaxation rate for that species. These data suggest that ATP binding increases the conformational strain of uncapped FeS^B and somewhat inhibits the strong interaction of the cap with the cluster in FeS^A. The FeS^A EPR signals from the BchL^{S17A} variant (Fig. 3.6c) exhibited strong rapid-passage distortion at 5 K and overall reduced signal intensities over the 5 - 17.5 K temperature range; the addition of ATP restored the intensity of the FeS^B signal somewhat, suggesting that relaxation properties were responsible for this phenomenon and that, therefore, the interaction of the cap region with the cluster is altered in BchL^{S17A}. The conformational changes around the [4Fe-4S] cluster in BchL upon ATP binding appear similar to

the BchL^{S17A} protein in the absence of ATP (Fig. 3.6d). Based on these results, it appears that the loss of auto-inhibition drives higher overall substrate reduction activity in BchL^{S17A}.

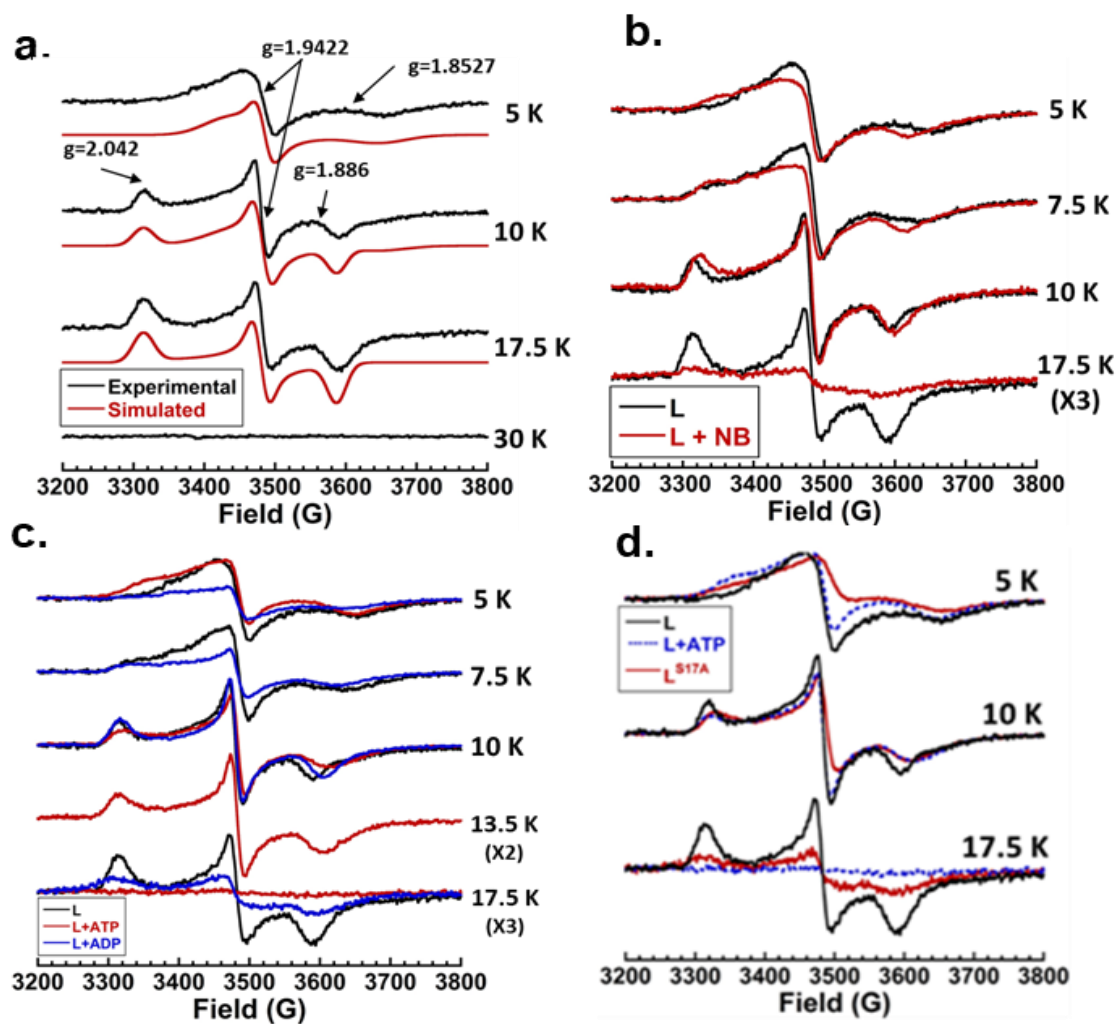


Fig. 3.6 EPR characteristics of BchL, BchNB and BchL tail mutant constructs under various nucleotide conditions.

a. Experimentally determined (black) and simulated (red) EPR spectra of BchL at 5 K, 10 K, 17.5 K, and 30 K. No absorbance was detected at 35K, typical of [4Fe-4S] clusters. There appear to be two species, a fast-relaxing almost-axial species ($g = [1.9750 \ 1.9422 \ 1.8527]$) and a slower-relaxing rhombic species ($g = [2.0420 \ 1.9442 \ 1.8860]$). The spectrum at 10 K was simulated using a 40 % axial:60 % rhombic mixture. The g -values for the axial signal are highly unusual in having all three values less than 2.0. In addition, the line shape could not be replicated well, probably due to rapid passage artifacts. The rhombic signal, on the other hand, is "well-behaved".

b. EPR spectra of BchL (black traces) and BchL with 1:1 BchNB (red traces) at indicated temperatures. Upon adding BchNB, there are spectral and relaxation changes. The high-field resonance of the axial signal occurs at a higher g -value (lower field) and features due to the g_1 of the rhombic signal persist (distorted by rapid passage) at 5 K. The rhombic signal is very similar in shape to that of the BchL protein alone, but in the presence of BchNB, the signal undergoes significant relaxation broadening at 17.5 K. **d.** EPR spectra of BchL (black traces), BchL incubated with excess ATP (red traces), and BchL incubated with excess ADP (blue traces) at indicated temperatures. ATP incubation produced the most drastic spectral and relaxation changes, particularly at higher temperatures, broadening relaxation almost entirely. ADP incubations produced similar, though not identical effects as BchNB incubation. **c.** EPR spectra comparing BchL (black solid lines) BchL incubated with excess ATP (blue dotted lines), and BchLS17A (Red solid lines) at 5 K, 10 K and 17.5 K where indicated.

3.3.4 A DFD amino-acid patch promotes inter-subunit cross-stabilization upon ATP binding.

The ATP-binding sites in BchL are situated away from the BchL:BchNB interaction interface (Fig. 3.7a). Thus, it may be possible that other regions between these two sites might function as a conduit for communication and be an important contributor to potential conformational changes and promote rearrangement of the flexible N-terminus. Comparison of the nucleotide-free (Fig. 3.7a), ADP-bound (Fig. 3.7b) and ADP-AlF₃-NB-bound (Fig. 3.7c) BchL crystal structures reveal a ‘DFD patch’ composed of amino acid residues Asp180, Phe181, Asp182 that undergo rearrangements and contact the hydroxyl groups of the sugar moiety of the bound nucleotide. Interestingly, the contacts only appear in the ADP-AlF₃-L-NB DPOR structure (Fig. 3.8c), and thus the DFD patch appears poised to be important for coordinating ATP-dependent conformational changes during complex formation and substrate reduction. D180 and D182 from one subunit form a network of interactions in *trans* with the sugar moiety of ATP bound to the neighboring subunit along with R244 in the nucleotide-bound subunit (Fig. 3.7c). This series of interactions was coined “inter-subunit cross stabilization of ATP”. These interactions appear to be stabilized in the ATP hydrolysis transition state- mimic structure when BchL is in complex with BchNB bound to Pchlide. One possibility is that ATP-binding drives inter-subunit cross stabilization and would provide the necessary conformational stability required to pry away the flexible N-terminal tail from binding across the [4Fe-4S] cluster, thus

relieving inhibition. If this were the case, mutations in the DFD patch would not affect ATP binding, but would perturb substrate reduction.

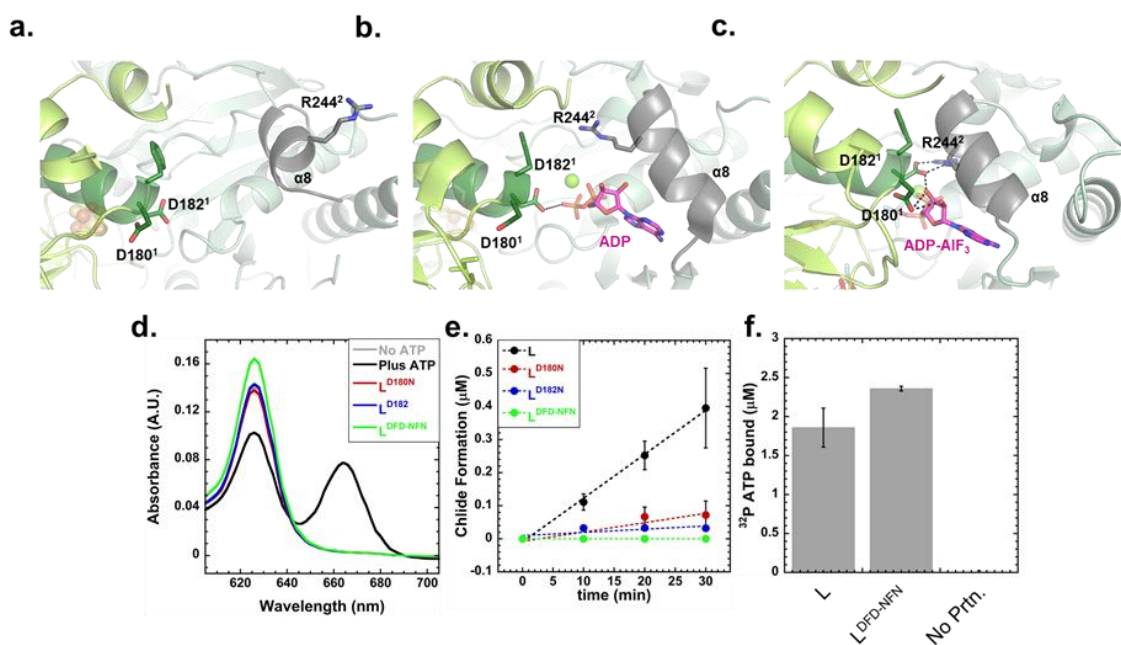


Fig. 3.7 Interactions between ATP and a DFD patch promotes inter-subunit cross stabilization and conformational changes in BchL.

Views of the DFD patch (highlighted in green) and associated interactions in three distinct conformations of BchL. **a.** In the absence of nucleotides, residues D180 and D182 on chain C form no notable interactions and are a large distance away from residue R244 on the opposing chain D. **b.** With ADP bound, the $\alpha 8$ -helix, highlighted in dark grey. Undergoes considerable motion, bringing R244 much closer to the DFD patch. Additionally, D182 now interacts with the bound ADP. **c.** When bound to ADP-AIF3 and in complex with BchNB, D180 and D182 have extensive interactions with both the bound nucleotide as well as inter-subunit interactions with R244. **d.** Pchlde reduction activity of BchL and variant proteins collected 60 minutes after addition of ATP. Chlide formation is monitored as a peak between 660-670 nm and occurs only in the presence of ATP. BchL^{D180N}, BchL^{D182N}, and BchL^{DFD-NFN}, are all defective for substrate reduction. **e.** Time course of Chlide formation for reactions containing BchNB, ATP and Pchlde in the presence of various BchL constructs. BchL reduces Pchlde to Chlide ($k_{obs} = 0.0126 \pm 0.0065 \mu\text{M}\cdot\text{min}^{-1}$), and no appreciable Chlide formation is observed for BchL^{D182N} or BchL^{DFD-NFN}. Severely impaired but detectable reduction activity is observed for BchLD180N ($k_{obs} = 0.0028 \pm 0.0042 \mu\text{M}\cdot\text{min}^{-1}$). **f.** Nitrocellulose filter binding analysis of ATP binding to BchL shows ~ 2 ATP bound per BchL dimer to both BchL and BchL^{DFD-NFN}, and no non-specific binding to the membranes is observed in the absence of BchL in the reaction.

To test this hypothesis, and the role of the DFD patch, I generated three BchL variants carrying amino acid substitutions wherein Asp180 (BchL^{D180N}), Asp182 (BchL^{D182N}), or both, (BchL^{DFD-NFN}) were substituted to Asn. Phe181 does not make contacts with the sugar and thus was not perturbed. BchL^{D180N} was poorly active for Pchlide reduction (Fig. 3.7d,e) whereas BchL^{D182N} and BchL^{DFD-NFN} were inactive (Fig. 3.7d,e), suggesting that both residues are important for function. Next, to precisely understand why mutations in the DFD patch affected substrate reduction, we analyzed the nucleotide binding, and EPR spectral properties of BchL^{DFD-NFN}. Nucleotide binding was measured by capturing the BchL:ATP complex using radiolabeled γ -³²P-ATP in a nitrocellulose filter binding assay. BchL binds to the nitrocellulose filter and ATP bound to the protein is retained on the membrane, while unbound ATP flows through the filter. Both BchL and BchL^{DFD-NFN} are capable of binding to ATP, and no ATP is retained on the membrane when no protein is present in the reaction (Fig. 3.7f). This finding is consistent with the ADP-bound crystal structure where no contacts between the DFD patch and the 5-carbon sugar of the nucleotide are observed (Fig. 3.7b). Thus, the loss in substrate reduction activity in the BchL^{DFD-NFN} protein occurs post ATP binding, and possibly due to a loss of the promotion of conformational changes necessary for multiple rounds of complex formation with BchNB.

EPR of BchL^{DFD-NFN} at 5 K (Fig. 3.8a,c) again revealed an FeS^A signal, though the rapid-passage distortions indicated that ATP binding enhanced relaxation in BchL^{DFD-NFN} whereas ATP inhibits relaxation in native BchL. The overall relaxation rates for FeS^A in native BchL and BchL^{DFD-NFN} can be summarized as BchL > BchL-ATP \approx BchL^{DFD-NFN}-ATP > BchL^{DFD-NFN}. At 10 K, the EPR spectra of both native BchL and BchL^{DFD-NFN} are almost indistinguishable and consist of 60% FeS^B, whereas the ATP complexes of both exhibit EPR signals indistinguishable from each other but containing only 35% FeS^B and 65% of the relaxation-inhibited FeS^A (Fig. 3.8b). The spectra of both native BchL and BchL^{DFD-NFN} at 17.5 K are again indistinguishable and are

due to FeS^{B} alone (Fig. 3.8b). In both cases, the signals are of diminished intensity upon addition of ATP due to enhanced relaxation, to about 25% in the case of $\text{BchL}^{\text{DFD-NFN}}\text{-ATP}$ and almost completely extinguished in native $\text{BchL}\text{-ATP}$. It is not clear whether the residual FeS^{B} signal from $\text{BchL}^{\text{DFD-NFN}}\text{-ATP}$ at 17.5 K is due to slower relaxation than in native $\text{BchL}\text{-ATP}$ or less than stoichiometric binding of ATP. So, overall, relaxation of FeS^{A} is markedly inhibited in $\text{BchL}^{\text{DFD-NFN}}$, indicating poorer coupling to a strained lattice in the capped species, while the cluster environments in the uncapped FeS^{B} species of native BchL and $\text{BchL}^{\text{DFD-NFN}}$ are indistinguishable by EPR (Fig. 3.8c); and the binding of ATP to both species provides very similar cluster environments for both FeS^{A} and FeS^{B} . Thus, ATP binding to $\text{BchL}^{\text{DFD-NFN}}$ does not elicit the complete portfolio of conformational changes required for substrate reduction.

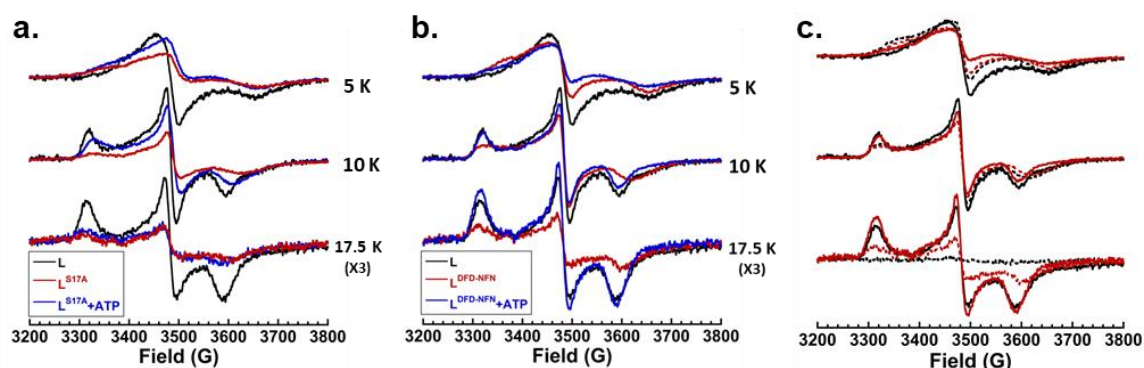


Fig. 3.8 EPR characteristics of BchL, and BchL DFD mutants.

a. EPR spectra of BchL (black traces), BchLS17A (red traces), and BchLS17A incubated with excess ATP (blue traces) at indicated temperatures. The slow relaxing axial species was distorted for BchLS17A compared to wildtype. The fast relaxing species was significantly broadened compared to wild-type and was unaffected by ATP incubation, though the mixed-species signal and axial species were both significantly diminished compared to wt. **b.** EPR spectra of BchL (black traces), $\text{BchL}^{\text{DFD-NFN}}$ (red traces), and $\text{BchL}^{\text{DFD-NFN}}$ incubated with excess ATP (blue traces). $\text{BchL}^{\text{DFD-NFN}}$ produced spectra similar to wt BchL with some minor distortions in the axial signal. ATP incubation with $\text{BchL}^{\text{DFD-NFN}}$ produced spectral changes similar to those produced for the wildtype BchL, though to a lesser extent. **c.** EPR spectra comparing wt BchL (black solid lines), BchL incubated with excess ATP (black dotted lines), $\text{BchL}^{\text{DFD-NFN}}$ (Red solid lines), and $\text{BchL}^{\text{DFD-NFN}}$ incubated with excess ATP (red dotted lines) at 5K, 10K, and 17.5K as denoted.

3.3.5 Binding of ATP to both subunits in the BchL dimer are required to generate a concerted motion to promote inter-subunit cross stabilization and drive substrate reduction.

Each BchL homodimer contains two sites for ATP binding (Fig. 3.1a), and the two subunits are covalently tethered by a single [4Fe-4S] cluster (Fig. 3.3a-c) (Fig. 2a-c). In the homologous NifH (Fe protein) of nitrogenase, it appears that the two sites bind to nucleotide with differing affinities, illustrated by a crystal structure of the Fe-protein with two different nucleotides occupying the dimer, suggesting that the two ATP sites could play distinct roles in substrate reduction (Fig. 3.9c). (Tezcan et al., 2015)

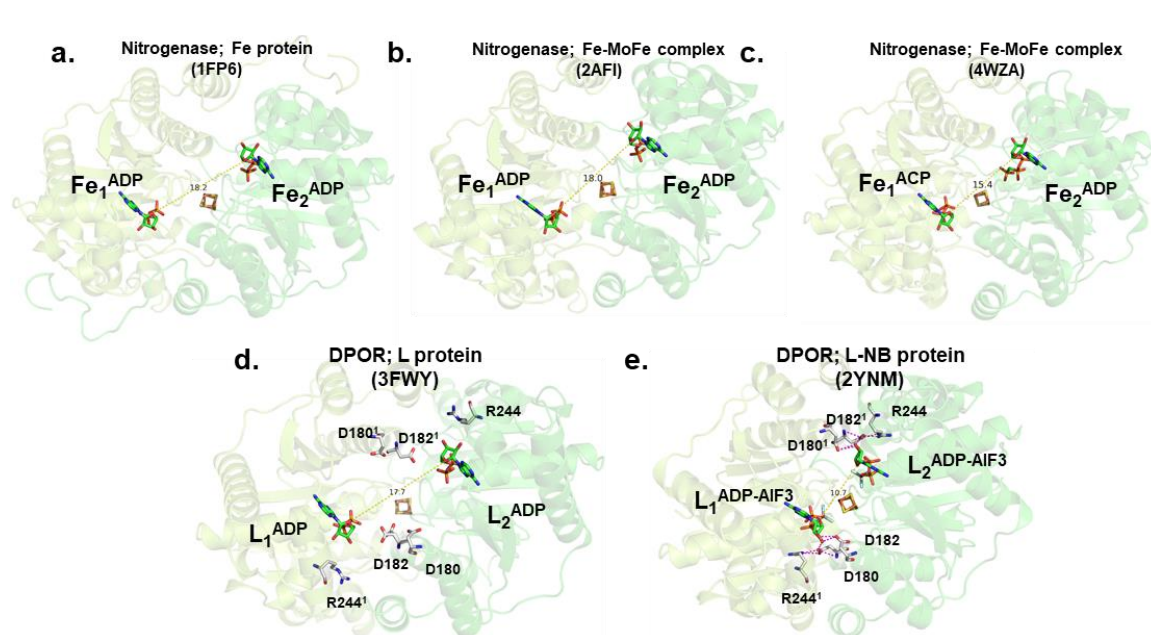


Fig. 3.9 Crystal structures of substrate-bound BchL and the Fe-protein from Nitrogenase.

Monomers are colored light and dark green as in previous figures, with highlighted residues and [4Fe-4S] clusters shown as sticks. Distance measurements are shown as dotted yellow lines. **a.** ADP-bound Fe-protein. **b.** ADP bound Fe-protein in complex with Mo-Fe protein. **c.** ADP and ACP bound Fe-protein in complex with MoFe protein. **d.** ADP bound BchL. **e.** ADP-AIF3 bound DPOR in complex with BchNB (not shown). BchL in 3FWY is from *R. sphaeroides*. BchL in 2YNM is from *P. marinus*.

To test the functional role of the two ATP-binding sites in BchL, I generated a covalently linked version of BchL by expressing the two subunits as a single polypeptide. The "linked" construct included an N-terminal 6x-poly histidine tag BchL followed by a Tobacco Etch Virus (TEV) protease site (the same N-terminal tag and protease site used for wild-type BchL, as well as all other described mutants). These subunits were either wild-type or a Walker A motif mutant which is unable to bind to ATP. This mutation in BchL is Lys44 (Fig. 3.10a), substituted with Ala in nucleotide binding mutant constructs. The two BchL subunits were covalently tethered by a flexible linker that connected the C-terminal end of the first monomer to the N-terminal end of the other (Fig. 3.10b). Covalent linkage of multimers can interfere with activity due to a variety of effects including conformational strain, non-specific interactions due to the linker, introduction of non-native secondary structures, or undefined effects. The linker was therefore constructed to carry TEV protease recognition sites bookending the linker region enabling proteolytic removal if the intact linker interfered with activity for any reason. (Fig. 3.10). I found that the length of the linker is a key determinant of protein activity. Linkers shorter than 15 amino acids are defective for substrate reduction, and optimal activity is obtained when linker lengths are longer than 20 amino acids (Fig. 3.11 a,c,d). The optimized linked-BchL behaved similarly to wild-type BchL during purification (Fig. 3.10c) and was stable and fully active for Pchlide reduction (Fig. 5d). Removal of the linker after protease cleavage also resulted in protein activity similar to the un-cleaved and wild-type BchL proteins (Fig. 3.11b). These results show that a linker of optimal length does not interfere with protein function. The linked L-protein appeared to have slightly faster activity. I believe that this is due to only one N-terminal tail being free to "cap" the [4Fe-4S] cluster, whilst the other is attached to the C-terminus of the first monomer and likely does not contribute to auto-inhibition of activity. This suggests that the 2 available N-terminal tails in the unlinked construct are dynamically interacting with the cluster.

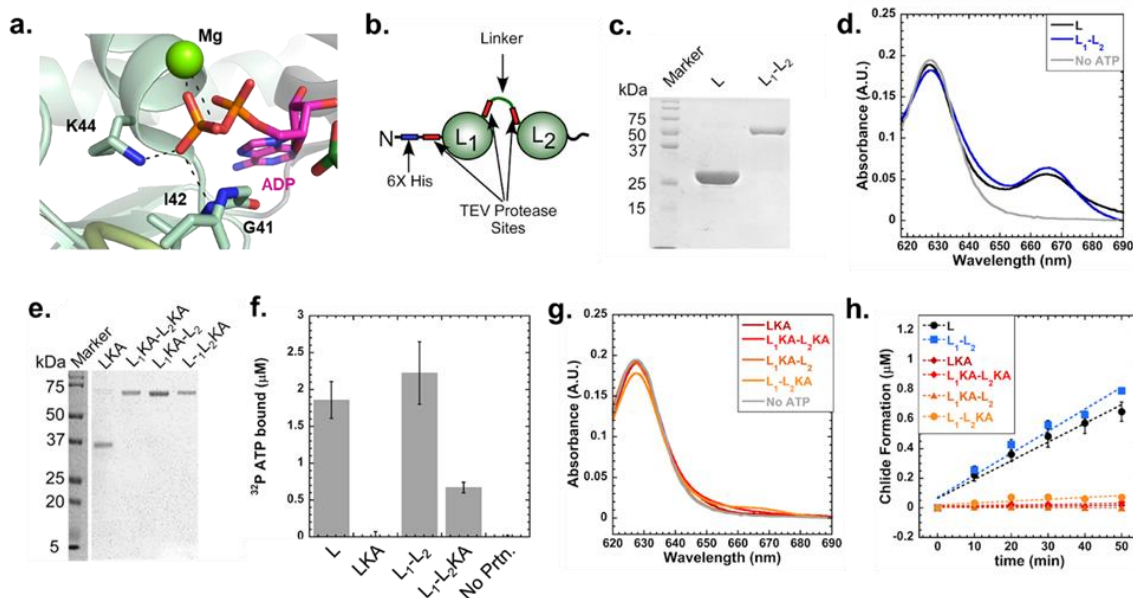


Fig. 3.10 Both ATP binding sites are required for DPOR activity.

a. Lys44 stabilizes nucleotide binding through interactions with the phosphate group of ADP (PDB: 3FWY). **b.** Schematic of the linked-L-protein design and the positions of the tobacco etch virus (TEV) protease cleavage sites. **c.** SDS-PAGE analysis of the purified BchL and linked-BchL-proteins. **d.** Spectroscopic analysis of Pchlde reduction activity of BchL (L, black trace), linked-BchL-protein (L_1 - L_2 , blue trace), and no ATP negative control (No ATP, grey trace). Pchlde absorbance is observed at 625 nm and Chlide formation is monitored at 665 nm 60 min post-incubation with ATP. **e.** SDS-PAGE analysis of the purified BchL^{K44A} (LKA) and versions of the singly (L_1 KA- L_2 or L_1 - L_2 KA) and doubly (L_1 KA- L_2 KA) mutated, linked, BchL-proteins. **f.** Nitrocellulose filter binding analysis of γ 32P-ATP binding by wildtype and Lys44 to Ala substituted BchL proteins. L and L_1 - L_2 are capable of binding ATP, whereas the singly substituted L_1 KA- L_2 is partially able to bind ATP. When both subunits are substituted with Lys44 to Ala, no ATP binding is observed. (g) Linked and unlinked BchL proteins carrying the K44A substitution are incapable of reducing Pchlde. Data shown were collected 60 min post-incubation with ATP. (h) Kinetics of Pchlde reduction measured as a function of Chlide formation is shown. L and L_1 - L_2 reduce Pchlde to Chlide ($k_{\text{obs}} = 0.01266 \pm 0.007 \mu\text{M}\cdot\text{min}^{-1}$ and $0.0148 \pm 0.0022 \mu\text{M}\cdot\text{min}^{-1}$, respectively.)

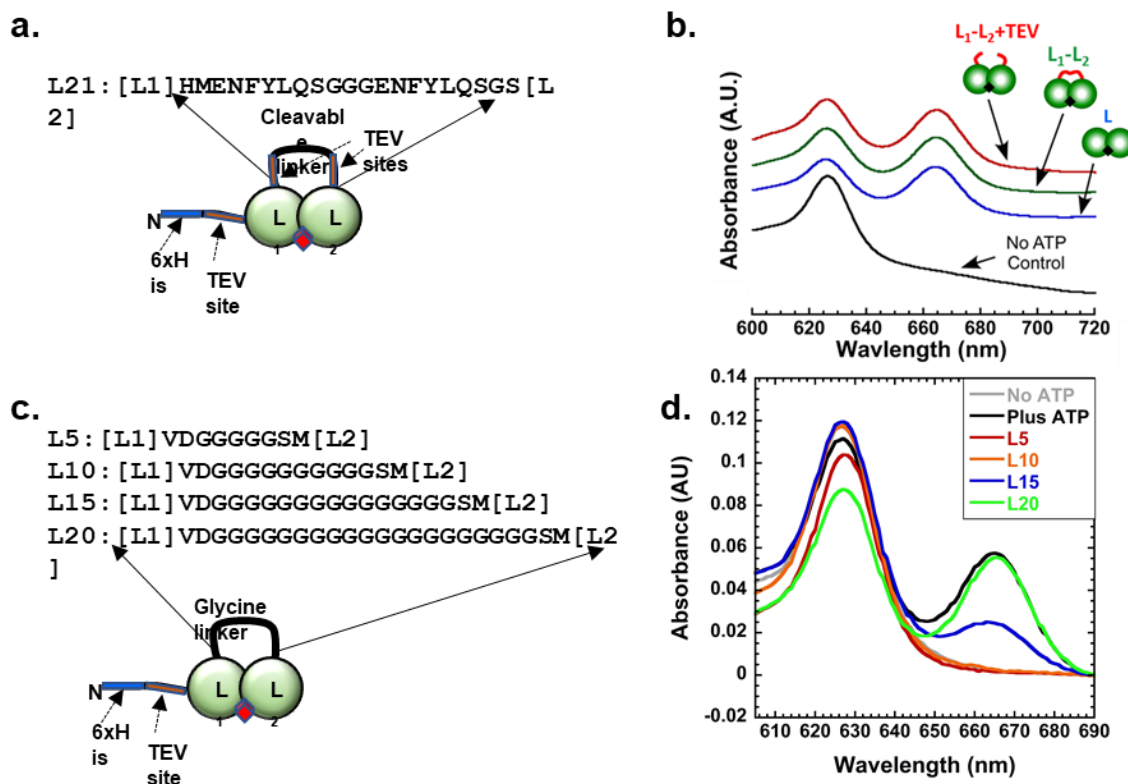


Fig. 3.11 Linked BchL dimer construction.

a. Cartoon representation of the generated cleavable linked BchL construct, and the amino acid sequence of the linker. **b.** Absorbance plot of acetone extraction of pigments after in vitro reaction. Cartoon representations of constructs are shown, and absorbance traces are shifted for clarity. The no ATP (negative control -black), WT reaction (positive control -blue), linked WT (green), and linked WT after cleavage with TEV protease (red) are shown. **c.** Cartoon representation of poly-glycine linkers lacking protease sites, with amino acid sequences of various linker lengths. **d.** Absorbance plot of acetone extraction of pigments after in vitro reaction. The no ATP negative control and WT reaction positive control shown as grey and black traces respectively. L5, L10, L15, and L20 construct traces are shown as red, orange, blue, and green lines, respectively.

Next, to assess the contribution of the individual ATP sites, I generated an ATP-binding (K44A) deficient mutation in one or both subunits in linked-BchL (Fig. 3.10e). Using filter binding analysis, I determined the amount of ATP bound to the linked and unlinked versions of BchL. BchL (L) and linked-BchL with unaltered ATP binding sites (L_1L_2) bind ATP to similar extents (Fig. 3.10f). The K44A substitution in the Walker-A ATP binding pocket of un-linked BchL (LKA) and in both subunits of the linked-BchL (L_1KA-L_2KA) abolishes ATP binding as expected (Fig. 3.10f). When only one of the two ATP binding sites are mutated ($L_1^{KA}-L_2$), partial ATP binding is observed (Fig. 3.10f). When ATP binding is perturbed in both sites, or in just one site, a complete loss of Pchlde reduction activity is observed (Fig. 3.10g,h). These data suggest that both ATP molecules in the BchL dimer are required for substrate reduction. These data sets suggest that binding of both ATP molecules likely causes cooperative conformational changes in the two halves of the L-protein homodimer and drive inter-subunit cross stabilization.

3.4 DISCUSSION.

Nitrogenase and nitrogenase-like enzymes such as DPOR and Chlorophyllide Oxidoreductase (COR) share structural similarity with respect to their electron donor and electron acceptor component proteins. These proteins catalyze multiple rounds of ET for substrate reduction, and transient association of the electron donor and electron acceptor is a prerequisite for each ET event. ATP binding to the electron donor is canonically assigned as the mechanistic trigger that promotes the assembly of the component proteins. However, the precise structural and functional principles underlying this ATP-driven process have largely remained unclear. The results presented in this study shed light on several ATP-binding driven changes in BchL that enable DPOR to function in an oxygenic environment.

In the nucleotide-free crystal structure, residues 16-29 are ordered in one of the four chains and suggest a novel regulatory role for the flexible N-terminus of BchL. Only one of the

four chains being ordered suggests that BchL has conformational diversity and suggests that a landscape exists of states where in one, the other, or neither tail are interacting with the cluster. Interestingly, the N-terminal tail binds across the [4Fe-4S] cluster and appears poised to block the docking surface for interaction with BchNB (Fig. 3.3a-c). The residues highlighted in purple (the surface that interacts with BchNB) of (Fig. 3.3c) occupying the same space as the tail in the nucleotide free structure. Six residues of each BchL chain are thought to interact with BchNB to form the DPOR complex. In the nucleotide free BchL structure, the disordered N-terminus from one subunit forms an inhibitory barrier across the docking surface, and hydrogen bonding affects three of the 12 docking residues (Cys 126, Gly 161, and Gln 168), suggesting that the N-terminus forms a barrier to docking and ET to BchNB. Mutations that perturb specific interactions in this region enhance the substrate reduction activity, supporting an auto-inhibitory role for this region in DPOR function (Fig. 3.5). Although binding of both ADP and ATP can be thought to trigger conformational changes leading to the displacement of N-terminal residues, only ATP hydrolysis drives the dissociation of the BchL-NB complex to complete the catalytic cycle. Therefore, the conformational change in the N-terminal region could be yet another way of coupling ATP-binding to BchL with Pchlide reduction in BchNB.

A BLAST-P analysis of residues 1-29 yielded BchL protein hits spread across ~150 species of bacteria. A nine-residue patch in the flexible N-terminus [DGEGSVQVH] (residues 13-21 in *R. capsulatus* BchL) is highly conserved, supporting functional significance (Fig. 3.3e). The flexible N-terminal region is unique to the DPOR system. The tail is not conserved in COR which catalyzes the subsequent reductive step in chlorophyll synthesis (Fig. 3.3e,3.4), and the entire N-terminal region does not exist in the Fe-protein of nitrogenase (Fig. 3.4a) The biological necessity for such a regulatory region remains to be established, though may exist as a mechanism to prevent off-target electron donation and the formation of free radicals in the cell.

The observations that substitutions in this region affect BchL stability *in vitro* suggests a potential role in protecting the [4Fe-4S] cluster against oxidation and off-target electron donation.

ATP binding to both subunits of BchL promotes a network of interactions between a conserved DFD patch and the sugar moiety of the nucleotide. This generates an inter-subunit cross stabilization as the DFD patch from one subunit contacts the nucleotide bound to the other. Such an ATP-binding dependent conformational change could generate an upward compaction of BchL leading to the release of the auto-inhibitory N-terminus from the docking interface and promote complex formation with BchNB (Fig. 3.12). Substitutions in either the DFD patch or rendering one subunit devoid for ATP binding abolishes substrate reduction activity. I propose a model where cooperative interactions between the DFD patch and the nucleotide relieves the auto-inhibition by the N-terminus of BchL and is a key regulatory step in transient assembly of the DPOR complex (Fig. 3.12). I propose that the interaction of the N-terminus is a dynamic equilibrium, and that ATP binding pushes the pool of BchL toward a more cluster-exposed one. This may be the result of the conformational changes induced by binding of ATP that alter distances necessary for ionic interactions between the tail and the dimer, the emergence of different competing ionic bonds not found in existing structures, or the free energy change associated with solvating an unfolded amino acid compared to being bound across the cluster. In any case, the larger pool of cluster exposed BchL is illustrated by the modest increase in activity upon mutation of the tail, and the slight increase in activity in the linked BchL construct where only tail is available to “cap” the cluster. It is also possible that there may also be cooperative effects in the binding of BchL to BchNB that are coordinated by the disordered N-terminus (or termini) that may be perturbed in the mutant construct(s). In the related nitrogenase complex, several crystal structures of the homologous Fe-protein have been solved in complex with a variety of nucleotides in the absence and presence of the MoFe-protein. In these structures, the relative distances between the two nucleotides does not change (Fig. 3.9). Since the flexible N-

terminal region is not conserved in the Fe-protein, it may indicate the presence of a different protective mechanism in the nitrogenase system.

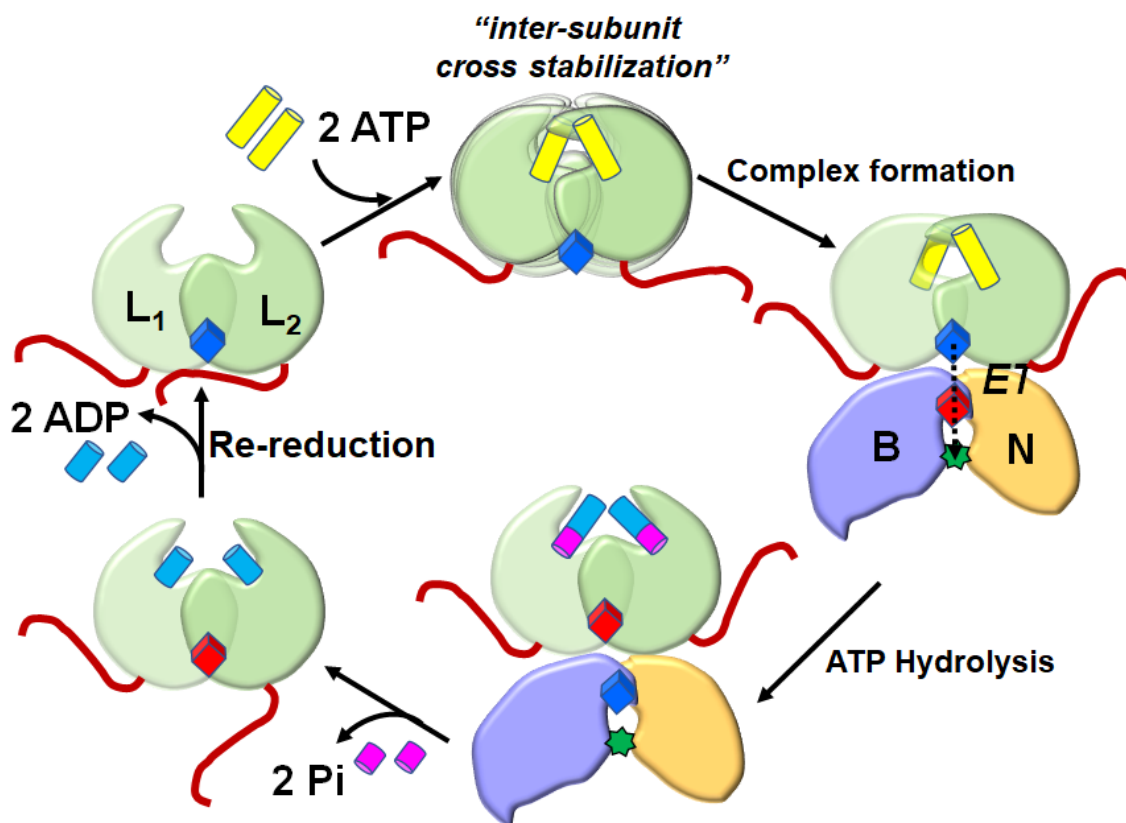


Fig. 3.12 Model for ATP-binding induced release of auto-inhibition by the flexible N-terminus of BchL.

Cartoons depict the BchL dimer (green) with one of the two disordered N-termini binding across the [4Fe-4S] cluster (blue; reduced form). ATP (yellow) binding promotes inter-subunit cross stabilization and associated conformational changes through interactions between the DFD patch and ATP; thereby releasing the flexible N-terminus from the docking surface. Complex formation to the BchNB protein ensues followed by electron transfer (ET), ATP hydrolysis, and product (ADP, Pi) release. The oxidized BchL [4Fe-4S] cluster is depicted in red. The BchL [4Fe-4S] cluster is subsequently re-reduced by ferredoxin.

In DPOR, the subtle structural changes observed between the ADP-bound and the nucleotide-free crystal structures indicate how nucleotide-binding enables BchL to carry out ET to BchNB. These changes likely play 2 tandem or cooperative roles of conformationally gating binding of BchL to BchNB, as well as modulating the redox properties of the cluster. This is made clear by the changes in the EPR spectra of the nucleotide free vs ATP-bound BchL and BchL tail mutants. This suggests that ATP binding both relieves conformational auto-inhibition by shifting the pool of BchL molecules toward a more cluster exposed state, as well as priming the cluster for ET by modulating its redox potential.

Predictable changes occur around the ATP-binding pocket: comparison of the two structures suggest that the Switch II region may act as a redox switch. The Switch II region is fully conserved between BchL and NifH (the nitrogenase Fe protein), including Phe135 in NifH (Phe163 in BchL), which has been demonstrated to be important for the redox properties of the [4Fe-4S] cluster of NifH. In the absence of ADP, the local environment immediately surrounding the BchL-cluster is more packed and hydrophobic, promoted by the interactions of Leu155, Val158, and Phe163 (Fig. 3.13). In general, for redox-active metal centers, hydrophobicity increases reduction potential, suggesting that in the absence of Mg-ADP, the BchL-cluster is less likely to become oxidized. While electrochemical data is not available for BchL, studies with NifH show that in the presence of ATP or ADP, the midpoint reduction potential is 120-160 mV more negative, indicating that oxidation of the [4Fe-4S] cluster of NifH for electron transfer to the P-cluster becomes more favorable in the presence of nucleotides. The conservation of Switch II sequence suggests that the redox properties of the [4Fe-4S] cluster of BchL could be similarly modulated. The van der Waals interaction observed between the [4Fe-4S] cluster of BchL, its ligand Cys160, and Phe163 (Fig. 3.13) could be a means of modulating the redox properties of the BchL-[4Fe-4S] cluster in the presence and absence of nucleotides.

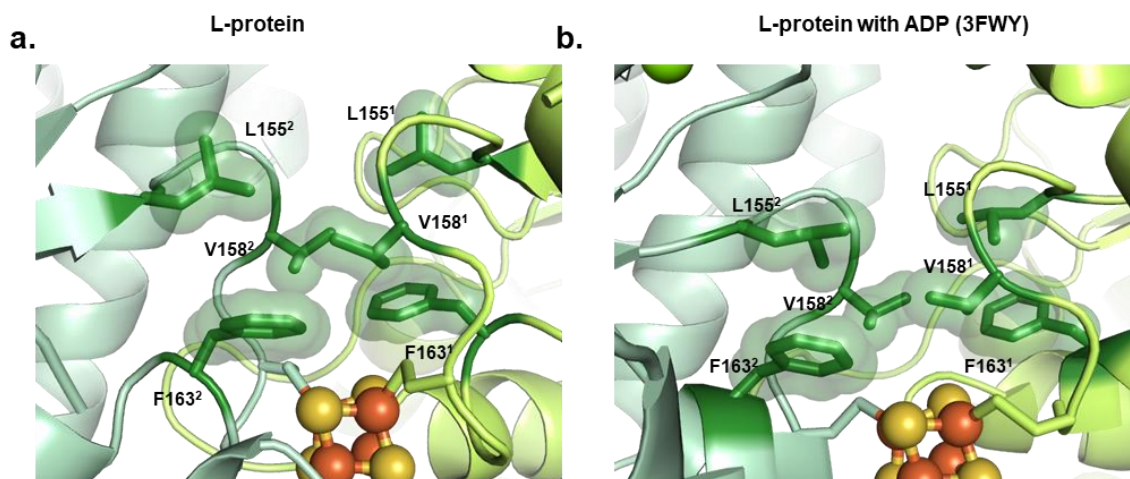


Fig. 3.13 Perturbations in the Switch-II region change the local environment around the [4Fe-4S] cluster.

a. Highlighted in dark green are the interactions of six hydrophobic residues, Leu155, Val158 and Phe163 on each chain, in the absence of nucleotide **a.** and presence of ADP **b.** The environment directly above the [4Fe-4S] cluster becomes less hydrophobic upon the addition of ADP, largely as a result of repositioning of the adjacent Phe163 residues relative to the cluster. More hydrophobic environments generally correlate with increased reduction potential for redox-active metal centers, suggesting that the binding of Mg-ADP acts as a form of redox control in BchL by increasing the tendency of the cluster to become oxidized.

CHAPTER 4. ESTABLISHMENT OF SEQUENTIAL ELECTRON TRANSFER IN BCHNB.
4.1 INTRODUCTION.

Many oligomeric enzymes that transfer electrons for catalysis or substrate reduction have two identical active sites and their subunits are arranged with a head-to-head or head-to-tail symmetry. The electron acceptor component proteins DPOR, COR and nitrogenase are arranged as $\alpha_2\beta_2$ tetramers, which are separable from their electron donor components, highlighted in (Fig. 4.1.a). A similar architecture is also seen in the nitric oxide synthase and ribonucleotide reductase family of enzymes, among others. Given the evolutionary and functional significance of these enzymes, a mechanistic significance must exist behind such structural assemblies. In gymnosperms, the cyanobacteria *Prochlorococcus marinus* and all photosynthetic eubacteria, DPOR catalyzes the reduction of protochlorophyllide (Pchl_{id}) to chlorophyllide (Chl_{id}), the penultimate step in the biosynthesis of chlorophyll and bacteriochlorophyll.

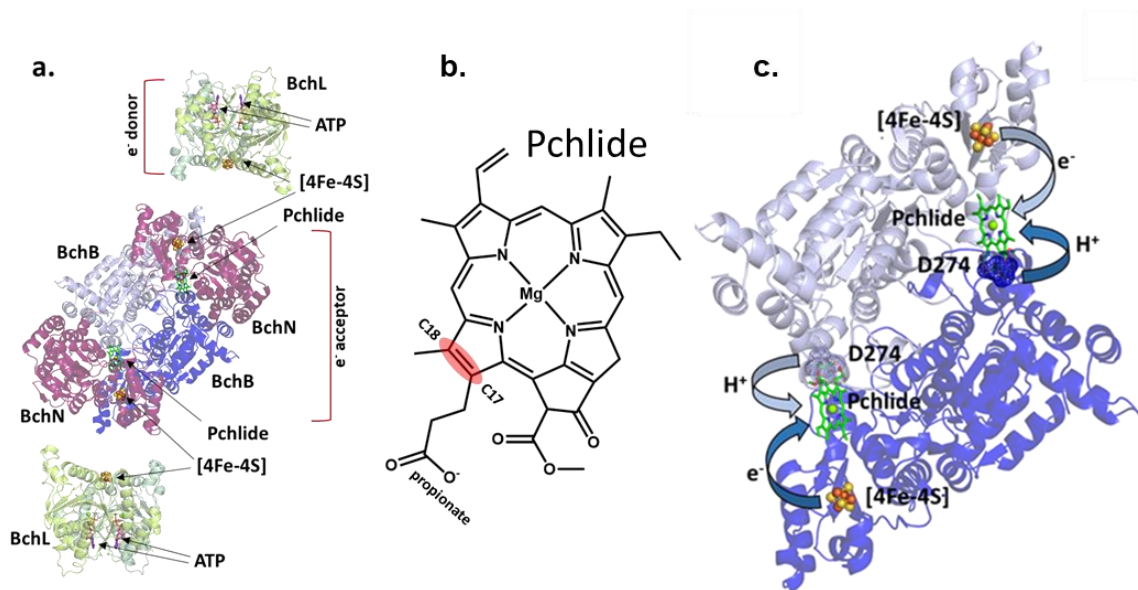


Fig. 4.1 DPOR components, reaction stoichiometry, and electron transfer pathways.

a. Crystal structure of DPOR components (PDB:2YNM). BchN, BchB, and Bch, are shown as purple, light and dark blue (emphasizing the boundaries between BchB subunits), and light and dark green cartoons respectively. Substrates and cofactors are shown as sticks and indicated by arrows. **b.** Crystal structure BchB shown as light and dark blue cartoon. Asp274 is shown as colored dots, Pchlido and [4Fe-4S] clusters are shown as sticks. Electron and proton donation directions are denoted with colored arrows.

DPOR consists of electron donor (BchL) and electron acceptor (BchN-BchB; BchNB) component proteins (Fig. 4.1a). BchL is a homodimer containing one [4Fe-4S] cluster ligated at the dimer interface by two cysteine residues per monomer and possesses one ATP binding site per monomer. BchNB is a $\alpha_2\beta_2$ tetramer carrying one [4Fe-4S] cluster and substrate (Pchlido) binding site per half of the tetramer. ATP binding to BchL drives the assembly of the BchL and BchNB proteins and the transient assembly of this complex promotes electron transfer (ET). The electron is transferred from the [4Fe-4S] cluster of BchL, to the [4Fe-4S] cluster of one half of BchNB and finally to the C17-C18 double bond of Pchlido. Two rounds of electron and proton transfer are required to reduce Pchlido to Chlide (see earlier chapters). In DPOR, one proton

required for reduction originates intrinsically from within the C17 propionate of Pchl_{ide} (Fig. 4.1b), and the second proton is donated in *trans* from an Asp274 of the opposing BchB subunit (Fig. 4.1c). (Muraki et al., 2010) Chl_{ide} is subsequently reduced by the structurally homologous Chlorophyllide Oxido-Reductase (COR) in the bacteriochlorophyll biosynthetic pathway. These reductive steps fine tune the spectral and reactive properties of bacteriochlorophyll to be optimally suited for photosynthesis.

An overarching question about these enzymes centers on their conserved architectural complexity: Why are these enzymes assembled as two functional halves, and how do they cooperatively function during substrate reduction? Since two rounds of ET (per half) are required for substrate reduction, multiple BchL binding and dissociation cycles occur at each BchNB half. The two BchL binding interfaces on BchNB are situated ~100Å apart. If their binding events are coordinated, long-range, inter-subunit allosteric communication is necessary. Here, I explored these fundamental mechanistic questions using DPOR. I show that the two halves indeed communicate, and that perturbation of substrate reduction activity at one half abolishes ET at the other, thus stalling the entire DPOR complex. Unique EPR signatures of the [4Fe-4S] cluster of the BchNB protein provide evidence that, in the presence of BchL and ATP, BchNB can be reduced before binding of Pchl_{ide}, enabling the first ET to Pchl_{ide} in the absence of the BchL protein. This process is similar to the ‘deficit-spending’ mechanism observed in nitrogenase. Finally, it is shown that Pchl_{ide} binding to BchNB sets the functional asymmetry within the complex and the initial ET event is used as a sensory mechanism to recognize Pchl_{ide} and trap it in the active site. I propose that the $\alpha_2\beta_2$ architecture in DPOR serves to correctly recognize and orient the incoming substrate. The recognition then triggers sequential ET which is coordinated through allosterically controlled conformational changes between the two halves of the BchNB complex. The findings explain key functional advantages of the oligomeric architecture found in many enzymes that catalyze electron transfer reactions.

4.2 MATERIALS AND METHODS.

4.2.1 Generation of protein expression constructs.

The coding regions for BchL, BchN, and BchB were PCR amplified from *Rhodobacter sphaeroides* genomic DNA and cloned into pRSF-Duet 1 or pET-Duet 1 plasmids as described. (Nomata, Kitashima, et al., 2006b). The appropriate C-terminal poly-histidine or strep-tags and D27A mutagenesis were engineered onto/into BchB using Q5 site-directed mutagenesis (New England Biolabs, Ipswich, MA).

4.2.2 Generation of Pchl_{ide}.

Pchl_{ide} was generated as described in chapter 2.2.5 of this document.

4.2.3 Protein synthesis and purification.

Wild-type/mutant BchNB and BchL protein complexes were purified as described in chapter 2.2.6 of this document. The following modified procedure was used for purification of the half-reactive BchNB complex. Plasmids encoding BchN, His-BchB and Strep-BchB were co-transformed into *E. coli* BL21(DE3) SufFeScient cells. The transformants were grown, and protein overproduction was induced as described for the wild-type BchNB complex. After lysis (as described), the clarified lysates from His-tagged or dual tagged constructs were loaded onto an Nickel-nitrilotriacetic acid (Ni²⁺-NTA; 1.6 mL suspended beads/L growth) column (Thermo Scientific) equilibrated with 10 column volumes (CVs) STD (100 mM HEPES PH7.5, 150 mM NaCl) buffer. Non-specifically bound proteins were washed off with 10 CVs STD buffer containing 20 mM imidazole. Bound proteins were eluted into a septum sealed bottle using 30 mL STD buffer containing 250 mM Imidazole. The clarified lysates from Strep-tagged BchNB were loaded onto a Strep-Tactin Sepharose column (IBA, Germany; 1.6mL resuspended beads/L

growth) equilibrated with 10 CVs STD buffer. Post washing with 10 CVs STD buffer, bound proteins were eluted using 30 mL STD buffer containing 2.5 mM Desthiobiotin (IBA).

Asymmetric or dual tagged BchNB constructs followed the methods described for Ni²⁺-NTA columns and for Strep columns but performed sequentially. Eluted BchNB proteins were concentrated using a spin concentrator (30 kDa molecular weight cut-off). Proteins were aliquoted in the glove box into 1.2 mL cryo-tubes which have a gasket sealed cap (Cat. #430487 Corning). Closed tubes with protein were removed from the glove box and flash frozen using liquid nitrogen and stored under liquid nitrogen. Protein concentrations were determined using Bradford reagent with bovine serum albumin as reference.

4.2.4 Western blotting.

Western blots were performed on samples after separation on 10% SDS-PAGE. Proteins were transferred (100 mA for 90 min) on to nitrocellulose membranes. Membranes were washed thrice with TBST (Tris buffered saline plus 0.1 % (v/v) Tween-20), and rocked for 15 minutes after the third rinse. Membranes were blocked with 5 % (w/v) milk in TBST for 1 hour at 25 °C. Membranes were then washed with TBST thrice as before, then exposed to primary antibody. Membranes were exposed to StrepMAB-Classic HRP conjugate (IBA) primary antibody (1:34000 dilution in TBST) for 1 hour while rocking at 25 °C and/or anti-poly-histidine antibody, HRP conjugate (Invitrogen) (1:1000 dilution in TBST plus 1 % (w/v) milk) overnight (~17 hours) while rocking at 4 °C. Membranes were then washed, rocked for 3 hours after the third rinse before adding detection reagent (Pierce Fast Western Blot Kit, ECL substrate, Thermo Scientific). Blots were imaged using an AI 600 imager (GE Healthcare).

4.2.6 Assay for substrate reduction by DPOR.

Reduction of Pchl_{ide} to Chl_{ide} was measured spectroscopically by mixing BchN-BchB protein (3 μ M tetramer), BchL-protein (9 μ M dimer), and 35 μ M Pchl_{ide}, in the absence or presence of ATP (3 mM) in STD buffer + 10mM MgCl₂. 40 μ l of these reactions were quenched with 160 μ l of 100 % acetone (80% v/v final concentration). The acetone extraction was then spun down in a tabletop centrifuge at 13,226 x g for 4 minutes to pellet precipitated protein components. 160 μ l of the supernatant was transferred to a cyclic olefin half-area well plate (catalog #4680 Corning) and absorbance scans from 600 nm to 725 nm were recorded on a SpectraMax i3x plate reader (Molecular Devices). Chl_{ide} appearance was represented as the absorbance value at 666nm.

4.2.7 EPR Spectroscopy.

EPR spectra were obtained at 10 K on an updated Bruker EMX-AA-TDU/L spectrometer equipped with an ER4112-SHQ resonator (9.48 GHz) and an HP 5350B microwave counter for precise frequency measurement. Temperature was maintained with a ColdEdge/Bruker Stinger S5-L recirculating helium refrigerator, and an Oxford ESR900 cryostat and MercuryITC temperature controller. Spectra were recorded with either 0.3 G (3×10^{-5} T) or 1.2 G (0.12 mT) digital field resolution with equal values for the conversion time and the time constant, 5.2 mW incident microwave power, and 12 G (1.2 mT) magnetic field modulation at 100 kHz. EPR simulations were carried out using Easyspin [Stefan Stoll, Arthur Schweiger. EasySpin, a comprehensive software package for spectral simulation and analysis in EPR. *J. Magn. Reson.* 178(1), 42-55 (2006)].

Samples for EPR Spectroscopy. Reactions contained various combinations of BchL, BchNB, Pchl_{ide}, and ATP. 200 μ L EPR samples contained 1.7 mM dithionite, and, where

indicated in the figure legends, 40 μM BchL, 20 μM BchNB, 40 μM Pchlde, and 3 mM ATP. Samples from Fig. 4.5a contained 60 μM BchNB, and/or 120 μM Pchlde. All samples were incubated in the glove box for 60 minutes unless otherwise denoted. Protein samples were prepared and transferred to the EPR tubes in the glove box and stoppered with a butyl rubber stopper. Samples were removed from the glove box and immediately flash frozen in liquid nitrogen and then analyzed by EPR.

4.2.8 Steady State Pchlde Binding Fluorescence titrations.

2.0 mL mixtures of BchNB (various concentrations) and Pchlde (20 μM) were made in the glove box in STD buffer with 10 mM MgCl_2 , then incubated for 20 minutes before being transferred to an airtight 2 mL SEPTA screw cap cuvette (Firefly Scientific). Fluorescence emission spectra were recorded on a PTI fluorometer (Photon Technology International) excited at 440 nm, with excitation and emission slit widths of 1.5 mm and 3.0 mm respectively. PMT voltage and slit widths were maintained between replicates.

4.3 RESULTS.

4.3.1 A half-reactive DPOR complex is defective for substrate reduction.

To test the importance of the $\alpha_2\beta_2$ architecture for function, I first generated a half-reactive version of DPOR and tested overall Pchlide reduction activity. BchN and BchB are expressed as separate open reading frames and form a constitutive tetramer in the cell. To generate a half-reactive BchNB complex, I employed a dual-affinity tag approach where two BchB open reading frames were generated coding for either a poly-histidine affinity tag or a Strep-tag affinity on the N-terminus. N-terminal positioning of either affinity tag does not affect Pchlide reduction activity as their rates of Pchlide reduction are similar (Fig. 4.2a,b; blue and red traces). Reduction of Pchlide to Chlide results in a spectral shift with appearance of an absorption maxima at 666 nm. It is worth noting that placing affinity tags on the C-terminus of BchB perturbs Pchlide reduction activity (data not shown). These tagged-BchB constructs were co-expressed along with an untagged version of the BchN polypeptide. This strategy generated an ensemble of BchNB tetramers carrying either two poly-histidine tagged BchB, two strep-tagged BchB, or one of each in the context of a BchNB tetramer (Fig. 4.2c). This dual-tagged approach enabled sequential fractionation of the mixed population of BchNB proteins over Ni^{2+} -nitriloacetic acid (NTA) and Strep-Tactin-agarose resins. The final purified BchNB complex had one BchB subunit carrying a poly-histidine tag and the other a Strep-tag (Fig. 4.2e). The presence of the appropriate affinity tags over the sequential purification steps were confirmed by western blotting using anti-His and anti-Strep antibodies (Fig. 4.2g,i).

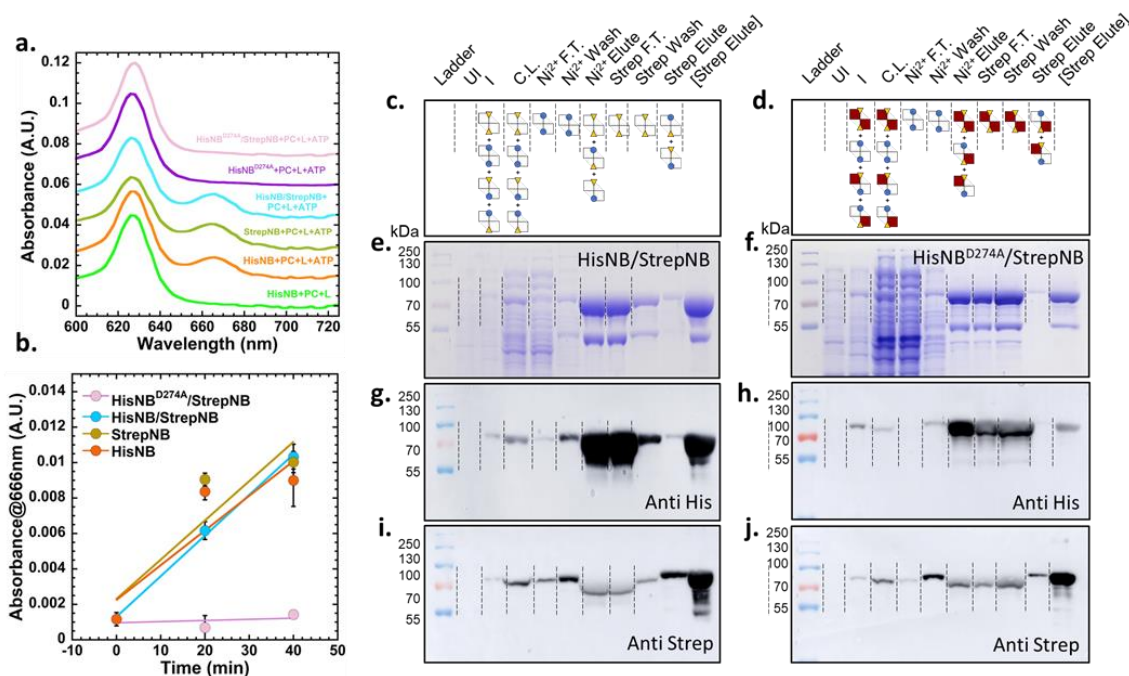


Fig. 4.2 Asymmetric BchNB mutants are incapable of complete Pchlide reduction.

a. Absorbance spectra of acetone extracted pigments samples after 60-minute reactions. Protein constructs and components included in reactions are denoted above absorbance spectral traces. Traces represent average of $n=3$ samples. **b.** Quantification of $n=3$ activity assays of half-reactive asymmetric mutant construct, asymmetric (dual tag) wt construct, strep-tagged BchB, and 6xHis tagged BchB shown as pink, light blue, brown, and orange circles respectively. **c,d.** Cartoon representation of theoretical protein pools in each sample. 6xHis tag(s) are shown as yellow triangles, Strep tag(s) are shown as blue circles. BchN, wild-type BchB, and BchB^{D274A} are shown as white triangles, white squares and colored (red and black) squares respectively. **e.** Coomassie-stained 10% SDS-PAGE gel tracking purification of wt asymmetric (dual tagged) protein preparation. **f.** Coomassie stained 10% SDS-PAGE gel tracking purification of asymmetric half-reactive protein preparation. **g.** Anti-6xHis western blot of identical samples from 4.2e. **h.** Anti-6xHis western blot of identical samples from 4.2f. **i.** Anti-Strep western blot of identical samples from 4.2e. **j.** Anti-Strep western blot of identical samples from 4.2f.

To generate a half-active BchNB complex, I introduced an Asp274 to Ala substitution only in the BchB subunit carrying the poly-histidine tag. Asp274 acts as one of the necessary proton donors for Pchl_{id}e reduction, the other coming from the Pchl_{id}e itself (Fig. 4.1b,c). (Muraki et al., 2010) Asp274 interacts with the Pchl_{id}e molecule and substitution of Asp274 to Ala has been shown to perturb substrate reduction in DPOR. (Muraki et al., 2010) When expressed along with wild-type BchN and wild-type Strep-tag BchB, a mixture of BchB complexes were generated (Fig. 4.2d) carrying either entirely wild-type BchNB (strep-B:[BchN]₂:strep-B); mutant BchNB (his-B^{D-A}:[BchN]₂:his-B^{D-A}); or half-active BchNB (his-B^{D-A}:^A:[BchN]₂:strep-B). Using the dual-affinity purification strategy, it was possible to isolate the half-reactive BchNB (his-B^{D-A}:^A:[BchN]₂:strep-B; Fig. 4.2f) and confirmed the presence of both affinity tags by western blotting using the above described antibodies (Fig. 4.2h,j). It should be noted that although the intensity of anti-his and anti-strep blots are not 1:1 in the final purified protein, this is likely due simply to the different antibodies. Future experimentation should incorporate a concentration standard with the two antibodies to confirm a 1:1 ratio of Strep and His-tagged NB in the final construct.

Next, Pchl_{id}e reduction activity of the dual-tagged wild-type and half-active BchNB complexes was monitored by mixing them with Pchl_{id}e, BchL and ATP. While wild-type BchNB carrying either affinity tag reduces Pchl_{id}e (Fig. 4.2a,b; green trace), the half-active BchNB is defective for Pchl_{id}e reduction (Fig. 4.2a,b; black trace). These data show that two functional halves in the context of the $\alpha_2\beta_2$ BchNB tetramer are required for substrate reduction.

The predicted sequence of Pchl_{id}e-reduction events in DPOR involve binding of Pchl_{id}e to BchNB, the binding of BchL to BchNB and the respective electron transfer events. In addition, ATP binding and hydrolysis within the BchL complex are elemental steps in substrate reduction. Since the half-active BchNB proteins were defective for overall Pchl_{id}e reduction, we next sought to identify where the enzyme stalled in the catalytic cycle. Thus, we focused on measuring

the electronic properties of the [4Fe-4S] clusters of BchNB using electron paramagnetic resonance (EPR) spectroscopy. Unfortunately, the protein yields of the half-active BchNB protein were minimal after the dual-affinity purification and hence precluded us from performing detailed EPR studies. The cause for the low yield could be due to many factors. First, even if the ratio of wild type to mutant to half reactive mutant was stochastic during synthesis, the yield of half reactive mutant compared to normal growth would be ~25%. I believe that this is also coupled to conformational instability of a BchNB complex that is in a pseudo-transition state (where one D274 has been mutated), which may be unstable, or that the synthesis machinery of *E. coli* prefers assembling proteins with the same sequence in both halves of the tetramer due to the conformations adopted. This explanation lends credence to the significant conformational role of the protonation state of Asp274. Due to the low yields of asymmetric BchNB, we investigated the spectral properties of wild type and variant (BchNB^{D274A}) DPOR complexes to capture the steps in the electron transfer cycle.

4.3.2 The [Fe-S] cluster of BchNB matches a simulated $s=7/2$ spin state which can be pre-reduced, and re-primed for sequential reactions – a ‘deficit spending’ model.

The Asp274 residue in BchB is unique in its role as a proton donor to Pchl_{ide}. Structurally, it functions in *trans*, where Asp274 from one half of the BchNB tetramer serves as the proton donor to the Pchl_{ide} molecule bound to the active site of the opposing half BchNB (Fig. 4.1c) (Muraki et al., 2010)(Sarma et al., 2008). Thus, this residue serves as a key communication element between the two halves of the $\alpha_2\beta_2$ BchNB tetramer. The [4Fe-4S] cluster of BchNB is ligated by three Cys residues from BchN (C29, C54 and C115) and one Asp residue from BchB (D36; Fig. 4.3a). To better understand the catalytic events in DPOR, I first focused on the intrinsic electron transfer properties of the [4Fe-4S] cluster of BchNB.

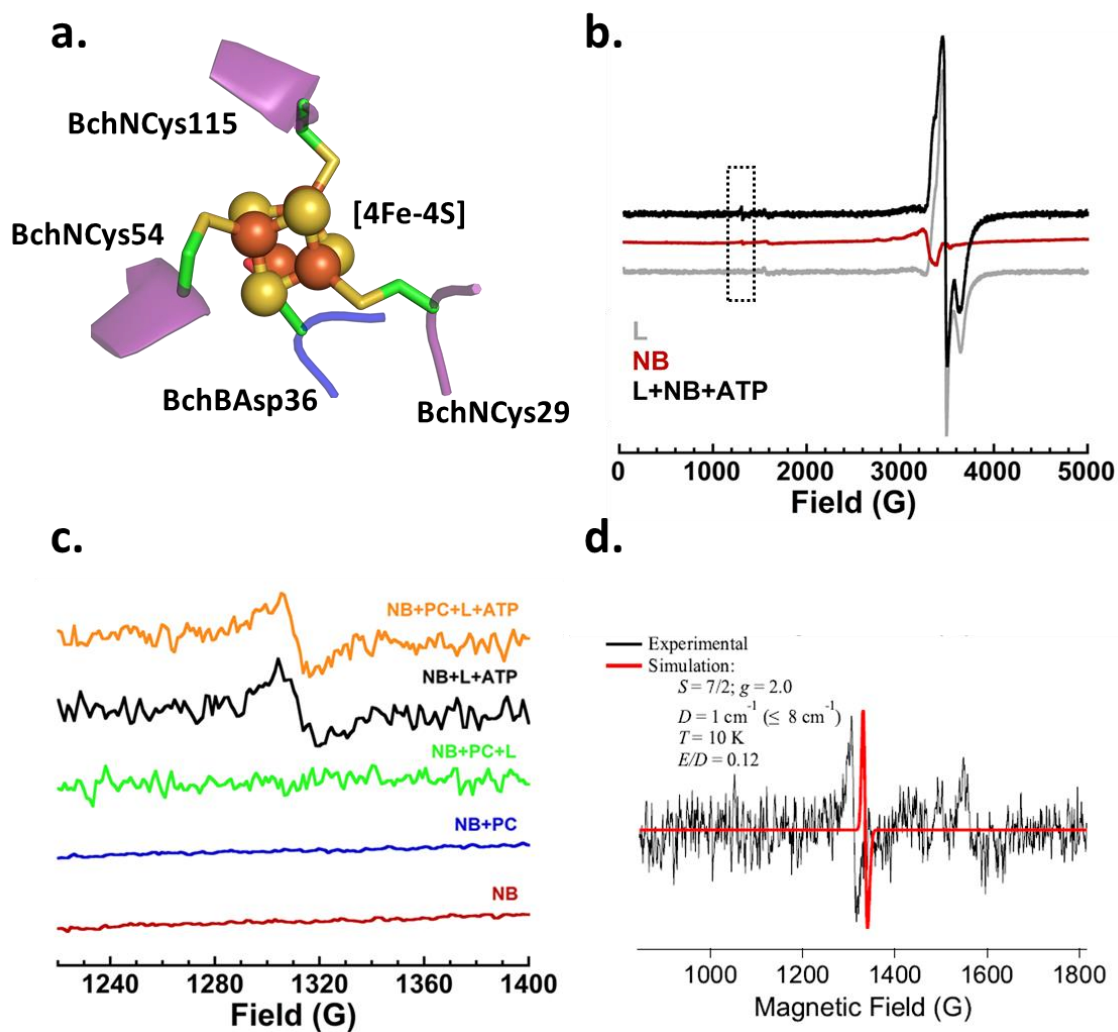


Fig. 4.3 The [4Fe-4S] Cluster of BchNB

a. Crystal structure of the [4Fe-4S] cluster of BchNB (PDBID:2YNM). Ligands are labeled, and colors of BchN and BchB are identical to Fig. 4.1. **b.** EPR spectra of DPOR components. Components in each spectrum are denoted in the figure legend. **c.** EPR spectra of DPOR components/reactions. Reaction components are denoted in above each trace. **d.** Experimentally derived (black) and simulated (red) EPR spectra of $S=7/2$ spin state cluster. Experimental and simulation conditions are denoted.

The EPR spectral properties of the BchNB [4Fe-4S] cluster have not been thoroughly characterized. Thus, the EPR spectra of BchNB alone was measured first, in complex with its substrate (Pchl_{ide}), and upon addition of BchL (+/- ATP). The [4Fe-4S] cluster of BchNB is EPR silent (Fig. 4.3b; red trace). In comparison, the [4Fe-4S] cluster of BchL produces a large signal in the ~3500 G range as reported previously (Fig. 4.3b; grey trace). Even at 3-fold higher BchNB concentrations (90 μM tetramer) in the EPR reactions no EPR signature is observed (Fig. 4.3c; red trace). When Pchl_{ide} is added to BchNB, a change in signal is not observed (Fig. 4.3c; blue trace). When BchNB, BchL and Pchl_{ide} are mixed together in the absence of ATP, the signal for the [4Fe-4S] cluster for BchL is observed, but no new signals for BchNB are observed (Fig. 4.3c; green) trace. This finding is not surprising, as ATP binding to BchL is required to drive complex formation between BchNB and BchL.

When BchL and ATP are introduced to the reaction containing BchNB in the absence of Pchl_{ide}, a peak appears at ~1300 G (Fig. 4.3b,c; black traces). This suggests that ATP-bound BchL forms a complex with BchNB in the absence of Pchl_{ide} and donates an electron to the [4Fe-4S] cluster of BchNB. When the entire reaction is reconstituted with BchL, BchNB, Pchl_{ide}, and ATP, the steady state reaction results in the presence of the ~1300 G peak (Fig. 4.3c; orange trace). By modulating the temperature and reaction conditions, this EPR signal of the uniquely ligated BchNB cluster was visible. The spectrum matches a simulated $s=7/2$ spin state (Fig. 4.3d). Previous models for DPOR suggest that the [4Fe-4S] cluster of BchNB exists in an oxidized state, binds to Pchl_{ide}, followed by complex formation with BchL and the transfer of the first electron from BchL to BchNB and then onto Pchl_{ide}. In these experiments, since BchL can reduce BchNB in the absence of Pchl_{ide}, an alternate possibility exists where BchNB could be pre-reduced in the cell followed by Pchl_{ide} binding, and the subsequent transfer of the first electron to Pchl_{ide}. This model is congruent with the “deficit spending” mechanism proposed for nitrogenase, wherein the

first electron donation to substrate is accomplished before ATP-dependent reduction from the Fe-protein (electron donor component). (Seefeldt et al., 2012)

Next the kinetics of substrate reduction in DPOR was measured by following the appearance of the absorbance signal at 666 nm (Fig. 4.4a), and the appearance of the ~ 1300 G EPR signal (Fig. 4.4b). Reduction reactions containing BchL, BchNB, and Pchlide were initiated by adding ATP and quenched samples were assessed for electron transfer (EPR) and Pchlide formation (absorbance). The appearance of the EPR signal correlates with the formation of Chlide, albeit at a slower rate (Fig. 4.4c), suggesting that a) the EPR signal represents electron transfer to the [4Fe-4S] cluster of BchNB, and b) Since rate of appearance of the EPR spectra lag behind the Chlide formation signals (absorbance signals), the EPR signal likely reflects the re-reduced cluster on BchNB. Thus, during the reaction, the BchNB cluster is always in a reduced state, and primed to donate an electron to Pchlide during the next substrate reduction cycle – as would be expected in the ‘deficit spending’ model.

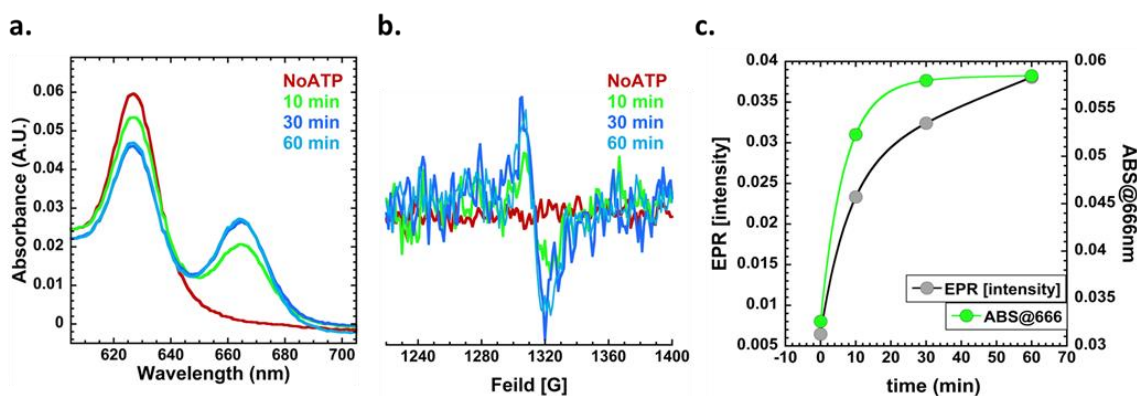


Fig. 4.4 Electrons are re-loaded onto BchNB after catalysis

a. Absorbance spectra of acetone extracted pigment from samples from EPR reaction shown in **b.** No ATP negative control, 10-minute sample, 30-minute sample and 60 minute samples shown as red, green, dark blue and light blue lines respectively. **b.** EPR spectra of samples from Fig. 4.1b, identical color traces. **c.** EPR intensity at 1300G (grey circles, left Y-axis) and absorbance at 666nm values (green circles, right Y-axis) vs time plot from 4.4a,b.

4.3.3 Asp274 to Ala substitution reveals unresolved electron transfer intermediates in BchNB and a sequential substrate reduction mechanism within the two halves.

Establishment of the order of Pchl_{ide} binding to BchNB is necessary to understand the mechanism of ET. From the half-reactive BchNB experiments I deciphered that multiple rounds of ET do not occur when one or both BchNB halves carry a substitution in the proton donor residue - Asp274. Thus, I proposed that a stalled BchNB intermediate could be identified through EPR for the BchNB^{D274A} complex. Interestingly, the EPR signature of BchNB^{D274A} (in the absence of Pchl_{ide}, BchL or ATP) showed the presence of a peak at ~1300 G, indicative of the presence of a reduced [4Fe-4S] cluster (Fig. 4.5a; brown trace). This is in stark contrast to wild type BchNB that is EPR silent (Fig. 4.5a; red trace). This suggests that the substitution at Asp274 influences the electronic properties of the [4Fe-4S] cluster either by physically promoting structural changes in the protein that make the cluster more accessible to the reductant (dithionite) in the reactions, or by propagating/perturbing a network of amino acid interactions that change the reduction potential of the cluster, making it EPR visible.

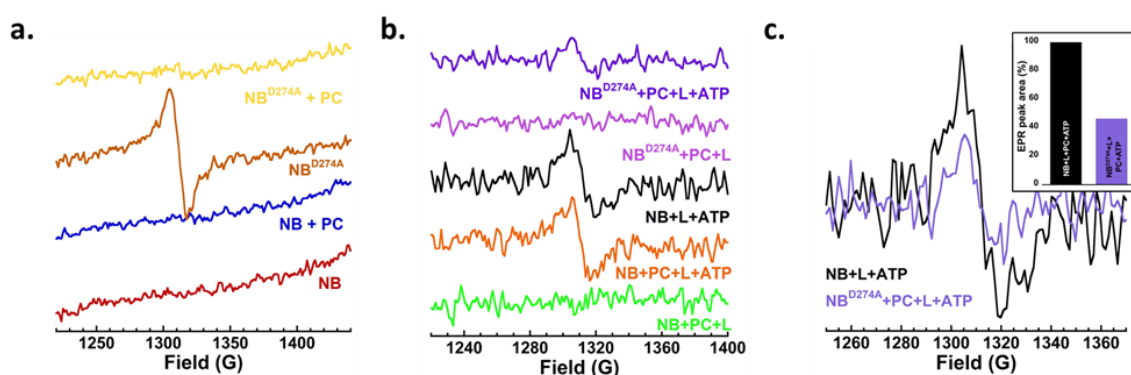


Fig. 4.5 BchNB^{D274A} is synthesized with electrons pre-loaded, reveals stalled intermediate.

a. and b. EPR spectra of various DPOR components/reactions. Protein(s) and/or substrate(s) are denoted above individual traces. **C.** EPR spectra of samples from Fig. 4.1b, identical color traces, highlighting area integrated for quantifying inset.

Analysis of the apo and Pchl_{id}-bound BchNB crystal structures show large scale conformational changes that might explain this difference (Fig. 4.6) The collapse of the binding pocket in wild type BchNB, in the absence of Pchl_{id}, also likely serves as a protective mechanism for the [4Fe-4S] cluster. Chapter 3 of this document describes the unique protective mechanism in the BchL protein where a flexible disordered region in the N-terminus bound across the [4Fe-4S] cluster and autoinhibited BchL activity. The inhibition is released through conformational changes upon ATP binding. It is possible that the collapse of the Pchl_{id} binding pocket might serve a similar protective role in BchNB as the cluster is not able to be reduced. Because the addition of BchL and ATP alone reduces the [4Fe-4S] cluster of BchNB, this suggests that binding of BchL alone plays a role in the conformational landscape that BchNB can/must navigate to successfully reduce Pchl_{id}. Binding of Pchl_{id} alone induces oxidation of the BchNB [4Fe-4S] cluster (at least in the D274A context), which unsurprisingly suggests that Pchl_{id} binding is also involved in the conformational landscape of BchNB. Therefore, The conformation of BchNB likely dictates the propensity of the [4Fe-4S] cluster to donate or accept electrons. In short, BchNB can bind to Pchl_{id} in the absence of BchL; similarly, BchL can bind to BchNB in the absence of Pchl_{id} and donate an electron (in the presence of ATP). Thus, Pchl_{id} or BchL binding to BchNB are likely not mutually exclusive events and a specific order of binding may not dictate overall substrate reduction activity.

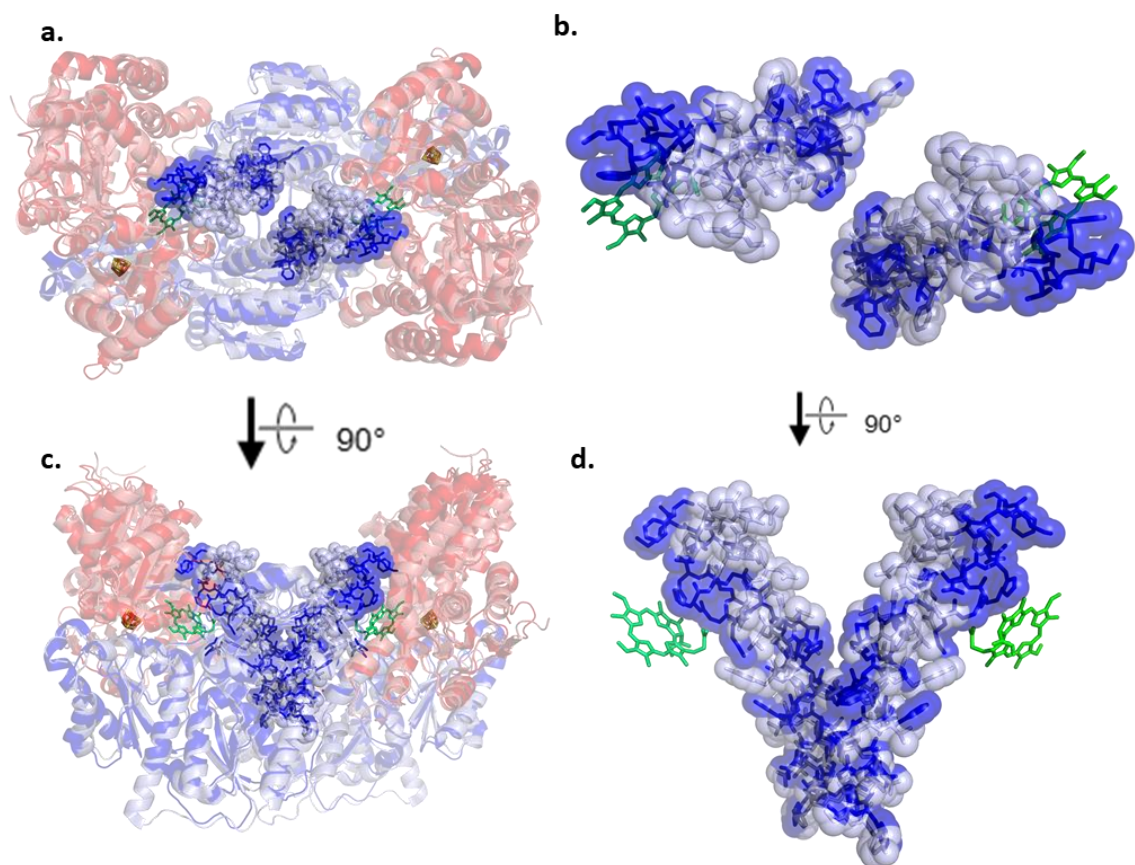


Fig. 4.6 Comparison of BchNB and Pchlde-bound BchNB crystal structures

a. Top view of crystal structure of BchNB (Dark red and blue, PDBID: 2XDQ) and Pchlde-bound BchNB (light red and blue, PDBID: 3AEK) after structural alignment, shown as semi-transparent cartoon(s). [4Fe-4S] clusters and Asp274 (*R. sphaeroides* numbering) are shown as sticks, and Pchlde is shown as green sticks. The last alpha helix of either structure is shown as semi-transparent balls, and opaque sticks. Color schema are maintained throughout entire figure. **b.** Same view as that of **a.**, showing only the terminal helix, highlighting conformational changes around the bound Pchlde molecule. **c.** Side view of the structure shown in **a.** **d.** Side view of the structure shown in **b.**

Since BchNB^{D274A} is defective for Pchl_{ide} reduction, but is preloaded with electrons, it was next tested whether ET occurs. When incubated with Pchl_{ide}, the EPR spectra for the [4Fe-4S] cluster of BchNB^{D274A} disappears (Fig. 4.5a; yellow trace). Thus, BchNB^{D274A} donates its preloaded electrons to Pchl_{ide}. The complete disappearance of the EPR signal implies that the first ET event occurs in both halves. Proton transfer may be necessary to stably oxidize the cluster of BchNB^{D274A}. It may be that the first proton donation always comes from Pchl_{ide} itself. Alternatively, the inability to protonate the radical Pchl_{ide} may induce substrate release. Upon release, the radical on Pchl_{ide} would likely form a hydroxide radical with the surrounding solvent. In either case, the electron is lost from the cluster of BchNB^{D274A}.

Interestingly, when BchNB^{D274A} is incubated with BchL, Pchl_{ide} and ATP, the EPR signal at ~1300 G is resurrected (Fig. 4.5b; violet trace). However, the intensity of the EPR peak is almost exactly 50% of the amplitude of the signal observed for wild-type BchNB under similar conditions (Fig. 4.5c). This is indicative of a stalled intermediate where re-reduction of only one of the two [4Fe-4S] clusters of BchNB has occurred. The data also affirm the interpretation that the EPR signal at ~1300 G for wild type BchNB (and the BchNB^{D274A} without Pchl_{ide}) reflects two total electrons per tetramer – one per BchNB half.

These findings further support the sequential ET model in DPOR where events in one half control activity in the other. If the two halves were to act independently, a) the half-reactive DPOR complex should have been able to retain partial Pchl_{ide} reduction activity, but this is not the case (Fig. 4.2). b) Similarly, in the EPR analysis, for an independent model, the amplitude of the spectra for BchNB^{D274A} should have been either around 100% or 0% that of wild-type BchNB, but this again is not the case (Fig. 4.5c). Thus, I propose that an intrinsic functional asymmetry exists in DPOR.

4.3.4 Direct measurements of Pchl_{ide} binding to BchNB reveals cooperative substrate binding and a substrate sensing mechanism that establishes functional asymmetry.

Since the two halves in the BchNB complex appear to transfer electrons to Pchl_{ide} in a sequential manner, I next tested how asymmetry is established. Either BchNB, when synthesized, is intrinsically endowed with asymmetric Pchl_{ide} binding properties through differences in active-site conformations between the two halves, or the first Pchl_{ide} binds stochastically to a symmetrical BchNB, establishes asymmetry, and allosterically controls the second Pchl_{ide} binding event. To test these models, I directly monitored Pchl_{ide} binding by capturing the changes in fluorescence upon binding to BchNB. A scan of the fluorescence properties of Pchl_{ide} shows an excitation and emission maxima at 440 and 636 nm, respectively (Fig. 4.7).

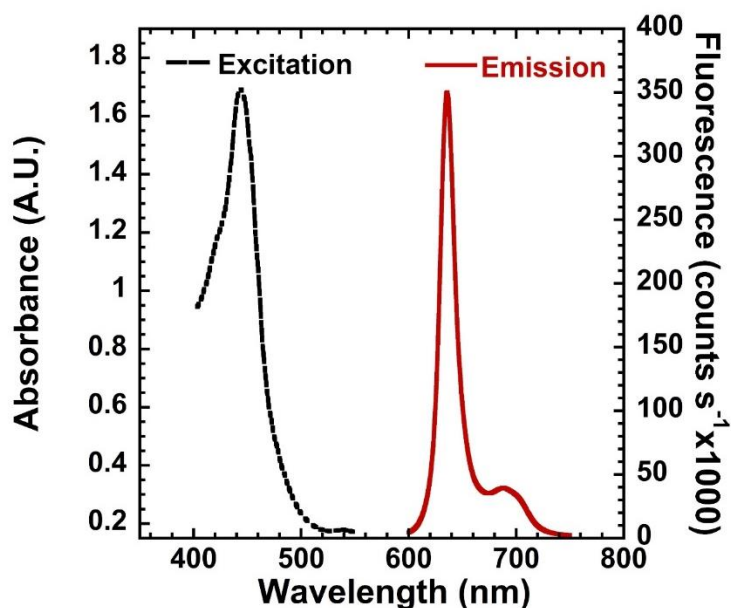


Fig. 4.7 Excitation/emission spectra of Pchl_{ide}

Excitation/absorbance maxima (black dotted line) and emission (red line) spectrum of BchNB-Pchl_{ide} complex.

Based on the spectral features, I excited a sample of Pchl_{id}e at 440 nm and measured the change in fluorescence (Fig. 4.8a; red trace). When BchNB is added to the reaction, the fluorescence emission of Pchl_{id}e increases ~750-fold (Fig. 4.8a; black trace). The utility of Pchl_{id}e fluorescence to investigate its binding to other proteins has been controversial. One such study using protochlorophyllide reductase (POR) showed no significant changes in Pchl_{id}e fluorescence upon binding to Pchl_{id}e; as non-specific binding to BSA also generated similar changes in fluorescence. Thus, such changes in Pchl_{id}e fluorescence were ascribed to non-specific solution partition effects. This is not the case for Pchl_{id}e binding to the BchNB complex. Under my reaction conditions, BSA does not produce a change in Pchl_{id}e fluorescence (Fig. 4.8a; blue trace). Thus, for the BchNB complex, changes in Pchl_{id}e fluorescence are an excellent measure of binding. The differences between fluorescence enhancement in Pchl_{id}e bound to BchNB vs POR are likely due to differences in the binding pocket. Fluorescence tends to increase the more hydrophobic the environment, and the binding pocket of DPOR is certainly more hydrophobic than the aqueous environment. A crystal structure does not exist for POR complexed with Pchl_{id}e. It may be that there is simply a much less hydrophobic interaction between POR Pchl_{id}e compared to BchNB and Pchl_{id}e. BchNB completely envelopes Pchl_{id}e, it is possible that POR does not exclude Pchl_{id}e from solvent to the same extent.

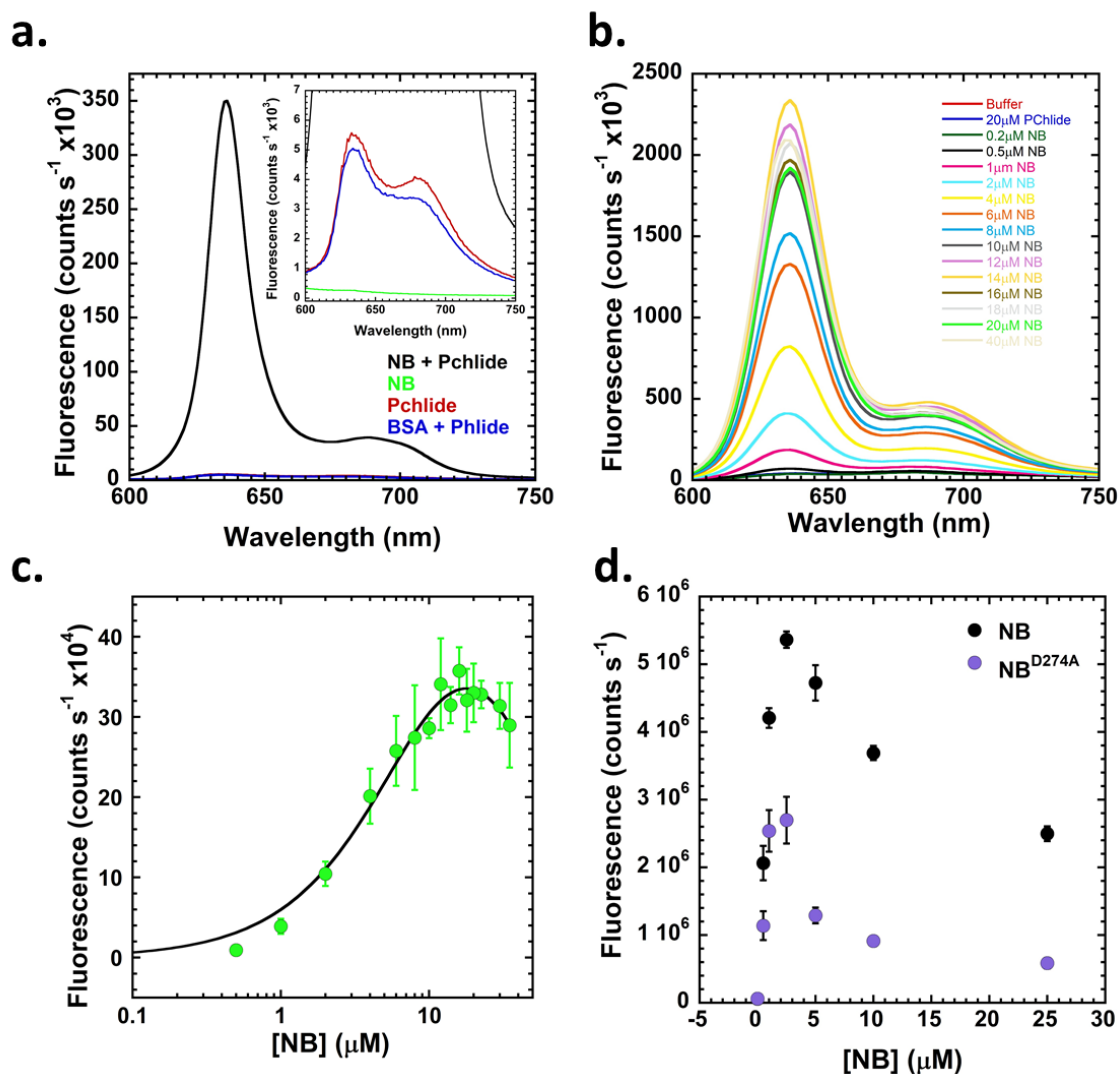


Fig. 4.8 Pchlde fluorescence as a measure of Pchlde binding

a. Fluorescence emission spectra of purified BchNB/Pchlde mixture (black), BchNB (green), Pchlde (red), and Bovine Serum Albumin (BSA)/Pchlde mixture (Blue). Inset, zoomed in on y axis to highlight fluorescence fold change. Representative Fluorescence spectra of Pchlde (20 μ M) titrated with BchNB (various concentrations). **c.** Fluorescence count at 636 nm plotted against BchNB concentration. **d.** Similar to 6c. Wild type BchNB and BchNB^{D274A} are shown as black and purple circles respectively.

Since the fluorescence signal arises from Pchl_{ide}, I performed binding experiments with a fixed concentration of Pchl_{ide} and titrated in increasing concentrations of the BchNB tetramer (Fig. 4.8b). An increase in Pchl_{ide} fluorescence is observed as a function of BchNB concentration (Fig. 4.8c). The signal plateaus when enough BchNB is present to bind all the Pchl_{ide} molecules in the reaction and fit well to a double exponential plus linear fit for the given titration. Curiously, when an excess of BchNB is added to the reaction the fluorescence does not plateau. Instead, a drop in the Pchl_{ide} fluorescence is observed (Fig. 4.8c), which did not fit well to the same fit used for Fig. 4.8c, and so was not fit in Fig. 4.8. As the concentration of BchNB is increased in the reaction, the equilibrium likely shifts from a 2-Pchl_{ide} bound BchNB complex (higher fluorescence) to a 1-Pchl_{ide} bound complex (lower fluorescence). The quantum yield of the 2-Pchl_{ide} bound complex is likely different than the 1-Pchl_{ide} bound complex. Given the asymmetry in BchNB activity, I propose that one Pchl_{ide} is bound in a conformation different than the other. The conformational differences likely contribute to two different quantum yields for Pchl_{ide} fluorescence when bound to BchNB.

When similar binding experiments are performed with the BchNB^{D274A} variant, I observed a similar overall profile where an increase in Pchl_{ide} fluorescence is observed. The signal saturates stoichiometrically, as observed for wild-type BchNB. Thus, both active sites are Pchl_{ide} bound. However, for BchNB^{D274A}, the fluorescence quantum yield upon reaching stoichiometry is half that observed for wild-type BchNB. These data suggest that either the conformational positioning or electronic landscape of the bound Pchl_{ide} molecules are different between BchNB^{D274A} and wild-type BchNB.

Extrapolating back to the EPR results, the spectra obtained for the wild type BchNB likely reflect one electron transferred to each Pchl_{ide} molecule. This could function as a sensing step to recognize and lock in the Pchl_{ide} within the active site. The EPR spectra for BchNB^{D274A}, measured under the same conditions, also show ET to the bound Pchl_{ide} molecules (Fig. 4.5a). In

BchNB^{D274A}, the inability to donate the second proton from Asp274 to Pchl_h is perturbed, the first coming from Pchl_h itself. In the presence of BchL and ATP, complex formation between Pchl_h-bound-BchNB and ATP-bound-BchL occurs. This re-reduces the [4Fe-4S] cluster on BchNB. The extent of re-reduction is 50% in the BchNB^{D274A} variant and thus Pchl_h reduction is not achieved in either active site. This evidence points to sequential ET in the DPOR system and the Asp274 residue serves as a key sensor in communicating the electron transfer status between the two halves.

4.4 DISCUSSION

The oligomeric $\alpha_2\beta_2$ structural arrangement observed in the BchNB complex of DPOR is found in a host of enzymes, especially in enzymes that catalyze ET reactions. These enzymes have two diametrically situated, identical active sites. In DPOR, extensive structural contacts between the two active sites are a prominent feature with one half contributing a key proton donor (Asp274) in *trans* to the Pchl_h molecule bound in the active site of the opposing subunit. Thus, allosteric and direct communication between the two halves likely controls the catalytic steps in the ET and Pchl_h reduction mechanisms. These findings support this model and show communication between the two active sites. In the half-reactive engineered version of BchNB, where one site is wild-type and other carries a D274A substitution, Pchl_h reduction activity in both halves is abolished. Thus, in this scenario, the half-reactive enzyme does not go through multiple rounds of ET required for Pchl_h reduction. The proposed sequence of catalytic events for DPOR activity involves:

1. Pchl_h binding to both active sites of BchNB. Upon synthesis in the cell, BchNB is either structurally asymmetric with respect to the organization of the two identical active site dictating the order of Pchl_h binding to the two active sites, or the active sites are identically poised to accept Pchl_h and stochastic binding of Pchl_h to one or the other site sets the

asymmetry within BchNB. Contrary to previous models, data presented here show that the [4Fe-4S] cluster of BchNB exists in a reduced state and can donate the first electron to Pchl_{id}e upon binding in the absence of BchL. In the steady state experiments, the EPR spectra corresponding to the [4Fe-4S] cluster of BchNB shows a persistent reduced state well after the time course of Pchl_{id}e reduction (Fig. 4.4). This mechanism is similar to the ‘deficit spending’ model proposed for nitrogenase, where the first ET in the MoFe-protein occurs before binding of the Fe-protein. Whether this first ET occurs sequentially in both active sites of BchNB, or just within one site (thus maintaining asymmetry) is yet to be determined. Another interesting observation is the difference in pre-reduced states of the presented wild-type BchNB and the BchNB^{D274A} variant. The [4Fe-4S] cluster of BchNB^{D274A} is always pre-reduced and is visible in EPR (Fig. 4.5a). The wild-type BchNB protein is EPR silent (Fig. 4.3c). This difference suggests conformational differences around the [4Fe-4S] cluster between the wild-type and variant BchNB complexes. However, both proteins bind to two Pchl_{id}e molecules (Fig. 4.8d).

I propose that the Asp276 residue is used to sense and communicate the presence of Pchl_{id}e molecule within the active site and the deficit spending mechanism might be an integral part of this process. This sensing and selection of Pchl_{id}e likely serves two roles - a) it correctly positions the porphyrin-ring structure of Pchl_{id}e within the active site, and b) it helps DPOR differentiate between Pchl_{id}e and Chl_{id}e. Chl_{id}e is the reduced product of Pchl_{id}e and must dissociate from the active site of DPOR. Chl_{id}e then binds to the active site of chlorophyllide oxidoreductase (COR), the next enzyme in the pathway. COR is structurally similar to DPOR, but the difference between Pchl_{id}e and Chl_{id}e is one double bond in the C17-C18 position of the porphyrin ring. Thus, the initial positioning and sensing of Pchl_{id}e by the Asp274 residue likely serves as a ‘substrate-check’ in the active site of BchNB.

2. The next step in the DPOR mechanism is the binding of BchL to BchNB. It is noteworthy that while it is logical to think of Pchlide binding to BchNB as the first step, followed by complex formation with BchL, these steps need not be sequential or even dependent on one another. BchL forms a complex with BchNB in the absence of Pchlide and transfers electrons (Fig. 4.3c). Thus, a direct measure of the kinetics and thermodynamics of complex formation between BchNB and BchL, and the influence of Pchlide, would be required to better understand the complexities underlying complex formation in DPOR. Similarly, when BchL binds to BchNB, these events occur on both halves of the BchNB complex. Whether these binding events are stochastic, cooperative/independent, and how they contribute to overall asymmetry remains to be investigated. The crystal structure of DPOR wherein BchL is bound to the ATP hydrolysis analog ADP-AlF₃ stabilizes a transition-state complex with BchNB bound to BchL on both halves. In the absence of ATP, there is no ET from BchL to BchNB (Fig. 4.3c). Thus, at a minimum, complex formation between BchL and BchNB is transient and coupled to ATP binding and hydrolysis within BchL. Chapter 3 of this document describes how a disordered region in the N-terminus of BchL is auto-inhibitory to overall reduction rates of DPOR, and how ATP-binding relieves the inhibition to drive complex formation with BchNB. This regulation appears unique to DPOR as neither the Fe-protein of nitrogenase or the BchX protein of COR possess this regulatory N-terminal region.

3. ET from the [4Fe-4S] cluster of BchL to the [4Fe-4S] cluster on BchNB and then onto Pchlide occurs upon complex formation. As stated above, whether ET occurs independently within the two halves remains to be established. Presented data provides strong evidence that communication regarding ET from one half is relayed to the other through Asp274. Substitution of Asp274 in just one half of BchNB stalls Pchlide reduction. Thus, the two halves are synchronized with respect to the steps in their Pchlide reduction cycles. In nitrogenase, it was shown that negative cooperativity and allosteric communication exist between the two halves.

(Danyal et al., 2016) ET occurs first in one half, and this process is suppressed in the other, thus establishing a sequential ET mechanism between the two halves. Since the half-active DPOR complex fails to reduce Pchlide in both halves, I propose that such asymmetry also exists in the DPOR system.

The commonalities between DPOR and nitrogenase, with respect to communication and allostery between the two halves suggest that sequential ET might be a theme embedded in other such $\alpha_2\beta_2$ structured enzymes. Evolutionary functional advantages to such structures could be used to direct the flow of electrons, provide substrate-binding selectivity, and overall efficiency of ET. Both nitrogenase and DPOR catalyze substrate reduction reactions requiring multiple rounds of ET. The allosteric and sequential ET process could also be utilized to count/calibrate the number of electrons accumulating at the metal clusters and/or on the substrate. It would be interesting to explore such mechanistic differences between $\alpha_2\beta_2$ enzyme complexes that catalyze single versus multiple ET dependent reduction chemistries.

CHAPTER 5: CONCLUSIONS

Oxidoreductases are abundant and diverse, with many biological, (Vedalankar & Tripathy, 2019) agricultural, (Garrone, Archipowa, Zipfel, Hermann, & Dietzek, 2015) industrial, (Martínez et al., 2017) and medicinal (Abu-Remaileh & Aqeilan, 2015) applications. Those with multiple subunits and oxygen sensitive [Fe-S] clusters are often difficult to study due to overall complexity and the necessity to maintain anaerobic environments to study them. It is often necessary to develop strategies to cope with several difficulties including but not limited to: an enzyme being made up of multiple separable components (this adds complexity, but can also be a strength allowing chimeric complexes to be formed (Wätzlich et al., 2009)), oxygen sensitivity (Cirpus et al., 2006), UV-invisibility (no strong absorbance peaks to exploit), EPR spectroscopic “invisibility” of individual electrons (electrons with very wide peak broadening due to anisotropic effects), fluorescent or highly absorptive substrates and/or reductants, etc. Strong absorbance and/or fluorescence of substrates can also be a positive, powerful tool. The intrinsic fluorescence of Pchl_a was used to study DPOR in chapter 4 of this document, but chlorophyll background fluorescence in cells can make microscopic imaging techniques challenging in photosynthetic organisms such as *Chlamydomonas reinhardtii* (Rasala et al., 2013), necessitating new techniques to study them. DPOR poses many of the listed challenges. The absorbance spectrum of the reductant used in all preparations of DPOR components, reduced dithionite, overlaps with the typically used 280nm absorbance value used to determine protein concentrations, (Layne, 1957) necessitating different colorimetric assays for determining protein concentrations. Absorbance at 280 nm is also the standard wavelength used to monitor elutions on HPLC machinery, which is masked by the absorbance of reduced dithionite. The [Fe-S] cluster of BchNB has very weak EPR absorbance under even the most ideal conditions. The oxygen sensitivity of DPOR makes all standard biochemical techniques more difficult and complicated. While studying these proteins can prove challenging, evolution has dictated that this complexity

is necessary for many of the extant oxidoreductases that are critical for a whole host of cellular process across all domains of life and are thus worthy of the attention of the scientific community.

DPOR presents an opportunity to attempt to address a fundamental conundrum regarding enzyme evolution. So-called “catalytically or kinetically perfect” enzymes are those that increase a reaction’s velocity to a high enough degree that the rate of catalysis is limited by the molecule finding the enzyme. (ZHOU & ZHONG, 2005) These enzymes, (carbonic anhydrase, catalase, fumarase, superoxide dismutase, etc.) operate at very high rates ($\sim 10^{10} \cdot \text{M}^{-1} \cdot \text{s}^{-1}$), roughly 11 orders of magnitude faster than that of DPOR ($\sim 0.2 \cdot \text{M}^{-1} \cdot \text{s}^{-1}$). (Yuichi Fujita & Bauer, 2000)

If evolution can produce “perfect” enzymes, why do some enzymes exist with very low rates of catalysis such as DPOR? This question can be addressed to some degree by abolishing the notion that selection pressures favor catalytic efficiency over the safety or fidelity of a reaction (avoiding off-target chemistry, etc.). This argument does not hold true with DPOR, as LPOR has increased catalytic rates as well as greater efficiency, requiring smaller chemical energy input(s). Of course, LPOR uses light as one of the inputs, which can be considered “free”. In that vein, all organisms that utilize DPOR are using it to create chlorophyll, so all must have access to light eventually, otherwise why reduce Pchl_a at all? Of course, some photosynthesis is better than none, so organisms in low light can occupy a less than ideal niche despite an inefficient metabolic strategy. Evergreen trees, for example, remain green by using DPOR while covered in snow and/or during short days of the year, while their angiosperm cousins hibernate. (Schoefs & Franck, 2003) This may be interpreted as an organism filling a niche that is present because it is willing (or able) to perform admittedly less efficient metabolic processes when others cannot perform them at all. It could therefore be argued that DPOR allows organisms to fill niches that organisms relying on LPOR could not but has not been determined empirically.

Further comparison of DPOR with LPOR prompts me to think that LPOR appears to have been rationally designed, where DPOR does not appear to be the product of a deliberate process. Of course, neither of these enzymes or any extant enzyme for that matter (that was not deliberately designed by humans) are not rationally designed. DPOR accomplishes the simplest of organic chemical reductions, albeit with high specificity at a very slow rate, requiring a large number (8) of subunits, and chemical energy input. Reducing just half of a double bond using DPOR ultimately requires 1 molecule of NADPH, a NADPH reductase, a second protein (a ferredoxin), BchL, 2 molecules of ATP, and one half of a BchNB tetramer. Because DPOR binds to 2 molecules of substrate, a full catalytic cycle costs 4 NADPH, 8 ATP, and a grand total of 20 polypeptides working in careful unison. In contrast, LPOR needs one molecule of NADPH and light energy. It also does not require the incorporation and maintenance of intact [Fe-S] clusters and can tolerate a variety of conditions in the cell. Why, then, are DPOR and structurally homologous enzymes like COR and Nitrogenase maintained?

DPOR is an ancient enzyme, and some parallels can be drawn to ancient organisms. Trilobites, for example were a dominant organism in the early earth biome, a huge contribution to the fossil record spanning the Cambrian period (~540million years ago) to the late Permian period (~300 million years ago). (Eldredge, 2008) . Among the first of arthropods, they had a segmented body with repeated segments in their body plan. These repeated segments allowed specialization in individual segments over millennia. (Loxdale & Wilmer, 1991) This type of expansion/duplication followed by specialization is a common evolutionary theme. This logic could be applied to DPOR and its relatives. DPOR, COR and Nitrogenase likely have a common ancestor that was duplicated and specialized, like the duplication(s) in body segments of the ancient trilobites. While that can explain of how the extant hetero-octameric enzymes came to be, it does not explain why DPOR is still maintained when LPOR exists. At least so far as why many organisms **only** use DPOR to reduce Pchlide. A likely answer has to do with the early earth

conditions (reducing atmosphere, no oxygen evolving complex in plants, etc.). There was no pressure to evolve an enzyme that required stability in oxygenic environments, and the strongest pressure was likely simply to develop any enzyme that could accomplish the correct chemistry. To answer why DPOR was ultimately maintained, the solution can be derived from the fitness of certain animals and plants. Crocodylians have remained essentially unchanged the late Cretaceous (~80 million years ago). (Dessauer, Glenn, & Densmore, 2002) Existing fern plants have also changed little since the late Cretaceous (~145 million years ago). (Smith et al., 2006) While evolution at an organismal scale is not identical to enzyme evolution, the logic behind the current existence of DPOR can be related to the crocodylians and fern plants. It is an ancient enzyme that served its purpose well enough, and despite the later emergence of the non-homologous LPOR, is robustly maintained like the extant ancient organisms that coincide with living “higher” plants and animals.

Philosophical evolutionary musings aside, DPOR and related enzymes ARE maintained, and are very critical to life. *The central aims of this document are to begin to address the controversial field of [Fe-S] cluster biogenesis and to address the complexity and symmetry of DPOR. In the case of the BchL, its c2 symmetry axis and how ATP is utilized to coordinate electron transfer, and how information is transmitted between subunits and to the [4Fe-4S] cluster. In the case of BchNB, its c2 symmetry axis and how substrate binding, electron transfer, and proton transfer are coordinated/communicated between halves.*

5.1 In most (or all) modern commercially available *E. coli* BL21(DE3) *E. coli* expression cell lines, one of two [Fe-S] cluster genesis operons is inoperative.

E. coli BL21(DE3) and its many derivatives all are used for the heterologous expression of enzymes/proteins in large enough quantities to allow for their in-vitro characterization. Some contain additional plasmids that express additional amino acids, have inserted tags on native

proteins to aid in purification, or have even been optimized to not contain a particular (such as TAG) stop codon to aid in the incorporation on non-canonical amino acids. (Kleber-Janke & Becker, 2000; Robichon, Luo, Causey, Benner, & Samuelson, 2011; Villarreal et al., 2008) *E. coli* cells have two operons (*isc* and *suf*) that are responsible for the generation and delivery of [Fe-S] clusters from Iron ions and sulfur derived from cysteine. Despite their redundant functionality, they are utilized differently in times of stress or nutrient limitation. It was discovered that a fusion of the first two genes of the *suf* operon have become fused and non-functional at some point since their isolation and derivations. 10 modern strains were determined to have this same non-functional Suf pathway. (Corless et al., 2020)

The field of [Fe-S] cluster biogenesis, even in the “simpler” organisms like *E. coli* is contested, with many of the enzyme components performing either multiple roles or have moonlighting activity in-vitro that are not relevant in-vivo, the protein CyaY is particularly contentious. (Adinolfi et al., 2004; Bedekovics, Gajdos, Kispal, & Isaya, 2007; di Maio, Chandramouli, Yan, Brancato, & Pastore, 2016; Roche et al., 2015) This is all to convey the idea that even from the scale of an entire operon being non-functional, the understanding of the entire process of [Fe-S] cluster genesis and delivery is still in its adolescence. Proper generation and insertion of [Fe-S] clusters is of particular importance to enzymes which rely on them for functionality. Because two systems exist in the wild, and the routine production of enzymes from distant relatives of *E. coli* such as human proteins in *E. coli* BL21(DE3) cell lines, it is likely that certain proteins prefer the components of one operon over the other, while certain proteins may not have a preference.

To this end, multiple cell lines were generated based off the *suf* deficient *E. coli* BL21(DE3) cell line. One line wherein the operon was restored maintaining its native regulatory elements, and one where the operon was restored and de-repressed, which were titled SuffeScient

cells. These cell lines were used to determine what effect (if any) would be revealed on the heterologous expression of components of DPOR.

5.2 SufFeScient cells increase BchL Yield, and [Fe-S] cluster occupancy, while BchNB was not affected.

BchL and BchNB were used to assay the effect of restoring and derepressing the *suf* operon in *E. coli* BL21(DE3) cell lines. When grown under identical conditions, *E. coli* BL21(DE3) and a cell line with a restored *suf* operon produced statistically identical results as far as yield and cluster occupancy for both BchL and BchNB. However, when the *suf* operon was genetically de-repressed, BchL showed a reproducible ~three-fold increase in the yield of protein per gram of wet cell paste/per liter of cells grown, and an increase in [Fe-S] cluster occupancy to nearly 100%. This increase was not seen for BchNB. This is the first evidence that under certain conditions of heterologous over expression, there is a clear preference for the *suf* operon being overexpressed as well. Regardless of cell line, all proteins were determined to be active after purification. Additionally, despite having similar doubling times once in lag phase, SufFeScient cells, regardless of protein being overexpressed, managed to reach log growth phase ~45 minutes sooner than *E. coli* BL21(DE3) cells. While not a tremendous increase in efficiency, in large scale processes this could be an additional time-saving feature of this cell line.

Due to the murky nature of the field of [Fe-S] cluster biogenesis and incorporation field, at this time the preference of a protein to the Isc or Suf pathway would have to be determined empirically using side-by-side comparisons. The potential increase in yield and occupancy will hopefully inspire multiple groups to try this cell line with their respective enzyme. Over time and as the number of proteins assayed increases, it is possible that patterns may begin to emerge that would help to clarify the waters of this field.

Finally, multiple enzymes that have an iron-sulfur cluster use them for sensing their environment. The redox capabilities of [Fe-S] clusters are also their Achilles heel. Exposure to oxygen can cause the destruction of an intact cluster. Some enzymes and proteins are still functional without their intact cluster, adopting a different conformation and activity to be used in the presence of oxygen. (Helmut Beinert et al., 1997; Crack, Green, Thomson, & Brun, 2014) There is also growing evidence that many of the nuclear enzymes have predicted [Fe-S] binding sites but are not expressed in a manner or cell that is optimized to incorporate them. This presents a solution to the apparent inactivity of certain purified proteins, as well as the opportunity to characterize the redox abilities of those proteins purified aerobically. (Wachnowsky, Fidai, & Cowan, 2018) The SuffeScient cell line may be a future workhorse or necessary cell line for characterizing these incompletely studied proteins.

5.3 BchL utilizes a novel “cap” structure to modulate its activity.

The homodimeric BchL from eubacterial species, as well as the cyanobacterium *Prochlorococcus marinus* (possibly the most prevalent single celled organism on earth) (Kettler et al., 2007) all have a conserved stretch of amino acids in near their N-terminus. Despite the conservation, existing crystal structures of BchL never had any electron density for this N-terminal region. With the help of a collaborator (Nozomi Ando) we successfully obtained density for these residues in a nucleotide free crystal structure. These alternating charged and uncharged residues from one half of the dimer interact with the [4Fe-4S] cluster of the L-protein, at least when not bound to nucleotide. This was a novel mechanism for interacting with and modulating [Fe-S] clusters. Interestingly, this feature is not present in homologous systems. Plant and most cyanobacterial BchL do not have this N-terminal extension (chapter 3 of this document). They do; however, all have an unresolved C-terminus. This region should be explored in the future. Chimeric versions where a eubacterial BchNB is mixed with a cyanobacterial or plant ChIL

protein are active, but to a lesser extent. (Yamamoto, Kurumiya, Ohashi, & Fujita, 2011) It's possible that the c-terminus of ChIL proteins serves a similar regulatory role to the N-terminus of BchL. Deletion of the C-terminus of this L-protein and characterizing its stability and enzymatic activity would shed light on this.

The Fe-protein of nitrogenase has neither region on either terminus. It also donates electrons to the MoFe protein at rates that are orders of magnitude higher than that of BchL. Chimeric complexes using the Fe-protein in lieu of BchL, or vice versa are very slow if at all active. It's possible that a N-terminally truncated BchL or C-terminally truncated ChIL would work in conjunction with the MoFe protein of Nitrogenase. If so, it's equally possible that copying the N-terminus of BchL onto the Fe-protein activity could be restored. These experiments would shed some light on the evolutionary path that was taken by these individual electron donor proteins for their respective systems.

5.4 BchL has a distinct patch of amino acids necessary for stabilizing the transition state.

The crystal structure of the full DPOR complex from *P. marinus* revealed that in the ATP hydrolysis transition state (simulated with ADP and AlF_3) a patch containing 2 Aspartic acids bridging a Phenylalanine ("DFD" patch") formed ionic interactions in trans with the 5-carbon sugar of the nucleotide bound to the opposing monomer. If one or both amino acids are mutated to the charge-reversed amino acid asparagine, activity was severely reduced or abolished entirely. The conformational landscape of BchL appears to be different from the Fe-protein of Nitrogenase.

DFD mutant constructs were able to bind to nucleotide despite losing overall activity. These constructs additionally do not have any theoretical basis for having lost the ability to hydrolyze ATP, though this was not determined experimentally. ATP binding was able to induce

a change is the local environment of the cluster confirmed by EPR, to about 50% of the extent of the effect seen for wild-type BchL. A similar patch is not obviously evident when comparing the sequence of BchL to BchX. Future work to obtain crystal structures of various forms of BchX would certainly shed light on if this phenomenon is conserved in COR, the trapped transition state would be most informative, though any nucleotide bound form may give relevant clues.

5.5 Both molecules of ATP are required for BchL activity.

The overall energetic cost of 2 ATP molecules per electron transfer event is high when compared to enzymes that perform similar reactions. While ATP will be regenerated by the product of DPOR (bacteriochlorophyll) and light energy, it is unclear if both molecules are necessary to perform catalysis. As a homodimer, it would be difficult for evolution to produce a version of BchL where only one half would be able to bind to ATP. A gene duplication event and a binding mutation in one of the duplicates feasibly could produce a pool of asymmetric dimers, but if the process of dimerization was stochastic, it would produce 50% wild-type/binding mutant, 25% binding mutant/ binding mutant, and 25% wild-type/wild-type. This may provide some benefit to the overall process if the asymmetric mutant was active to the same degree, but it would also produce a substantial portion of nonfunctional enzyme.

Modern molecular biology tools allow the creation of an asymmetric mutant using a variety of strategies including co-expression of wild-type and mutant proteins harboring different affinity tags followed by dual column purification, or in some select instances covalent attachment via an amino acid linker. The latter strategy was used to probe the functionality of a BchL construct wherein only one half could bind to ATP. Various linkers were tried, and in this case 20 or more amino acids between the two halves of the dimer was determined to be the required length.

Perturbation of the binding ability of either half (or both halves) in the linked context or without a linker abolished the ability of BchL to reduce Pchl_{ide} to Chl_{ide} in conjunction with BchNB. While a less efficient process than that of LPOR, DPOR has clearly fine-tuned the existing methodology over evolutionary time. Often when looking at existing structures it becomes clear that nature does not stem from a planned outcome, rather it refines existing strategies, even when other convergent evolutionary pathways (LPOR) have come into being.

5.6 BchNB requires both catalytic sites to accomplish full reduction.

BchNB exists as a hetero tetramer comprised of two molecules of BchN and two of BchB, with two binding sites for its substrate Pchl_{ide}. Older models for DPOR's reaction cycle were depicted focused on only the chemistry occurring in one binding site. This may have been the trend for the sake of simplicity, the C₂ axis of symmetry of BchNB, or the assumption that the catalytic halves of BchNB are independent. Due to the size of BchNB (206kDa) it is possible that the two halves indeed are independent and the rest of the structure of the tetramer exists only as a form of scaffolding to hold the proteins together. Structural evidence suggests that this is not the case. One of the protons necessary for Pchl_{ide} reduction comes from Pchl_{ide} itself, the other from a conserved Aspartic acid residue (D274) in BchB. (Moser et al., 2013) This proton is being delivered in trans to the opposing half of the tetramer, depending on how it's divided. The phenomenon of interactions occurring in trans appears to be a prevalent strategy for DPOR. Like BchL, the interaction across symmetry lines suggests that communication between the two halves of the tetramer may be possible or necessary for the full catalytic cycle.

To address the question of whether both halves are necessary, an asymmetric mutant was created wherein one half cannot perform the proton transfer, where the other half presumably can if it is independent from the other side. This was accomplished by co-expression of a wild-type and mutant (D274A) version of BchB with BchN. The wild type and mutant versions of BchB

contained N-terminal StrepTactin and 6X poly-histidine affinity tags respectively. This produced a mixture of species, with a small portion hopefully existing as the asymmetric mutant. The appropriate controls were performed to ensure that co-expression of multiple copies of BchB, nor the affinity tags chose were affecting the activity of the tetramer. After a dual column purification of the asymmetric construct, the resulting purified protein was assayed with western blot to determine the presence of both tags, as a proxy for the mutation in one half. In lock step with BchL, this asymmetric mutant was inactive.

5.7 BchNB donates electrons one at a time.

The inability to produce product in the mutant construct only implies that one of the steps of the reaction are not possible. Because two electron transfers must occur, and the order of proton donation between Pchlide and D274 remains unknown, it is necessary to observe the electrons harbored in the [4Fe-4S] cluster of BchNB. EPR spectroscopy proved difficult for monitoring BchNB [Fe-S] clusters, due to the very rare ligation used by BchNB. Most [Fe-S] clusters utilize the terminal sulfur of 4 cysteines to ligate the Fe atoms in the cluster. Many other ligands are possible, but BchNB uses an Aspartic acid residue for its 4th ligand, which is extremely rare. Despite the rarity of such a cluster, in collaboration with Brian Bennet, we were able to reproducibly visualize, and simulate, and determine the spin state the $s=7/2$ electrons in BchNB after optimizing the signal to relaxation rates to achieve resolution. This ligation, and the resulting spin state are critical to the function of DPOR specifically. Mutation of the 4th ligand to cysteine abolishes almost all activity, and the cluster found in COR's equivalent structure (BchYZ) is likely ligated by 4 cysteines, though the effect of mutating a 4th ligand in COR to asparagine has not been attempted. (Kiesel et al., 2015; Kondo, Nomata, Fujita, & Itoh, 2011)

The ability to directly monitor electrons in BchNB was paramount to key discoveries. First and foremost is that BchNB can be pre-reduced by BchL in the presence of ATP. The

previous assumption was that BchNB existed in an oxidized state (but stable) state after synthesis and before Pchl_{id}e binding. Secondly, wild-type BchNB is synthesized with oxidized clusters, while the D274A mutant is synthesized with reduced clusters, or is capable of being reduced (once) by the chemical reductant dithionite in solution. This suggests that the oxidation/protonation state of D274 is important for the conformational landscape and reductive properties of BchNB. Finally, in the presence of Pchl_{id}e, BchL, and ATP, the D274A mutant, while incapable of full reduction, regains almost exactly 50% of its EPR spectra compared to the fully reduced spectra. This suggest that the D274A mutant is stalled in one of the intermediates, where only one cluster has been re-reduced, and is waiting for the proton donation to occur in either the same or opposing half. This is the first EPR evidence that electrons are donated to BchNB in a stepwise fashion, where each side performs electron transfer in one-electron steps, while the other half is stalled. It is a reasonable assumption to make that individual proton donations occur at similarly gated intervals, but this remains unknown.

Study of COR provides a unique opportunity to validate some these key findings in BchNB. Due to the structural and sequence similarity between DPOR and COR, some key hypotheses should be challenged going forward. It's possible that the specificity of which double bond is being reduced is dictated solely via the location of just the proton donors, acting as sinks to trap the excited electron delocalized in the pi-stacked ring of Pchl_{id}e/Chl_{id}e. This would be a testable hypothesis once a structure or the proton donor(s) are determined for BchYZ. In the case of BchYZ, where both protons needed for reduction may come from the protein, (Kiesel et al., 2015) it may be possible alter the specificity of the double bond, or even the substrate. Enzymes are much better at chemistry than chemists tend to be, so one can image a scenario where an engineered enzyme could produce mass quantities of a designed porphyrin. While the idea of enzyme engineering is still in its prepubescence, and the fact that these enzymes must be made anaerobic to work, there are significant hurdles to jump before this architecture of enzyme could

be useful on a large scale. One ameliorating factor is that the products of these enzymes are excreted into media when the subsequent enzyme is mutated, as described in 2.2.5. This could allow the in-culture production of desired compounds, foregoing the need for an anaerobic setup.

5.8 Stepwise electron donation in BchNB may be established by cooperative Pchl_{id}e binding.

Steady and pre-steady state kinetics of binding of Pchl_{id}e can be determined through an assay that takes advantage of the intrinsic fluorescence of Pchl_{id}e. While in aqueous solution, Pchl_{id}e is a good fluorophore, with strong absorbance bands and red-shifted fluorescence spectra at almost all wavelengths in the UV-visible range. Pchl_{id}e, when in the hydrophobic binding site of BchNB becomes a stellar fluorophore. The fluorescence yield by exciting at 420nm increase by 500-750-fold in terms of photon counts (Fig. 4.8). This increase allows titrations of Pchl_{id}e by NB to monitor the steady state fluorescence as well as rapid mixing in a stopped-flow instrument to monitor pre-steady state reaction kinetics. The sigmoidal shape of a steady state titration suggests a cooperativity in binding like that of hemoglobin, with only two sites for binding. At the pre-steady state scale, 2 distinct phases of fluorescence enhancement can be visualized within the first 10 seconds of their interaction. These traces can be well fit to a 2-exponential plus linear fit. Interestingly, the D274A mutant of BchNB binds at similar rates, though exhibits what appears to be a dissociation phase after the initial two events I am attributing to the binding of 2 substrate molecules. This suggests that having the proton donor from the protein present allows for longer lasting binding and is further evidence that conformational changes are communicated through the protonation state of D274 of BchB.

Once the hurdle of maintaining an anaerobic atmosphere has been jumped, DPOR is an excellent candidate for single molecule visualization. The substrate Pchl_{id}e, as mentioned earlier is a stellar fluorophore, and that the change in intensity upon binding could be used to monitor binding events in real time. Additionally, the fluorescence properties of Pchl_{id}e and Chl_{id}e are

separable. This would feasibly allow the visualization of binding events, dissociation events, and with the proper context and filter set the visualization of substrate conversion. Since the final protonation event presumably establishes the shift in absorbance and fluorescence of the substrate Pchl_{id}, it may even be able to establish the rates at which the final step of Pchl_{id} reduction occur. Finally, BchL is amenable to non-canonical amino acid incorporation and labeling. This could (again using an appropriate excitation wavelength and filter set) the real time single molecule visualization of BchL binding with and dissociating from BchNB.

A comparative analysis of DPOR, COR and Nitrogenase may help to highlight key evolutionary steps that led to the currently existing protein complexes. COR is a closer relative of DPOR than Nitrogenase. The evolutionary branch point of these two enzymes would be a great candidate for ancestral reconstruction. This construct may be capable of donating electrons to both BchNB and BchYZ meaning it is a more promiscuous enzyme, may have differential oxygen stability, or any number of differing characteristics. The ancestral recreation of the BchNB/BchYZ may be able to bind to a multitude of porphyrin-based substrates, or even perform multiple modifications to Pchl_{id} and/or Chl_{id}. This type of reconstruction is very high risk, high reward, but may be worth pursuing. As stated, a structural comparison between DPOR and COR would greatly aid in any of the comparative endeavors. Sequence alignment and structure prediction are of course very powerful tools, but a sequence in the context of the actual shape of the enzyme is always much more informative and can work congruently with more alignment-based techniques. Finally, in lieu of a crystal structure, less traditional structural techniques may be uniquely applicable to anaerobic systems like DPOR, COR, and Nitrogenase. Electron Microscopy, and Cryo-EM seem attractive targets for probing the conformational and complex stoichiometry dynamics of these systems.

5.9 Overarching themes and contributions.

This work describes the characterization of an optimized cell line for heterologous [Fe-S] cluster containing proteins. The wide-scale use of this cell line will likely have many downstream ramifications. First, it will aid in the characterization of known proteins by potentially drastically increasing protein yields. Second, The SuffeScient line described in chapter 2 of this document can be applied to any number of known [Fe-S] cluster-containing proteins and may be used to discover novel [Fe-S] cluster-containing proteins that have been previously overexpressed in traditional BL21(DE3) cell lines. These proteins may require the restored *suf* operon to have properly incorporated [Fe-S] clusters. This is particularly important for the discovery of new roles in well studied enzymes, particularly those involved in DNA repair, but the applications are widespread. Finally, this cell line hints at the unknown specific role(s) of individual components of the *isc* and *suf* operons, generating new research directions for those studying this pathway.

This work describes a series of discoveries that address fundamental questions in the field of multimeric enzymes, and the class of hetero-octameric oxidoreductases containing [Fe-S] clusters specifically. A core misconception of symmetrical multimeric enzymes is that it is possible to assume that one symmetric unit is behaving in the same fashion as the other, and/or that each symmetrical part is independent of the other. Every symmetry axis of DPOR was shown to critical for overall functionality. The work described by (Tezcan et al., 2015) show that NifH of nitrogenase can bind asymmetrically to nucleotides but did not demonstrate that both nucleotides are required for functionality. Their work did not reveal the series of interactions that occur in trans in the homodimeric electron donor component that occur in BchL. This work details the specific amino acids required for the long-range allosteric communication necessary to convey information about the nucleotide state to the electron donating [Fe-S] cluster of BchL. Probing the conserved regions of BchL, the conserved disordered N-terminus was shown to regulate DPOR activity and possibly stability in solution. This highlights that the unstructured

regions of BchL, BchX, and NifH likely play a regulatory role in overall activity. The molecular details of how these unstructured regions interact with their own [Fe-S] clusters, as well as whether/how they interact with their respective electron acceptor component will provide key insights into how these enzymes are regulated. This discovery again provides a platform for studying the regulation and function of these proteins.

The work of (Danyal et al., 2016) show that there is negative cooperativity in the ET cycle of NifKD. While compelling evidence for communication between the halves, it did not determine that the activity of one half was necessary. The work described in chapter 4 of this document show that both halves of the tetramer must be functional, and that information is communicated about the electronic state(s) of the other half through the oxidation state of the in-trans proton donor of BchBD274. Furthermore, it revealed a stalled intermediate wherein only one half of the complex had been re-reduced after the initial electrons had been donated. This is the first hard evidence that ET is a stepwise phenomenon in DPOR. This knowledge provides hints as to the role of the heterotetramer, and the dual binding sites of these enzymes. It suggests that ET and proton donation are key regulatory steps that are necessary for sensing the electronic state of the other, possibly providing the overall ability to carefully donate electrons one at a time, ensuring that they are directed to the correct location. This hints at the way that specificity is provided for DPOR and COR, though likely cannot be proven without structural information about COR. Overall this work has proven the existence of key phenomena in these enzymes that were previously only speculation and provided several new questions and directions for future work. While this document describes several strides made in this avenue of scientific pursuit, more than anything it proves that there remains tremendous work to be done to fully understand and DPOR and related enzymes in order to leverage them to our advantage.

REFERENCES CITED

- Abu-Remaileh, M., & Aqeilan, R. I. (2015). The tumor suppressor WW domain-containing oxidoreductase modulates cell metabolism. *Experimental Biology and Medicine (Maywood, N.J.)*, 240(3), 345–350. <https://doi.org/10.1177/1535370214561956>
- Adams, P. D., Afonine, P. V., Bunkóczi, G., Chen, V. B., Davis, I. W., Echols, N., ... Zwart, P. H. (2010). PHENIX: A comprehensive Python-based system for macromolecular structure solution. *Acta Crystallographica Section D: Biological Crystallography*. <https://doi.org/10.1107/S0907444909052925>
- Adinolfi, S., Nair, M., Politou, A., Bayer, E., Martin, S., Temussi, P., & Pastore, A. (2004). The factors governing the thermal stability of frataxin orthologues: How to increase a protein's stability. *Biochemistry*, 43(21), 6511–6518. <https://doi.org/10.1021/bi036049+>
- Ayala-Castro, C., Saini, A., & Outten, F. W. (2008). Fe-S Cluster Assembly Pathways in Bacteria. *Microbiology and Molecular Biology Reviews*, 72(1), 110–125. <https://doi.org/10.1128/MMBR.00034-07>
- Bedekovics, T., Gajdos, G. B., Kispal, G., & Isaya, G. (2007). Partial conservation of functions between eukaryotic frataxin and the Escherichia coli frataxin homolog CyaY. *FEMS Yeast Research*, 7(8), 1276–1284. <https://doi.org/10.1111/j.1567-1364.2007.00296.x>
- Beinert, H. (2000). Erratum: Iron-sulfur proteins: Ancient structures, still full of surprises (Journal of Biological Inorganic Chemistry (2000) 5 (2-15)). *Journal of Biological Inorganic Chemistry*. <https://doi.org/10.1007/s00775-000-0014-3>
- Beinert, Helmut, Holm, R. H., & Münck, E. (1997). Iron-sulfur clusters: Nature's modular, multipurpose structures. *Science*. <https://doi.org/10.1126/science.277.5326.653>
- Blanc, B., Gerez, C., & Ollagnier de Choudens, S. (2015). Assembly of Fe/S proteins in bacterial systems. Biochemistry of the bacterial ISC system. *Biochimica et Biophysica Acta - Molecular Cell Research*. <https://doi.org/10.1016/j.bbamcr.2014.12.009>
- Boyd, E. S., Thomas, K. M., Dai, Y., Boyd, J. M., & Outten, F. W. (2014). Interplay between Oxygen and Fe-S Cluster Biogenesis: Insights from the Suf Pathway. *Biochemistry*. <https://doi.org/10.1021/bi500488r>
- Bröcker, M. J., Schomburg, S., Heinz, D. W., Jahn, D., Schubert, W. D., & Moser, J. (2010). Crystal structure of the nitrogenase-like dark operative protochlorophyllide oxidoreductase catalytic complex (ChlN/ChlB)₂. *Journal of Biological Chemistry*, 285(35), 27336–27345. <https://doi.org/10.1074/jbc.M110.126698>
- Burgess, B. K., & Lowe, D. J. (1996). Mechanism of molybdenum nitrogenase. *Chemical Reviews*, 96(7), 2983–3011. <https://doi.org/10.1021/cr950055x>
- Chandramouli, K., Unciuleac, M. C., Naik, S., Dean, D. R., Boi, H. H., & Johnson, M. K. (2007). Formation and properties of [4Fe-4S] clusters on the IscU scaffold protein. *Biochemistry*, 46(23), 6804–6811. <https://doi.org/10.1021/bi6026659>
- Cirpus, I. E. Y., Geerts, W., Hermans, J. H. M., Op den Camp, H. J. M., Strous, M., Kuenen, J. G., & Jetten, M. S. M. (2006). Challenging protein purification from anammox bacteria. *International Journal of Biological Macromolecules*.

<https://doi.org/10.1016/j.ijbiomac.2006.02.018>

- Corless, E. I., Mettert, E. L., Kiley, P. J., & Antony, E. (2020). Elevated expression of a functional suf pathway in *Escherichia coli* BL21(DE3) enhances recombinant production of an iron-sulfur cluster-containing protein. *Journal of Bacteriology*.
<https://doi.org/10.1128/JB.00496-19>
- Crack, J. C., Green, J., Thomson, A. J., & Brun, N. E. L. (2014). Iron-sulfur clusters as biological sensors: The chemistry of reactions with molecular oxygen and nitric oxide. *Accounts of Chemical Research*. <https://doi.org/10.1021/ar5002507>
- Daegelen, P., Studier, F. W., Lenski, R. E., Cure, S., & Kim, J. F. (2009). Tracing Ancestors and Relatives of *Escherichia coli* B, and the Derivation of B Strains REL606 and BL21(DE3). *Journal of Molecular Biology*. <https://doi.org/10.1016/j.jmb.2009.09.022>
- Danyal, K., Mayweather, D., Dean, D. R., Seefeldt, L. C., & Hoffman, B. M. (2010). Conformational gating of electron transfer from the nitrogenase Fe protein to MoFe protein. *Journal of the American Chemical Society*. <https://doi.org/10.1021/ja101737f>
- Danyal, K., Shaw, S., Page, T. R., Duval, S., Horitani, M., Marts, A. R., ... Antony, E. (2016). Negative cooperativity in the nitrogenase Fe protein electron delivery cycle. *Proceedings of the National Academy of Sciences*, *113*(40), E5783–E5791.
<https://doi.org/10.1073/pnas.1613089113>
- Dessauer, H. C., Glenn, T. C., & Densmore, L. D. (2002). Studies on the molecular evolution of the crocodylia: Footprints in the sands of time. In *Journal of Experimental Zoology*.
<https://doi.org/10.1002/jez.10208>
- di Maio, D., Chandramouli, B., Yan, R., Brancato, G., & Pastore, A. (2016). Understanding the role of dynamics in the iron sulfur cluster molecular machine. *Biochimica et Biophysica Acta - General Subjects*, *1861*(1), 3154–3163. <https://doi.org/10.1016/j.bbagen.2016.07.020>
- Duval, S., Danyal, K., Shaw, S., Lytle, A. K., Dean, D. R., Hoffman, B. M., ... Seefeldt, L. C. (2013). Electron transfer precedes ATP hydrolysis during nitrogenase catalysis. *Proceedings of the National Academy of Sciences of the United States of America*, *110*(41), 16414–16419. <https://doi.org/10.1073/pnas.1311218110>
- Eldredge, N. (2008). PALEONTOLOGY AND EVOLUTION. *Evolution*.
<https://doi.org/10.1111/j.1558-5646.2008.00382.x>
- Fontecave, M. (2006). Iron-sulfur clusters: Ever-expanding roles. *Nature Chemical Biology*.
<https://doi.org/10.1038/nchembio0406-171>
- Fujita, Y., Takagi, H., & Hase, T. (1998). Cloning of the gene encoding a protochlorophyllide reductase: the physiological significance of the co-existence of light-dependent and -independent protochlorophyllide reduction systems in the cyanobacterium *Plectonema boryanum*. *Plant & Cell Physiology*, *39*(2), 177–185.
<https://doi.org/10.1093/oxfordjournals.pcp.a029355>
- Fujita, Yuichi, & Bauer, C. E. (2000). Reconstitution of light-independent protochlorophyllide reductase from purified Bchl and BchN-BchB subunits: In vitro confirmation of nitrogenase-like features of a bacteriochlorophyll biosynthesis enzyme. *Journal of Biological Chemistry*, *275*(31), 23583–23588. <https://doi.org/10.1074/jbc.M002904200>
- Fujita, Yuichi, Takagi, H., & Hase, T. (1996). Identification of the chlB gene and the gene product essential for the light-independent chlorophyll biosynthesis in the cyanobacterium

- Plectonema boryanum. *Plant and Cell Physiology*.
<https://doi.org/10.1093/oxfordjournals.pcp.a028948>
- Garrone, A., Archipowa, N., Zipfel, P. F., Hermann, G., & Dietzek, B. (2015). Plant protochlorophyllide oxidoreductases A and B: Catalytic efficiency and initial reaction steps. *Journal of Biological Chemistry*. <https://doi.org/10.1074/jbc.M115.663161>
- Gräwert, T., Kaiser, J., Zepeck, F., Laupitz, R., Hecht, S., Amslinger, S., ... Rohdich, F. (2004). IspH protein of Escherichia coli: Studies on iron-sulfur cluster implementation and catalysis. *Journal of the American Chemical Society*. <https://doi.org/10.1021/ja0471727>
- Jacobson, M. R., Cash, V. L., Weiss, M. C., Laird, N. F., Newton, W. E., & Dean, D. R. (1989). Biochemical and genetic analysis of the nifUSVWZM cluster from Azotobacter vinelandii. *MGG Molecular & General Genetics*. <https://doi.org/10.1007/BF00261156>
- Jeong, H., Barbe, V., Lee, C. H., Vallenet, D., Yu, D. S., Choi, S. H., ... Kim, J. F. (2009). Genome Sequences of Escherichia coli B strains REL606 and BL21(DE3). *Journal of Molecular Biology*. <https://doi.org/10.1016/j.jmb.2009.09.052>
- Kettler, G. C., Martiny, A. C., Huang, K., Zucker, J., Coleman, M. L., Rodrigue, S., ... Chisholm, S. W. (2007). Patterns and implications of gene gain and loss in the evolution of Prochlorococcus. *PLoS Genetics*. <https://doi.org/10.1371/journal.pgen.0030231>
- Kiesel, S., W??tzlich, D., Lange, C., Reijerse, E., Br??cker, M. J., R??diger, W., ... Jahn, D. (2015). Iron-sulfur cluster-dependent catalysis of chlorophyllide a oxidoreductase from Roseobacter denitrificans. *Journal of Biological Chemistry*, 290(2), 1141–1154. <https://doi.org/10.1074/jbc.M114.617761>
- Kiley, P. J., & Beinert, H. (2003). The role of Fe-S proteins in sensing and regulation in bacteria. *Current Opinion in Microbiology*. [https://doi.org/10.1016/S1369-5274\(03\)00039-0](https://doi.org/10.1016/S1369-5274(03)00039-0)
- Kim, H., Kim, S., & Yoon, S. H. (2018). Metabolic network reconstruction and phenome analysis of the industrial microbe, Escherichia coli BL21(DE3). *PLoS ONE*. <https://doi.org/10.1371/journal.pone.0204375>
- Kim, S., Jeong, H., Kim, E. Y., Kim, J. F., Lee, S. Y., & Yoon, S. H. (2017). Genomic and transcriptomic landscape of Escherichia coli BL21(DE3). *Nucleic Acids Research*. <https://doi.org/10.1093/nar/gkx228>
- Kleber-Janke, T., & Becker, W. M. (2000). Use of modified BL21(DE3) Escherichia coli cells for high-level expression of recombinant peanut allergens affected by poor codon usage. *Protein Expression and Purification*. <https://doi.org/10.1006/prep.2000.1265>
- Kondo, T., Nomata, J., Fujita, Y., & Itoh, S. (2011). EPR study of 1Asp-3Cys ligated 4Fe-4S iron-sulfur cluster in NB-protein (BchN-BchB) of a dark-operative protochlorophyllide reductase complex. *FEBS Letters*, 585(1), 214–218. <https://doi.org/10.1016/j.febslet.2010.11.044>
- Kriek, M., Peters, L., Takahashi, Y., & Roach, P. L. (2003). Effect of iron-sulfur cluster assembly proteins on the expression of Escherichia coli lipoic acid synthase. *Protein Expression and Purification*. [https://doi.org/10.1016/S1046-5928\(02\)00680-0](https://doi.org/10.1016/S1046-5928(02)00680-0)
- Krissinel, E., & Henrick, K. (2007). Inference of Macromolecular Assemblies from Crystalline State. *Journal of Molecular Biology*. <https://doi.org/10.1016/j.jmb.2007.05.022>
- Kurnikov, I. V., Charnley, A. K., & Beratan, D. N. (2001). From ATP to electron transfer:

- Electrostatics and free-energy transduction in nitrogenase. *Journal of Physical Chemistry B*. <https://doi.org/10.1021/jp002540o>
- Lanz, N. D., Grove, T. L., Gogonea, C. B., Lee, K. H., Krebs, C., & Booker, S. J. (2012). RlmN and AtsB as models for the overproduction and characterization of radical SAM proteins. In *Methods in Enzymology*. <https://doi.org/10.1016/B978-0-12-394291-3.00030-7>
- Layne, E. (1957). [73] Spectrophotometric and turbidimetric methods for measuring proteins. *Methods in Enzymology*. [https://doi.org/10.1016/S0076-6879\(57\)03413-8](https://doi.org/10.1016/S0076-6879(57)03413-8)
- Lill, R., Broderick, J. B., & Dean, D. R. (2015). Special issue on iron-sulfur proteins: Structure, function, biogenesis and diseases. *Biochimica et Biophysica Acta - Molecular Cell Research*. <https://doi.org/10.1016/j.bbamcr.2015.03.001>
- Loxdale, H. D., & Wilmer, P. (1991). Invertebrate Relationships: Patterns in Animal Evolution. *The Journal of Animal Ecology*. <https://doi.org/10.2307/5473>
- Martínez, A. T., Ruiz-Dueñas, F. J., Camarero, S., Serrano, A., Linde, D., Lund, H., ... Alcalde, M. (2017). Oxidoreductases on their way to industrial biotransformations. *Biotechnology Advances*, 35(6), 815–831. <https://doi.org/10.1016/j.biotechadv.2017.06.003>
- MCNARY, J. E., & BURRIS, R. H. (1962). Energy requirements for nitrogen fixation by cell-free preparations from *Clostridium pasteurianum*. *Journal of Bacteriology*.
- Mettert, E. L., & Kiley, P. J. (2014). Coordinate regulation of the Suf and Isc Fe-S cluster biogenesis pathways by IscR is essential for viability of *Escherichia coli*. *Journal of Bacteriology*. <https://doi.org/10.1128/JB.01975-14>
- Mettert, E. L., Outten, F. W., Wanta, B., & Kiley, P. J. (2008). The Impact of O₂ on the Fe-S Cluster Biogenesis Requirements of *Escherichia coli* FNR. *Journal of Molecular Biology*. <https://doi.org/10.1016/j.jmb.2008.09.080>
- Monk, J. M., Koza, A., Campodonico, M. A., Machado, D., Seoane, J. M., Palsson, B. O., ... Feist, A. M. (2016). Multi-omics Quantification of Species Variation of *Escherichia coli* Links Molecular Features with Strain Phenotypes. *Cell Systems*. <https://doi.org/10.1016/j.cels.2016.08.013>
- Moser, J., Lange, C., Krausze, J., Rebelein, J., Schubert, W., Ribbe, M. W., ... Jahn, D. (2013). Structure of ADP-aluminium fluoride-stabilized protochlorophyllide oxidoreductase complex. *Proceedings of the National Academy of Sciences of the United States of America*, 110(6), 2094–2098. <https://doi.org/10.1073/pnas.1218303110>
- Munn, C. (2011). Microbes in the Marine Environment. *Marine Microbiology Ecology and Applications*.
- Muraki, N., Nomata, J., Ebata, K., Mizoguchi, T., Shiba, T., Tamiaki, H., ... Fujita, Y. (2010). X-ray crystal structure of the light-independent protochlorophyllide reductase. *Nature*, 465(7294), 110–114. <https://doi.org/10.1038/nature08950>
- Nakamura, M., Saeki, K., & Takahashi, Y. (1999). Hyperproduction of recombinant ferredoxins in *Escherichia coli* by coexpression of the ORF1-ORF2-iscS-iscU-iscA-hscB-hscA-fdx-ORF3 gene cluster. *Journal of Biochemistry*. <https://doi.org/10.1093/oxfordjournals.jbchem.a022409>
- Nascimento, S. M. D., Zou, Y., & Cheng, Q. (2016). Review of Studies on the Last Enzymes in Bacteriochlorophyll (<i>Bchl</i>) and Chlorophyll (<i>Chl</i>)

- Biosynthesis. *American Journal of Plant Sciences*. <https://doi.org/10.4236/ajps.2016.712155>
- Nesbit, A. D., Giel, J. L., Rose, J. C., & Kiley, P. J. (2009). Sequence-Specific Binding to a Subset of IscR-Regulated Promoters Does Not Require IscR Fe-S Cluster Ligation. *Journal of Molecular Biology*. <https://doi.org/10.1016/j.jmb.2009.01.055>
- Nomata, J., Kitashima, M., Inoue, K., & Fujita, Y. (2006a). Nitrogenase Fe protein-like Fe-S cluster is conserved in L-protein (BchL) of dark-operative protochlorophyllide reductase from *Rhodobacter capsulatus*. *FEBS Letters*, 580(26), 6151–6154. <https://doi.org/10.1016/j.febslet.2006.10.014>
- Nomata, J., Kitashima, M., Inoue, K., & Fujita, Y. (2006b). Nitrogenase Fe protein-like Fe-S cluster is conserved in L-protein (BchL) of dark-operative protochlorophyllide reductase from *Rhodobacter capsulatus*. *FEBS Letters*, 580(26), 6151–6154. <https://doi.org/10.1016/j.febslet.2006.10.014>
- Nomata, J., Kondo, T., Mizoguchi, T., & Tamiaki, H. (2014). Dark-operative protochlorophyllide oxidoreductase generates substrate radicals by an iron-sulphur cluster in bacteriochlorophyll biosynthesis. *Scientific Reports*, 4, 5455. <https://doi.org/10.1038/srep05455>
- Nomata, J., Mizoguchi, T., Tamiaki, H., & Fujita, Y. (2006). A second nitrogenase-like enzyme for bacteriochlorophyll biosynthesis: Reconstitution of chlorophyllide a reductase with purified X-protein (BchX) and YZ-protein (BchY-BchZ) from *Rhodobacter capsulatus*. *Journal of Biological Chemistry*, 281(21), 15021–15028. <https://doi.org/10.1074/jbc.M601750200>
- Nomata, J., Swem, L. R., Bauer, C. E., & Fujita, Y. (2005). Overexpression and characterization of dark-operative protochlorophyllide reductase from *Rhodobacter capsulatus*. *Biochimica et Biophysica Acta - Bioenergetics*, 1708(2), 229–237. <https://doi.org/10.1016/j.bbabi.2005.02.002>
- Nomata, J., Terauchi, K., & Fujita, Y. (2016). Stoichiometry of ATP hydrolysis and chlorophyllide formation of dark-operative protochlorophyllide oxidoreductase from *Rhodobacter capsulatus*. *Biochemical and Biophysical Research Communications*, 470(3), 704–709. <https://doi.org/10.1016/j.bbrc.2016.01.070>
- Olson, J. M., & Blankenship, R. E. (2004). Thinking about the evolution of photosynthesis. In *Photosynthesis Research*. <https://doi.org/10.1023/B:PRES.0000030457.06495.83>
- Outten, F. W., Djaman, O., & Storz, G. (2004). A suf operon requirement for Fe-S cluster assembly during iron starvation in *Escherichia coli*. *Molecular Microbiology*. <https://doi.org/10.1111/j.1365-2958.2004.04025.x>
- Pence, N., Tokmina-Lukaszewska, M., Yang, Z., Ledbetter, R. N., Seefeldt, L. C., Bothner, B., & Peters, J. W. (2017). Unraveling the interactions of the physiological reductant flavodoxin with the different conformations of the Fe protein in the nitrogenase cycle. *Journal of Biological Chemistry*, 292, jbc.M117.801548. <https://doi.org/10.1074/jbc.M117.801548>
- Pérard, J., & Ollagnier de Choudens, S. (2018). Correction to: Iron–sulfur clusters biogenesis by the SUF machinery: close to the molecular mechanism understanding (JBIC Journal of Biological Inorganic Chemistry, (2018), 23, 4, (581–596), 10.1007/s00775-017-1527-3). *Journal of Biological Inorganic Chemistry*. <https://doi.org/10.1007/s00775-018-1571-7>
- Pinske, C., Bönn, M., Krüger, S., Lindenstrauß, U., & Sawers, R. G. (2011). Metabolic deficiencies revealed in the biotechnologically important model bacterium *Escherichia coli*

- BL21(DE3). *PLoS ONE*. <https://doi.org/10.1371/journal.pone.0022830>
- Py, B., & Barras, F. (2010). Building Feg-S proteins: Bacterial strategies. *Nature Reviews Microbiology*. <https://doi.org/10.1038/nrmicro2356>
- Rasala, B. A., Barrera, D. J., Ng, J., Plucinak, T. M., Rosenberg, J. N., Weeks, D. P., ... Mayfield, S. P. (2013). Expanding the spectral palette of fluorescent proteins for the green microalga *Chlamydomonas reinhardtii*. *Plant Journal*. <https://doi.org/10.1111/tpj.12165>
- Reinbothe, C., Bakkouri, M. El, Buhr, F., Muraki, N., Nomata, J., Kurisu, G., ... Reinbothe, S. (2010). Chlorophyll biosynthesis: Spotlight on protochlorophyllide reduction. *Trends in Plant Science*, *15*(11), 614–624. <https://doi.org/10.1016/j.tplants.2010.07.002>
- Robichon, C., Luo, J., Causey, T. B., Benner, J. S., & Samuelson, J. C. (2011). Engineering *Escherichia coli* BL21(DE3) derivative strains to minimize *E. coli* Protein contamination after purification by immobilized metal affinity chromatography. *Applied and Environmental Microbiology*. <https://doi.org/10.1128/AEM.00119-11>
- Rocha, A. G., & Dancis, A. (2016). Life without Fe-S clusters. *Molecular Microbiology*. <https://doi.org/10.1111/mmi.13273>
- Roche, B., Agrebi, R., Huguenot, A., Ollagnier de Choudens, S., Barras, F., & Py, B. (2015). Turning *Escherichia coli* into a Frataxin-Dependent Organism. *PLoS Genetics*, *11*(5), 1–22. <https://doi.org/10.1371/journal.pgen.1005134>
- Sarma, R., Barney, B. M., Hamilton, T. L., Jones, A., Seefeldt, L. C., & Peters, J. W. (2008). Crystal structure of the L protein of *Rhodobacter sphaeroides* light-independent protochlorophyllide reductase with MgADP bound: A homologue of the nitrogenase Fe protein. *Biochemistry*, *47*(49), 13004–13015. <https://doi.org/10.1021/bi801058r>
- Schoefs, B., & Franck, F. (2003). Protochlorophyllide Reduction: Mechanisms and Evolution. *Photochemistry and Photobiology*. [https://doi.org/10.1562/0031-8655\(2003\)078<0543:prmae>2.0.co;2](https://doi.org/10.1562/0031-8655(2003)078<0543:prmae>2.0.co;2)
- Seefeldt, L. C., Hoffman, B. M., & Dean, D. R. (2012). Electron transfer in nitrogenase catalysis. *Current Opinion in Chemical Biology*. <https://doi.org/10.1016/j.cbpa.2012.02.012>
- Seefeldt, L. C., Peters, J. W., Beratan, D. N., Bothner, B., Minter, S. D., Raugei, S., & Hoffman, B. M. (2018). Control of electron transfer in nitrogenase. *Current Opinion in Chemical Biology*, *47*, 54–59. <https://doi.org/10.1016/j.cbpa.2018.08.011>
- Smith, A. R., Pryer, K. M., Schuettpelz, E., Korall, P., Schneider, H., & Wolf, P. G. (2006). A classification for extant ferns. *Taxon*. <https://doi.org/10.2307/25065646>
- Stephens, P. J., Jollie, D. R., & Warshel, A. (1996). Protein control of redox potentials of iron-sulfur proteins. *Chemical Reviews*, *96*(7), 2491–2513. <https://doi.org/10.1021/cr950045w>
- Stoll, S., & Schweiger, A. (2006). EasySpin, a comprehensive software package for spectral simulation and analysis in EPR. *Journal of Magnetic Resonance*. <https://doi.org/10.1016/j.jmr.2005.08.013>
- Studier, F. W., Daegelen, P., Lenski, R. E., Maslov, S., & Kim, J. F. (2009). Understanding the Differences between Genome Sequences of *Escherichia coli* B Strains REL606 and BL21(DE3) and Comparison of the *E. coli* B and K-12 Genomes. *Journal of Molecular Biology*. <https://doi.org/10.1016/j.jmb.2009.09.021>

- Takahashi, Y., & Tokumoto, U. (2002). A third bacterial system for the assembly of iron-sulfur clusters with homologs in Archaea and plastids. *Journal of Biological Chemistry*. <https://doi.org/10.1074/jbc.C200365200>
- Tanaka, N., Kanazawa, M., Tonosaki, K., Yokoyama, N., Kuzuyama, T., & Takahashi, Y. (2016). Novel features of the ISC machinery revealed by characterization of *Escherichia coli* mutants that survive without iron-sulfur clusters. *Molecular Microbiology*. <https://doi.org/10.1111/mmi.13271>
- Tezcan, F. A., Kaiser, J. T., Howard, J. B., & Rees, D. C. (2015). Structural evidence for asymmetrical nucleotide interactions in nitrogenase. *Journal of the American Chemical Society*, 137(1), 146–149. <https://doi.org/10.1021/ja511945e>
- Tokumoto, U., Kitamura, S., Fukuyama, K., & Takahashi, Y. (2004). Interchangeability and distinct properties of bacterial Fe-S cluster assembly systems: Functional replacement of the *isc* and *suf* operons in *Escherichia coli* with the *nifSU*-like operon from *Helicobacter pylori*. *Journal of Biochemistry*. <https://doi.org/10.1093/jb/mvh104>
- Tsai, C. L., & Tainer, J. A. (2018). Robust Production, Crystallization, Structure Determination, and Analysis of [Fe–S] Proteins: Uncovering Control of Electron Shuttling and Gating in the Respiratory Metabolism of Molybdopterin Guanine Dinucleotide Enzymes. In *Methods in Enzymology*. <https://doi.org/10.1016/bs.mie.2017.11.006>
- Vedalankar, P., & Tripathy, B. C. (2019). Evolution of light-independent protochlorophyllide oxidoreductase. *Protoplasma*, 256(2), 293–312. <https://doi.org/10.1007/s00709-018-1317-y>
- Villarreal, D. M., Phillips, C. L., Kelley, A. M., Villarreal, S., Villaloboz, A., Hernandez, P., ... Henderson, D. P. (2008). Enhancement of recombinant hemoglobin production in *Escherichia coli* BL21(DE3) containing the *Plesiomonas shigelloides* heme transport system. *Applied and Environmental Microbiology*. <https://doi.org/10.1128/AEM.01291-08>
- Vinella, D., Brochier-Armanet, C., Loiseau, L., Talla, E., & Barras, F. (2009). Iron-sulfur (Fe/S) protein biogenesis: Phylogenomic and genetic studies of A-type carriers. *PLoS Genetics*. <https://doi.org/10.1371/journal.pgen.1000497>
- Wachnowsky, C., Fidai, I., & Cowan, J. A. (2018). Iron-sulfur cluster biosynthesis and trafficking-impact on human disease conditions. *Metallomics*. <https://doi.org/10.1039/c7mt00180k>
- Watt, G. D., Bulen, W. A., Burns, A., & Hadfield, K. L. M. (1975). Stoichiometry, ATP/2e Values, and Energy Requirements for Reactions Catalyzed by Nitrogenase from *Azotobacter Vinelandii*. *Biochemistry*. <https://doi.org/10.1021/bi00690a019>
- Wätzlich, D., Bröcker, M. J., Uliczka, F., Ribbe, M., Virus, S., Jahn, D., & Moser, J. (2009). Chimeric Nitrogenase-like enzymes of (bacterio)chlorophyll biosynthesis. *Journal of Biological Chemistry*, 284(23), 15530–15540. <https://doi.org/10.1074/jbc.M901331200>
- Wayne Outten, F. (2015). Recent advances in the Suf Fe-S cluster biogenesis pathway: Beyond the Proteobacteria. *Biochimica et Biophysica Acta - Molecular Cell Research*. <https://doi.org/10.1016/j.bbamcr.2014.11.001>
- Winn, M. D., Ballard, C. C., Cowtan, K. D., Dodson, E. J., Emsley, P., Evans, P. R., ... Wilson, K. S. (2011). Overview of the CCP4 suite and current developments. *Acta Crystallographica Section D: Biological Crystallography*. <https://doi.org/10.1107/S0907444910045749>

- Yamamoto, H., Kato, M., Yamanashi, K., & Fujita, Y. (2014). Reconstitution of a sequential reaction of two nitrogenase-like enzymes in the bacteriochlorophyll biosynthetic pathway of *Rhodospirillum rubrum*. *Biochemical and Biophysical Research Communications*, 448(2), 200–205. <https://doi.org/10.1016/j.bbrc.2014.04.087>
- Yamamoto, H., Kurumiya, S., Ohashi, R., & Fujita, Y. (2011). Functional evaluation of a nitrogenase-like protochlorophyllide reductase encoded by the chloroplast DNA of *Physcomitrella patens* in the cyanobacterium *Leptolyngbya boryana*. *Plant and Cell Physiology*, 52(11), 1983–1993. <https://doi.org/10.1093/pcp/pcr132>
- Yang, Z. Y., Ledbetter, R., Shaw, S., Pence, N., Tokmina-Lukaszewska, M., Eilers, B., ... Seefeldt, L. C. (2016). Evidence That the Pi Release Event Is the Rate-Limiting Step in the Nitrogenase Catalytic Cycle. *Biochemistry*, 55(26), 3625–3635. <https://doi.org/10.1021/acs.biochem.6b00421>
- ZHOU, G.-Q., & ZHONG, W.-Z. (2005). Diffusion-Controlled Reactions of Enzymes. *European Journal of Biochemistry*. <https://doi.org/10.1111/j.1432-1033.1982.tb06976.x>

APPENDIX

Appendix 1 DPOR growth protocol

Media

Lauria Broth, autoclave for 40-minute cycle

Proper Antibiotic(s) (1X)

1mM Fe(III)Citrate (make 50mM stock in H₂O, stir at 200°C until see through orange) add 20 mL/Liter media

1mM L-cysteine (50mM stock in H₂O stirred at RT until clear) add 20 mL/Liter media

Growth

Incubate @37°C, shaking at 220 RPM until OD₆₀₀ = 0.6 (Take uninduced sample)

Induce with 30 µM IPTG (make 100 mM stock, 10 mL, add 300 µL)

Induction may also include 4AZP for TAG constructs (See notes)

Move to 25°C, 150 RPM, let shake overnight (~17 hours)

Cluster formation

Move growth to 1L centrifuge tubes

(Take Induced Sample)

Add 1.7 mM (0.3 g) Dithionite/Liter growth, cap immediately after addition and turn bottles end over end to mix

Incubate @ 17°C (no shaking) for 3 hours

Spin @4200 RPM for 20 minutes

Decant media in glovebox

Resuspend cells in at least 25 ml/Liter growth STD degassed buffer (100mM Hepes PH7.5, 150 mM NaCl, 1.7mM Dithionite)

Place into serum bottle, cap, add nitrogen (~5 PSI) to top, and freeze away.

NOTES

4AZP: For each 1L growth add:

206 mg 4AZP resuspension

Thoroughly vortex in 1 mL methanol

Add 1 additional mL methanol, vortex until clear

Bring volume up to 5 mL with MQ H₂O

Add entire quantity at time of induction

Appendix 2 DPOR lysis and preparation protocol

Buffers (All buffers must be properly degassed, at least 3 cycles of >15min each vacuum and Nitrogen on schlenk line.) Resuspend DT (10mMoles) in 10 mL degassed buffer, and vacuum until it stops forming bubbles. Make fresh DT stock every day.

STD

100mM HEPES (PH7.5)

150mM NaCl

WASH

100mM HEPES (PH7.5)

150mM NaCl

20 mM Imidazole

ELUTE

100mM HEPES (PH7.5)

150mM NaCl

250 mM Imidazole

A

100 mM HEPES (PH7.5)

B

100mM HEPES (PH7.5)

1M NaCl

For linked constructs, I also add 3X PIC and 1mM PMSF (1 mL of 100 mM in isopropanol.)

Lysis

1. Add lysozyme (.02g/100mL) to top of frozen cells, add 1.7 mM DT.
2. Thaw cells under nitrogen, stirring. Incubate on ice for at least 30 min after fully thawed.
3. Move cells into glovebox, with icebox. Pour cells+lysozyme into appropriately sized beaker, place in ice.
4. Sonicate @50% duty cycle, 1.7 amplitude. 1minute on, 1 minute off, 3 repetitions.

5. Pour sonicated cells into centrifuge tubes (~40mL each), make sure tubes have rubber seals.
6. Spin cells at 17,000 RPM for 1 Hr.
7. Decant clarified lysate into a clean serum bottle and cap it inside the glovebox.

Nickel NTA column 2mL/min

1. Equilibrate ~6 ml fresh nickel beads with ~90 mL STD, 2.0 mL/minute using either a peristaltic pump or the AKTA or equivalent. Check that buffer is reducing at the end of the column with Methyl-Violagen (~.2g in ~10 mL MilliQ water)
2. Load clarified lysate onto column using pump or AKTA (I always use the peristaltic pump for this step, it is much easier to clean.
3. Wash with at least 90mL WASH buffer.
4. Elute with ELUTE buffer. Proteins usually come off in the first 30 mL depending on column size.

Q-Sepharose column 2mL/min

1. Equilibrate column (~10mL) first with 80 mL buffer B. The high salt must be run first to get Dithionite throughout the whole column. If you just run A, the DT will just stay at the top of the column and the prep will fail.
2. Equilibrate with 80 mL Buffer A
3. Load Protein
4. Wash with 80 mL STD
5. Elute with a linear gradient, 140 mL (100% to 0%) (STD to B), collecting 1.8- or 2.0-mL fractions. Protein usually comes off column in elution 15-30.

6. run gel to determine where the protein is, pool fractions, concentrate in spin column (I usually do ~500 μ L for a 4L growth, usually get ~120 μ M.) and flash freeze in liquid nitrogen, in cryo-tubes. Store protein in liquid nitrogen doer. It is helpful to take a sample of the concentrated protein (I use 40 μ L) to perform subsequent SDS gel to determine purity and so you have a small quantity for Bradford assay protein concentration determination.

If you want to run an additional S200 polishing step, I recommend only concentrating down to either 2.5 or 1mL depending on the size of the growth.

S200 SEC gel filtration 2.7mL/min

1. Equilibrate the S200 column with at least 500mL STD buffer, running at 2.7mL/min if not in a cold room.
2. Equilibrate the syringe port with STD buffer by running through 5-10-fold the volume of the loop via syringe.
3. Once the column is equilibrated, load your sample then run the column at 2.7mL/min. Collect fractions after the void volume, I use 2 mL fractions every time just because there are so many.
4. Run brown fractions on a gel to determine which ones are desired, then concentrate selected fractions and freeze away as described.

Appendix 3 Bradford Assay

Reagents:

Bradford reagent

1 mg/mL Bovine Serum

H₂O

Cuvettes

Trendline:

1. Dilute Bradford reagent (1-part reagent to 4-parts water). You will need 10 mL for the trendline, and then I usually do 6 samples per protein, triplicates at 2 concentrations. (e.g. for 2 proteins, make 25 mL total, 5mL reagent + 20 mL H₂O)

2. Make 2 or 3 each, I make them directly in the bottom corner of the cuvettes:

(50 µg/mL) 2.5 µL BSA + 47.5 µL H₂O

(100 µg/mL) 5.0 µL BSA + 45.0 µL H₂O

(150 µg/mL) 7.5 µL BSA + 42.5 µL H₂O

(200 µg/mL) 10.0 µL BSA + 40.0 µL H₂O

(250 µg/mL) 12.5 µL BSA + 37.5 µL H₂O

NOTE 1µL sample + 49 µL H₂O (50X dilution factor) is a good place to start with concentrated (~100uM or greater) proteins. 10 µL sample + 40 µL H₂O (5X dilution factor) is a good place to start for more diluted (~10-20uM) proteins, depending on the size of course. Adjust your dilution factor until the values you get for the sample are within those of the trendline

3. Add 1 mL of diluted Bradford reagent to each sample and trendline cuvette.

4. Measure the absorbance of all cuvettes @595nm (simple reads application on the spec)

5. For the trendline, plot each absorbance value vs its concentration in kaleidagraph, and add a linear trendline.
6. Solve for X using the trendline values.
7. Multiply concentrations by dilution factor
8. Divide concentrations (mg/mL) by the molecular weight (in Daltons) and then multiply by the appropriate factor (10^6 for μM).
9. Average values and record concentration.